To the Graduate Council:

I am submitting herewith a thesis written by Douglas A. Shamblin entitled "Control of Oscillations in a Suspended Payload Transport System." I have examined the final copy of the thesis for form and content and recommend that it be accepted in partial fulfillment of the requirements for the degree of Master of Science, with a major in Electrical Engineering.

Mohan M. Trivedi

Dr. Mohan M. Trivedi, Major Professor

We have read this thesis and recommend its acceptance:

Robert E. Bodenheimer

Reid Kress

Accepted for the Council:

Associate Vice Chancellor and
Dean of The Graduate School

Statement of Permission to Use

In presenting this thesis in partial fulfillment of the requirements for a Master's degree at The University of Tennessee, Knoxville, I agree that the Library shall make it available to borrowers under rules of the Library. Brief quotations from this thesis are allowable without special permission, provided that accurate acknowledgement of the source is made.

Permission for extensive quotation from or reproduction of this thesis may be granted by my major professor, or in his absence, by the Head of Interlibary Services when, in the opinion of either, the proposed use of the material is for scholarly purposes. Any copying or use of the material in this thesis for financial gain shall not be allowed without my written permission.

Signature Douglas A. Shamblin

Date 7/13/95

Control of Oscillations in a Suspended Payload Transport System

A Thesis

Presented for the

Master of Science

Degree

The University of Tennessee, Knoxville

Douglas A. Shamblin

August 1995

Dedication

I would like to dedicate this thesis to my wife Wendy Shamblin and to my daughters Mary and Samantha who through their support and sacrifice have made this possible. I love you.

Acknowledgements

First I would like to thank my family and friends for their untiring support throughout my education. They have constantly encouraged me and helped me through the difficult times. My success is due in no small part to them.

I wish to express a special thanks to Dr. Mohan Trivedi for the opportunity to pursue my graduate studies. Dr. Trivedi extended assistance and encouragement at times when it was most important. I would like to express my gratitude to Dr. John Jansen who has provided direction and encouragement and shown unending patience during the development of my thesis. I would also like to express my appreciation to Dr. Kress and Dr. Bodenheimer for their help throughout my education.

I would like to thank my sister Pamela Shamblin for her invaluable assistance in editing this thesis. I owe additional thanks to all the members of the Computer Vision and Robotics Research Laboratory and the staff of the Electrical and Computer Engineering Department.

Abstract

This thesis addresses the design and testing of control systems to reduce and avoid oscillations in a suspended payload transport system, specifically the Integrated Product Development (IPD) crane located at the Oak Ridge National Laboratory (ORNL) Robotics and Process Systems Division. The IPD crane is an overhead gantry style industrial crane. The avoidance of payload oscillation was accomplished by operator input filtering using the Robust Notch Filter(RNF). The reduction or damping of payload oscillations was achieved with a closed-loop control system using inclinometers for each axis of motion as the feedback device. Both controllers were implemented using a Zilog Z180 based microcontroller board. The RNF provided avoidance of payload oscillation from operator input for changes in crane cable length of up to one half. The closed-loop oscillation damping system proved capable of damping oscillations within 2.5 to 3.0 cycles.

Table of Contents

List of Tables

List of Figures

1. Introduction

This thesis concerns itself with the development of control systems which will reduce or avoid oscillations in a suspended payload transport system. In particular, the system for providing oscillation reduction or avoidance is focused on the Integrated Process Development (IPD) crane in use at the Oak Ridge National Laboratory (ORNL). The IPD crane is an industrial crane which actuates in x-y directions and lifts the payload by means of a cable lifting system. The goals of the solution are to avoid or reduce oscillation in the crane payload resulting from both operator input and other possible external disturbances and to concentrate on making the proposed solution cost effective to implement.

1.1 Motivation of the Problem

To provide motivation for the solution to oscillations in a suspended payload transport system, it is necessary to give a physical description of the crane and an example of its operation. The physical description will address the structure of the crane as well as the components that make up the existing drive and control systems. The description of operation will concentrate on a typical scenario and the operating problems encountered.

The IPD crane's physical structure consists of two major pieces: the bridge and the trolley. The bridge spans the width of the area of operation for the crane.

The bridge moves along tracks near the ceiling of the crane's operating area. The trolley resembles a car moving along the bridge unit. The trolley carries the wench for the cable lifting system back and forth along the bridge. Together, the bridge and trolley provide perpendicular axes of motion for the cable lifting system.

The motion of the bridge and trolley is provided by AC induction motors. There are two primary reasons for using AC motors. First, power for AC motor operation is typically directly available as part of the building's electrical distribution system. On the other hand, DC motors require additional power conversion to make necessary operating power available. The second reason for using AC motors is that they do not use comutating brushes, which are necessary in DC motors. Therefore, AC motors require less periodic maintenance than is normally associated with changing DC motor brushes.

Control for the crane is provided by a control pendant. The control pendant consists of four buttons for actuating the bridge and the trolley in their available directions. Also, the pendant has buttons for raising and lowering the payload as well as any other buttons or switches required for safety purposes. The buttons for controlling the motion of the bridge and trolley provide for single speed operation.

Given the physical description of the crane, it is next necessary to consider a typical scenario of operation and the problems encountered which contribute to oscillation of the payload. The scenario will address both the average and the experienced operator and suggest the more significant issues to be addressed by any proposed solution.

Typical operation of the crane takes place in four steps. The first step is to attach and lift the payload to a height that will avoid collision with other objects. The second step is to actuate the bridge and trolley to transport the payload to the desired end location. Third, the payload must be steadied. It is necessary to steady the payload in preparation for the fourth step, which is lowering the payload to a resting position. The steps in the moving process which contribute to the motivation for solution to the oscillation of payload are the point-to-point movement and the steadying of the payload. The point-to-point motion causes oscillation of the payload. Also, any contact of the payload with other objects during the point-to-point move will result in additional oscillations. Once the payload is near the final resting position, it is necessary to either physically steady the payload or to wait until the oscillations have been sufficiently reduced by the natural damping of the cable system. Steadying of the payload is necessary to allow the payload to be lowered safely into position.

Operator skill plays a role in the amount of oscillation induced in the payload as a result of crane operation. A technique which can result in reduced payload oscillation is called "jogging" the crane. Jogging the crane consists of the operator momentarily depressing and releasing the button to start motion in a desired direction. Then at a point in time equal to half the period of oscillation for the payload, the operator depresses the same button to provide constant motion. A similar sequence of operator commands is carried out when the payload reaches the desired end position. The operator releases the motion button and then, at a time equal to half the period of payload oscillation, depresses the reverse direction button. If the jogging technique is employed by an experienced operator, it can result in no noticeable residual oscillation of the payload. However, the jogging technique is not easily mastered. Most operators do not successfully employ the technique, and those who do are not able to employ it at all possible payload elevations.

The key concepts to be considered based on the typical operating scenario are (1) the need to avoid or reduce the oscillation resulting from operator input to allow less experienced operators to work more efficiently, and (2) to provide a means to damp oscillations of the payload which may result from collision of the payload with other objects. Successful solution of both of these problems would result in a more useful crane system.

1.2 Focus of Thesis

This thesis proposes to evaluate the alternatives for avoiding or reducing oscillations of the payload for the IPD crane system resulting from operator input and external disturbances. The solutions to the problems of input shaping to avoid oscillation and closed-loop control to reduce oscillations will be examined separately because the oscillations resulting from operator input may be characterized as unwanted commands which introduce oscillation in the crane system. Conversely, system sensors will be required to detect oscillations caused by external sources, thereby allowing the externally induced oscillations to be damped.

The approach to reducing oscillations resulting from operator input will focus on techniques of input shaping. Input shaping techniques are essentially the application of a filter to operator inputs to eliminate or reduce causes of system oscillation. This may either employ removal of unwanted signals or the alternation of signals to conform with a known profile which will reduce payload oscillations. Previous work in these areas will be examined and a solution proposed.

Reduction of oscillations caused by external disturbance of the system will require the use of a feedback control system. This thesis will examine the use of an inclinometer as the feedback sensor providing necessary feedback. Both the feedback control system and the input shaping system will be designed with attention to their operating together as a part of the overall crane control system.

Finally, the proposed solutions will be evaluated with regard to the cost to an industrial crane manufacturer. This includes the selection of components to operate with an AC induction motor driven system requiring the minimum in alterations to existing crane designs. The controller itself also must be realizable without significantly affecting the space requirements for the crane or without unduly affecting the ability of the crane operator to use the crane effectively.

2. Review of Literature

The field of vibration reduction through input shaping has concentrated on two main approaches: impulse sequences and acceleration profiles, and notch filtering based on frequency-domain filtering. The overall approach for both has been to avoid oscillation in a system by modifying operator input to avoid exciting the system's modes of vibration. The impulse sequence and acceleration profile techniques are time-domain solutions; frequency-domain filters, as the name implies, are designed and specified in the frequency domain. In each case the singular criterion sought for all has been to reduce residual vibration while providing acceptable controllability for the operator.

2.1 Time-Domain Filtering

The development of the impulse sequence solution to oscillation avoidance has concentrated on the analysis and testing of filters based upon convolving user input with a sequence of impulses designed to cancel residual vibration. Except for the approach of using acausal filtering, each new development in the area of impulse sequences has been a refinement of first the technique for deriving the impulse sequence and second improving efficiency of design. All of these enhancements to the impulse sequence technique have been experimentally verified by computer simulation and by implementation in actual systems.

2.1.1 Acausal Filtering

Initial work on the problem of input shaping and vibration reduction were addressed in the paper by Singer and Seering [1], which took the approach of acausal filtering to adjust command inputs. The technique requires a priori trajectory specification. The inputs required to accomplish the desired trajectory are then convolved with a notch filter designed to eliminate frequencies that may excite the device's vibrational modes. The frequency based notch filter was selected because of the computational constraints. A finite-impulse response (FIR) filter design could have been used; however, the specific requirements of the project addressed would have, according to the authors, required a one thousand point FIR. An advantage of taking this approach is that because the filter is acausal, it can be designed with a phase shift of zero.

The final filter was tested using a simulation model of the Space Shuttle Remote Manipulator Systems developed by Draper Laboratories for NASA. These tests indicated reduction in residual vibration by a factor of four. However, the requirement that the desired trajectory be generated a priori limits the ability of this technique to operate as part of an interactive control system.

2.1.2 Impulse Sequence

The next step in the development of preshaping by impulse sequence was also generated by Singer and Seering [2]. The approach had as its goals the use of the system's natural tendency to vibrate to cancel residual vibration, treatment of the transient residual vibration as a function of its transient input, modification of the input to include insensitivity to uncertainties, and examination of the case of arbitrary system inputs. The proposed technique is based upon the fact that an uncoupled, linear, vibratory system of any order may be specified as a system of cascaded second order poles with a decaying sinusoidal response. The authors proceed to solve for a series of two impulses that will result in no residual vibration. The solution is based on equation 2.1, where A_j is the amplitude of the jth impulse, t_j is the time of the jth

$$\begin{aligned} \sum_{j=1}^{N} A_j e^{-\zeta\omega(t_N - t_j)} \sin(t_j \omega \sqrt{1-\zeta^2}) &= 0 \\ \sum_{j=1}^{N} A_j e^{-\zeta\omega(t_N - t_j)} \cos(t_j \omega \sqrt{1-\zeta^2}) &= 0 \end{aligned} \tag{2.1}$$

impulse, t_N is the time at which the sequence ends, ω is the undamped natural frequency, ζ is the damping ratio of the plant, and N is the number of impulses. The solution of the equations resulted in the impulse train illustrated in figure 2.1, which is a finite impulse response (FIR) filter. The two-impulse input was only able to maintain residual vibration under 5% for a deviation in system frequency of ±5% of the design frequency.

The robustness of the two-impulse input solution, improved upon by solving for three impulses, was achieved by including the derivatives with respect to frequency, ω, of equation 2.1. The resulting impulse sequence is illustrated in figure 2.2. This sequence maintains less than 5% residual vibration for system frequency variations of ±20%. Following the same techniques, other impulse sequences may be derived. The technique also may be extended to include higher modes of vibration. Essentially, the system is solved for a set of impulses that eliminate each successive

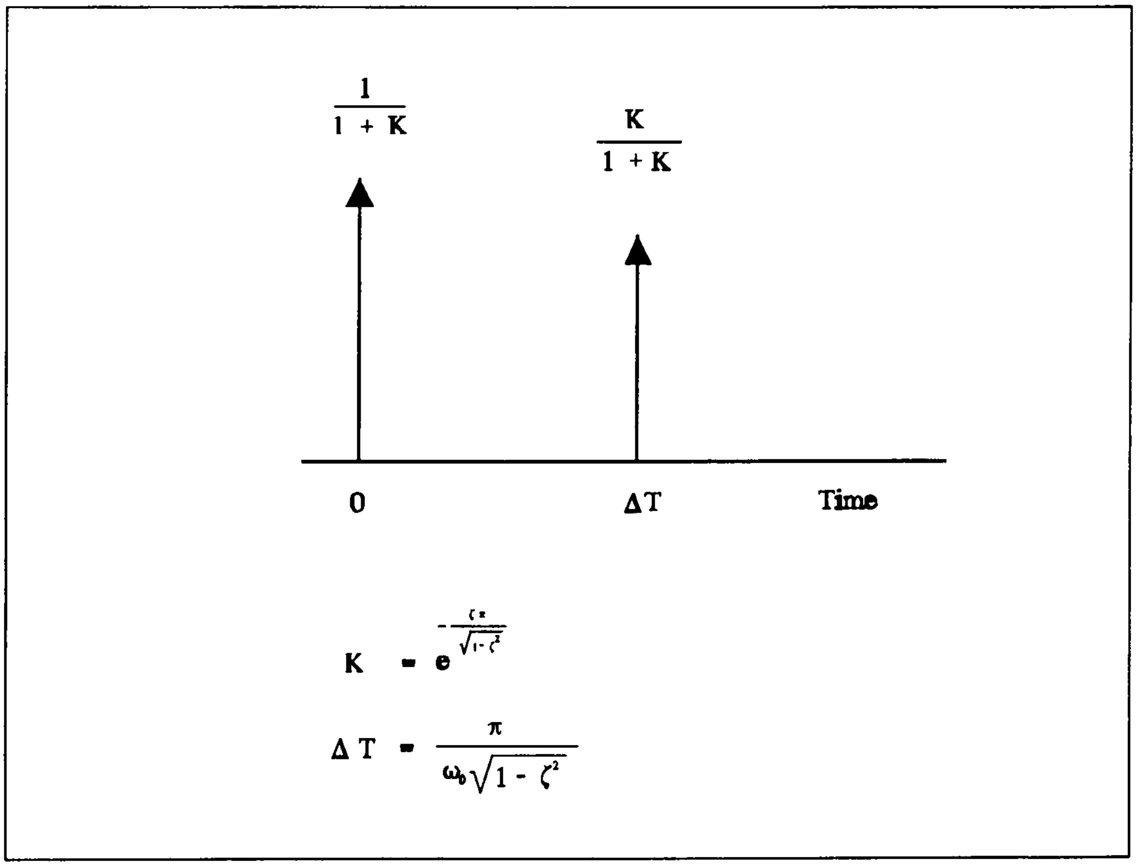

Figure 2.1: *Two impulse sequence derived from equation 2.1.*

mode to be considered. Simultaneous solution of all the equations results in a series of impulses that will cancel all the vibrational modes addressed, but with less duration than would be required if the separate sets of impulses were simply convolved together to create the single sequence.

The results of this work were tested on a computer model of the Space Shuttle Remote Manipulator System developed by Draper Laboratories. Residual vibration was shown to be reduced by a factor of 25 for the unloaded shuttle arm. Delay in input to output was on the order of one half cycle of vibration for the lowest mode used to develop the filter.

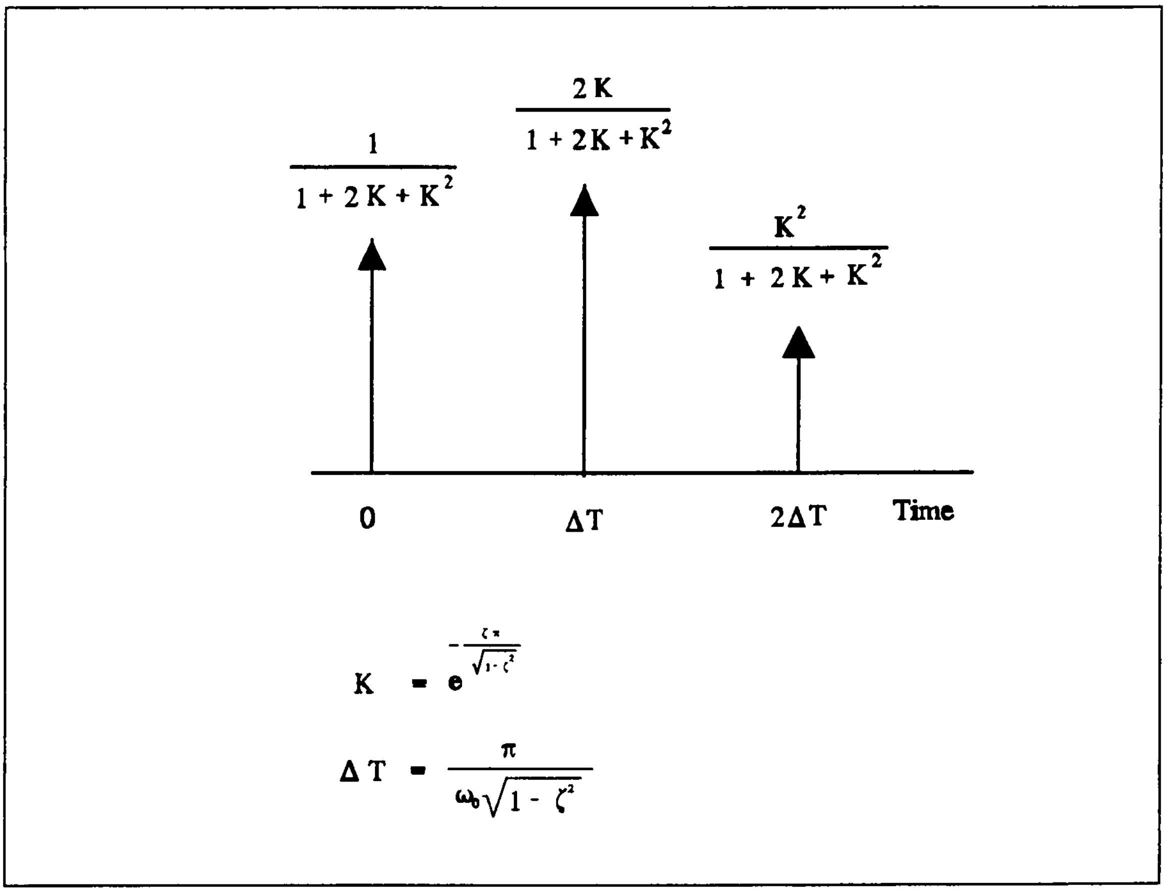

Figure 2.2: *Three impulse sequence.*

Following the derivation of the impulse sequence method, Singer and Seering compared their technique to other filtering techniques [3]. As previously mentioned, the three-impulse filtering technique is an FIR filter. It can be considered a notch filter in a frequency domain. The criteria for evaluation were the duration of the impulse response, residual vibration, and robustness to uncertainties. The other filters considered were ideal lowpass, FIR lowpass using a Hamming window with a duration of 5 periods, an FIR Parks-McClellan filter consisting of 256 points over one period, an infinite impulse response (IIR) Butterworth filter, an IIR Chebyshev filter, an IIR elliptic filter, a Hamming window notch filter, and a Parks-McClellan notch filter of 256 points over one period. Of those tested, the Parks-McClellan notch filter came closest in performance to the three-impulse filter. Singer and Seering concluded that frequency-domain filter techniques were less effective for shaping vibration-reducing inputs to systems.

In 1990 Singhose, Seering, and Singer [4] addressed design of impulse sequence filters by using a vector diagram approach. By letting ω of the diagram equal the natural frequency of the system and placing the initial impulse at $t = 0$, residual vibration in the system may be shown to be proportional to the magnitude of the resultant vector for the diagram. The representation of the correspondence between an impulse sequence and the associated vector diagram is illustrated in figure 2.3. This technique allows any arbitrary number of impulses to be canceled by adding one additional vector, which causes the resultant to equal zero. Following this design technique, the authors show that shifting the position of the impulses results in shifting the response from the design model frequency. Assuming that residual vibration of less than 5% is considered acceptable, this allows design of a filter which is more robust to variations in frequency than previous techniques had produced.

Returning to the application of impulse-based filters to multiple-mode systems, Hyde and Seering [5] documented a technique for solving for multiple modes simultaneously. The solution for a single-mode system was developed to create a three-impulse filter. Additional modes were addressed by solving for all modes as opposed to combining individual impulse sequences by convolution. The solution is achieved by selecting a time for the sequence's final impulse and then dividing the

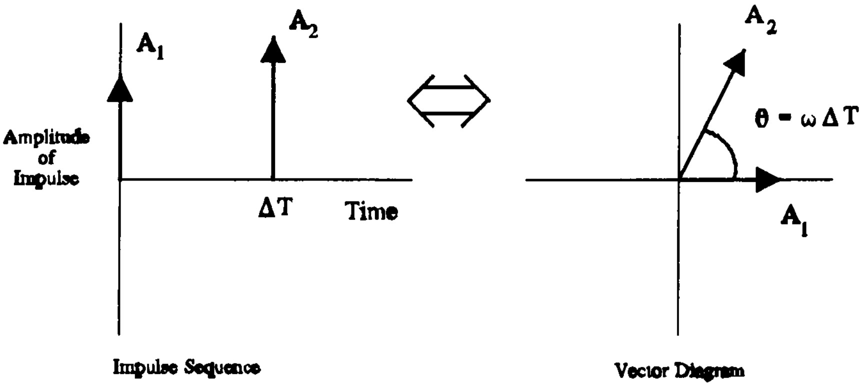

Figure 2.3: *Impulse sequence versus vector diagram.*

length into a fine time mesh. An impulse with unknown amplitude was then placed at each time slot. An optimization software package was then used to generate an impulse train with less than $(4 * M) + 1$ impulses, where M is the number of vibrational modes of the system. The result of this optimization was then processed using Mathematica to further reduce the number of impulses. The results of this work were tested using a model of the Mid-deck Active Control Experiment (MACE), a flexible system jointly designed by MIT and NASA to study methods for controlling flexible systems. The shortcoming of this solution is the complexity of solving for the optimal impulse sequence. The successful solution is dependent upon the manner in which the system is specified.

Singer and Seering [6], in a 1992 paper, take an approach similar to that taken by Singhose and Seering [4]. The approach is to sample frequencies for a system in which the natural frequency changes. Given the range over which the frequency may vary, a solution is then obtained to improve response for the widest possible range of frequencies. The result is similar in appearance to the vector design approach outlined by Singhose [4] in that the response to residual vibration is made more broadly insensitive by placing impulses that are shifted to account for varied frequencies.

Most of the work on impulse sequences has been performed by Singer, Seering, and Singhose. All of this work has approached the problem of input preshaping as a matter of applying an FIR filter. Although the FIR filter has the advantage of a "crisper" performance, the convolution operation is more computationally intensive. The practical implications of this fact have not been an issue because most of the system verification and testing was performed in a simulation environment.

2.1.3 Acceleration Profile

The acceleration profile solution to input shaping is another time-domain technique which is essentially the same as impulse sequencing. Basically the approach is to develop an overall profile to avoid vibration. This does not necessarily involve constantly filtering user input so much as restricting user input to an acceptable profile. The work on this technique has been applied to both single and multiple mode systems. In both cases, the systems were actual hardware implementations.

The initial work from Jones and Petterson [7] in 1988 concentrates on oscillation reduction for a simple suspended payload. The system is modelled as a simple pendulum. The resulting equations were examined both as linear and nonlinear approximations. The authors illustrated that the linear approximation stayed with 1% for maximum amplitudes less than 20 degrees; the same error could be obtained by use of the nonlinear approximation for amplitudes of up to 70 degrees. This does not cause any concern for a suspended payload system because in practice, amplitudes would not normally exceed two degrees. The approach taken to reduce oscillations was to produce identical acceleration profiles separated by some interval, T, which would be derived based upon the resonant frequency of the device and the length of the acceleration input. The resulting profile is shown in figure 2.4. The system has a constant acceleration for time t_a. After time t_a the system moves at a constant velocity for time T. At time $(t_a + T)$ the system accelerates again for time t_a. T is selected such that the oscillation imposed on the system from the second acceleration is 180 degrees out of phase with those imposed by the first acceleration. For small angle deflections, the value T was found to be one half the period for the small angle. The concept was tested using a 50-pound weight suspended by an 80-inch cable. The period of the pendulum was measured to be 2.87 seconds. Although the theory indicates that there should be no residual vibration, actual results did show some vibration. This vibration was attributed to model inaccuracies and servo loop delays.

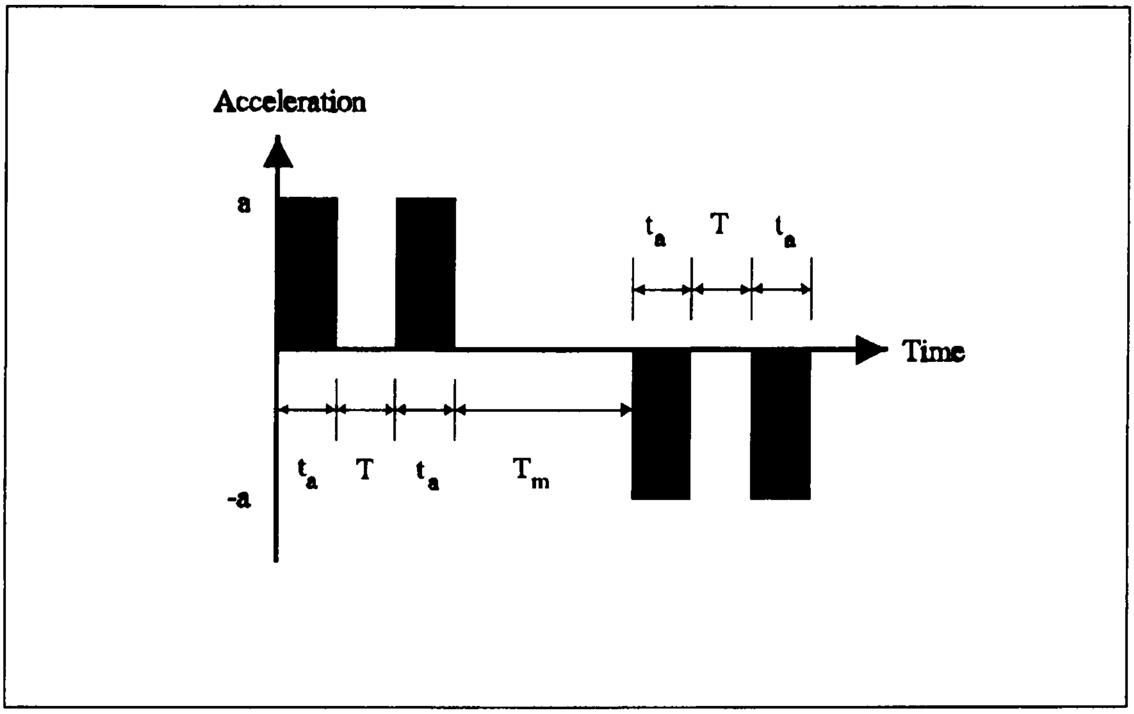

Figure 2.4: *Acceleration profile to eliminate residual vibration in a suspended payload.*

The above work was extended in Petterson, Robinett, and Werner [8] to the control of flexible rods. This technique differs from Singer's work in that it addresses strategy for damping the in- and out-of-plane oscillations in a coupled structure. This damping is accomplished by placing various masses at the tip of a flexible rod. A parameter-scheduled trajectory planner is then used which permits rapid movement of the rod while suppressing vibrations at the move endpoint.

Additional use of acceleration profiles was detailed in Noakes, Petterson, and Werner [9] as it applied to reduction of oscillations in the overhead crane transporter for the Advanced Integrated Maintenance System (AIMS) developed as an operations testbed for remote maintenance and handling studies by the Consolidated Fuel Reprocessing Program at ORNL. The original acceleration profile was changed to a constant acceleration with duration equal to half the period of the pendulum motion of the crane, followed by a constant velocity for travel. The actual implementation required updating the crane control hardware to allow for velocity control inputs. Extensive tests showed that residual swing of less than 0.5 inches was consistently obtained, permitting reduction in payload handling times.

In all cases the acceleration profile approach to vibration reduction showed acceptable results on actual hardware systems. The technique was applied to systems with a single mode of vibration—the small crane models and eventually the full size AIMS crane. Additionally, the technique was applied to a flexible arm which has multiple modes of vibration. The results of all these implementations was to reduce the residual vibration to less than 5% of maximum amplitude. The restriction, however, was on the allowable trajectories of movement.

2.2 Robust Notch Filter

Work by Noakes and Jansen [10] connected elements of Petterson's [7] and Singer's [2] work to address vibration reduction for the AIMS crane at ORNL. The system was modelled as a second-order oscillator where the natural frequency is known. The system will have damping, but it is unknown. It is then shown that a series of two impulses 180 degrees out of phase will result in no residual vibration. Convolving this impulse sequence with a desired acceleration command was then shown to be equivalent to the acceleration profile used by Noakes et al [9] in previous work on the AIMS crane.

Work presented by Jansen [11] further developed the frequency-domain filtering techniques for input shaping. The technique has similarities to the impulse sequence technique of Singer [2] and is outlined in the paper by Murphy and Watanabe [12] which illustrates the correlation between impulse sequence filters and frequency-domain filters. Beginning with the development of the two- and three-impulse sequence filters, Murphy [12] then transforms the filter to the Z-domain for analysis. Examination of the poles and zeroes of the filter in the Z-plane show that the impulse sequence filter simply places zeroes at the location of the vibratory system's poles. This essentially indicates that the impulse sequence is a notch filter in the discrete domain. Also, it is shown that robust insensitivity to residual vibration may be achieved by implementing successively higher order notch filters for input shaping. The author further develops a digital filter that provides the same performance while allowing arbitrary digital sampling rates.

The following sequence of equations demonstrates the effect of the two-impulse sequence and its response in the frequency domain. Starting with the time-domain equation for the two-impulse sequence

$$f(t) = \delta(t) + \delta\left(\tau - \frac{T}{2}\right). \tag{2.2}$$

Taking the Laplace transform, L, the equation becomes

$$L\left[\delta(t) + \delta\left(\tau - \frac{T}{2}\right)\right] = F(s) = 1 + e^{-\frac{T}{2}s}. \tag{2.3}$$

where

$$T = \frac{2\pi}{\omega_n}. \tag{2.4}$$

Substituting $s=j\omega_n$, the result is shown to have a value

$$F(s) = 1 + e^{-j\pi} = 0. \tag{2.5}$$

For the three impulse sequence, the time-domain equation is

$$f(t) = \delta(t) + \delta\left(\tau - \frac{T}{3}\right) + \delta\left(\tau - \frac{2T}{3}\right). \tag{2.6}$$

Taking the Laplace transform, the equation becomes

$$L[f(s)] = F(s) = 1 + e^{-\frac{T}{3}s} + e^{-\frac{2T}{3}s}. \tag{2.7}$$

Then, if $s = j\omega$, equation 2.8 becomes

$$F(s) = 1 + e^{-j\frac{2\pi}{3}} + e^{-j\frac{4\pi}{3}} = 0. \tag{2.8}$$

Following the fact that the impulse sequence filter is essentially a digital notch filter, Jansen [11] presented an implementation which improved on the robustness of the classical notch filter. The Robust Notch Filter (RNF) consists of two second-order notch filters and a lag filter. The frequency of the notch filters is set to the predicted harmonic frequency of the system. The effect of multiple notch filters is to broaden the insensitivity to system parameter variation as illustrated in figure 2.5. The similarity of this broadening effect to that of increasing the number of impulses in an impulse sequence, see figure 2.6, leads to the conclusion that both techniques place zeroes at the poles of the system.

2.3 Current Work

Extending the previous work at ORNL, it is desirable to generate the RNF solution primarily because of the ease with which frequency-domain filters are formulated and implemented on a computer. This has been previously applied to use with the IPD overhead crane. An RNF was used to provide operator input shaping to the crane. By setting the frequency of the RNF to the frequency corresponding to the maximum period of the crane, it has been shown that the RNF provides a simple and effective solution to vibration reduction.

Following from this open-loop solution to vibration reduction, this thesis shows the application of similar concepts to the solution of closed-loop vibration control. The techniques discussed to this point have been applied as an open-loop solution to system vibration. Although it has been suggested that the techniques may be applied to closed-loop implementation [1], the literature has not at this point reflected any such application. This thesis examines the characteristics of the IPD suspended payload transport system to identify possible techniques for eliminating vibration

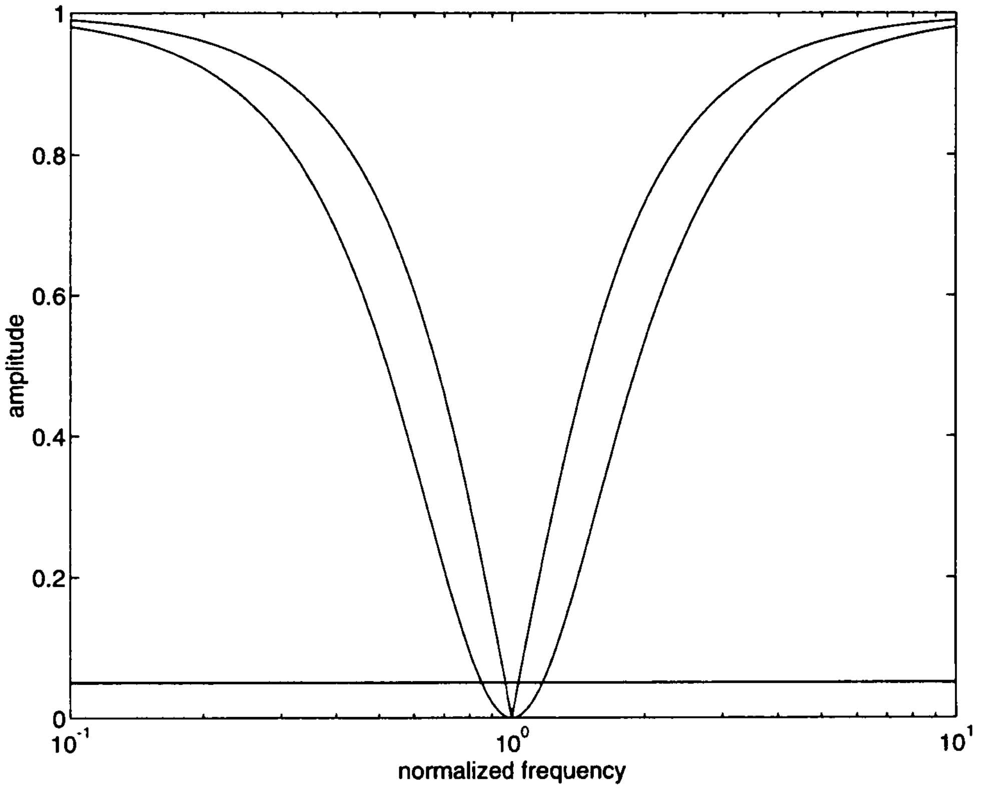

Figure 2.5: *Comparison of single and double second-order notch filters.*

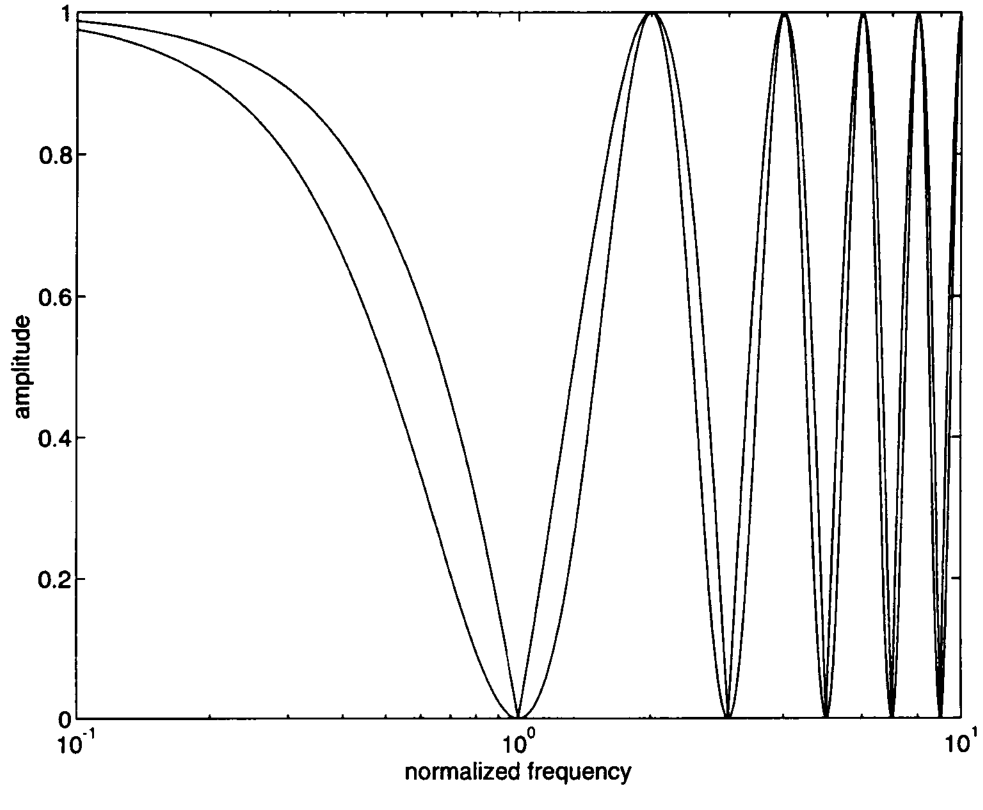

Figure 2.6: *Comparison of two and three impulse sequence input filters.*

induced by perturbations from sources other than the command input.

Given the requirements of actual hardware implementation as well as concern with the cost and effectiveness of transferring the solution to industry, the RNF seems the most likely candidate for the input-shaping implementation. Also, given that the RNF is formulated as a frequency-domain filter, efforts to derive a closed-loop solution to vibration damping will be directed toward frequency-domain control system analysis.

3. Analytic Models

In this section, models will be derived and justified for use in providing a solution to the problem of vibration damping for the IPD crane. In particular, it will be essential to develop models for the crane, the motor drive system, and the inclinometers. Linear models will be acceptable for analysis of the system because only small perturbations of the system will be encountered. The linear models developed will be for analysis in the s domain. Also, possible inaccuracies in the models will be identified for consideration during the design process. Finally, the discrete equivalents will be presented in preparation for their use during time simulations to predict system performance.

3.1 Crane Model

The first step in specifying the model for the IPD crane is to determine the significance of motion from movement as a two degree-of-freedom manipulator. It can be shown [11] that the general formulation for the continuous undamped distributive parameter system can be transformed to the set of infinite, uncoupled, ordinary differential equations:

$$\ddot{x} + w_i^2 x_i = f_i(t) \quad i = 1,2,3,\dots \,, \tag{3.1}$$

where x_i = i[th] generalized coordinate, w_i = i[th] eigenfunction associated with the problem, and f_i is the force. This may further be converted into state- variable form as shown in equation 3.2.

$$\frac{d}{dt}\begin{bmatrix} x_0 \\ \dot{x}_0 \\ x_1 \\ \dot{x}_1 \\ \vdots \\ \dot{x}_n \end{bmatrix} = \begin{bmatrix} 0 & 1 & & & & \\ -\omega^{2}_0 & -2\zeta_0\omega_0 & & & & \\ & & 0 & 1 & & \\ & & -\omega^{2}_1 & -2\zeta_1\omega_1 & & \\ & & & & \ddots & \\ & & & & -\omega^{2}_n & -2\zeta_n\omega_n \end{bmatrix} \begin{bmatrix} x_0 \\ \dot{x}_0 \\ x_1 \\ \dot{x}_1 \\ \vdots \\ \dot{x}_n \end{bmatrix} + \begin{bmatrix} 0 \\ f_1(t) \\ 0 \\ f_2(t) \\ \vdots \\ f_n(t) \end{bmatrix} \tag{3.2}$$

This may done by the usual approximation of truncating the series to include n modes by including damping terms ζ_i. For the specific problem of the IPD crane, the eigenvalues associated with the state variable form are distinct, which means that a complete set of eigenvectors, $\bar{v}_i$, can be found such that equation 3.3 can be transformed into the standard uncoupled canonical form:

$$\dot{\bar{z}} = D\bar{z} + \bar{u}, \tag{3.3}$$

where

$$\begin{aligned} \bar{x} &= T\bar{z}, \\ D &= diag\ (p_i), \\ \bar{u} &= T^{-1}\bar{f}, \\ T &= [\bar{v}_i] \end{aligned} \tag{3.4}$$

The implication of this is that each degree of freedom may be considered separately when developing analytical models. This will permit the solution to be formulated for the single-axis pendulum.

Using figure 3.1, the linear approximation to a pendulum modeled as a simple second-order undamped oscillator may be expressed as:

$$\ddot{\theta} + \frac{g}{l}\theta = -\frac{\ddot{x}_t}{l} \,. \tag{3.5}$$

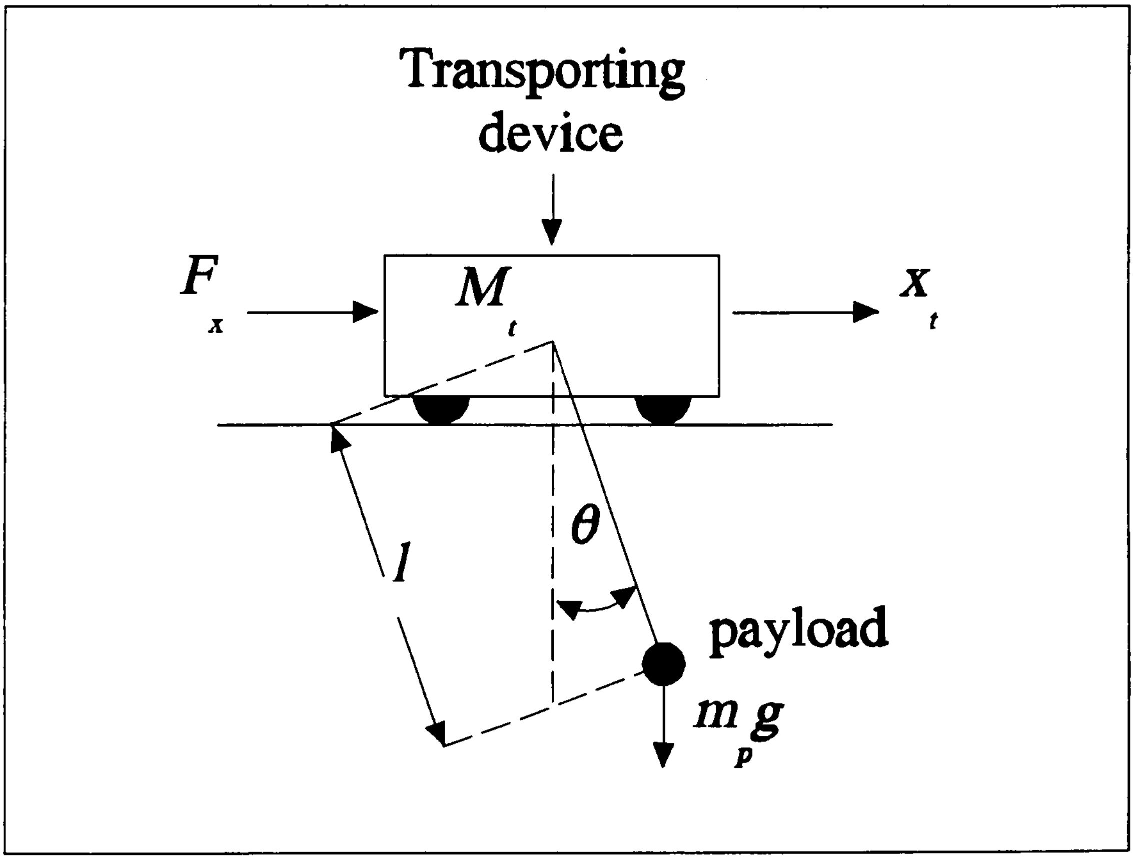

Figure 3.1: *Single axis pendulum model: suspended payload transport system.*

The parameters are as shown in figure 3.1 where θ is the angle of the cable, g is the gravitational constant, x_t is the position of the transport device, and l is the length of the cable to the center of mass for the payload and cable. The form of the model is based on the assumptions that the mass of the transport device, M, is much greater than the mass of the payload, m, and that the mass of the payload is sufficient to locate that overall center of mass for the pendulum at or near the payload. Also, for this linear approximation to remain acceptable, the angle θ must be small such that $sin(\theta) \equiv \theta$. This assumption may be made because the maximum speed of the crane transport device has been limited to constrain the potential amplitude of vibration. Taking the Laplace transform of the pendulum equation and setting the initial conditions to zero, the s domain transfer function would be:

$$G_\theta(s) = \frac{\theta}{\dot{x}} = \frac{-\frac{1}{g}s}{\frac{s^2}{\omega^2_p} + 1} . \tag{3.6}$$

It may be noted that this equation for the crane as a pendulum contains no damping. Although the actual crane will have some amount of damping, it is assumed that the proposed design will be sufficiently robust to compensate for uncertainty in the damping and system frequency.

3.2 Vector Drive Model

The transport devices for the IPD crane are powered by AC motors. The devices used to control these motors, variable frequency drives (referred to as vector drives), have been installed to permit better speed control of the motors than is normally available through the AC induction motors provided by the crane manufacturer. The motor drive system used on the crane accepts a velocity signal command. Therefore, change in the input voltage results in a velocity component for the crane transport device. This is the reason for the pendulum equation being formulated as the output angle over the transport device velocity.

For the purposes of this problem, the control provided by the vector drives provide for modeling them as a simple DC amplifier and a low-pass filter. Its associated s domain transfer function is

$$G_v(s) = \frac{\dot{X}}{V_c} = \frac{K_v}{\dfrac{s}{\omega_v} + 1}. \tag{3.7}$$

By observing the time required to respond to a step input command, the frequency response was estimated to be between 0.5 and 1.0 Hz. This was done using the observed, estimated rise time, t_r, and equation 3.8 [13].

$$f_0 \approx \frac{0.35}{t_r} \tag{3.8}$$

The result of the above information is a vector drive transfer function which will provide an approximate model for the controller design phase of this thesis. The unknown aspects of this model include the possible range of values for frequency response, which varies from 0.5 to 1 Hz., the exact velocity output per volt of input, and to a lesser degree, the assumption that the amplifier may be treated as a first order low-pass filter.

3.3 Inclinometer Model

The sensor provided for use on this project is an inclinometer. In general, these devices return a voltage which corresponds to the incline angle of an object to which they are attached. Typically, the inclinometer only responds to a single-axis of motion. This is important to the premise that the system may be modeled and a solution derived based on the single-axis of motion models. To arrive at a model it was necessary to begin with a generic model for inclinometers and then resolve particulars of the actual devices by testing.

3.3.1 General Model

The general model for an inclinometer was taken from Doebelin's [14] description for pendulous (gravity-referenced) angular-displacement sensors. The configuration used by Doebelin does not apply to all possible types of sensors, but it is sufficiently representative to provide the basis model for analysis. Doebelin [14] states that the model for this sensor holds for conditions in which the angular displacement is small such that the sine of the angle is approximately equal to the angle measurement, which is true for the problem being addressed in this thesis. The general transfer function for the inclinometer is

$$\frac{e_o}{\theta_c}(s) = \frac{K_i\left(\dfrac{s^2}{\omega_1^2} + 1\right)}{\dfrac{s^2}{\omega_2^2} + \dfrac{2\zeta s}{\omega_2} + 1}\,, \tag{3.9}$$

where e_o is the voltage signal out, θ_c is the angular displacement of the device, K_i is the DC gain constant, and ω_1 and ω_2 are zero and pole frequencies that specify the frequency response of the device.

Another characteristic of the inclinometer which deserves consideration is its susceptibility to linear acceleration effects. Doebelin [14] states that a steady horizontal acceleration, A_x will cause an output voltage KA_x/g for the general sensor model which incorporates no springs. For the application as a sensing device for the crane payload's angular displacement, it is necessary to consider two possible sources of acceleration: the linear acceleration of the transport device and the tangential component of acceleration for the payload resulting from angular displacement. The effects of linear acceleration on the inclinometer will be similar to those already stated for the crane as a pendulum, the exception being that the inclinometer will include a damping coefficient. The transfer function for the linear acceleration effects is shown in equation 3.10.

$$H_L(s) = \frac{e_o}{\dot{x}_t}(s) = \frac{\dfrac{K_i\, s}{g}}{\dfrac{s^2}{\omega^2_2} + \dfrac{2\zeta_i s}{\omega_2} + 1} \qquad \textbf{(3.10)}$$

The constant K_i and the frequency ω_2 are the same as those for the base inclinometer model. From this assumption, the tangential acceleration is given in equation 3.11.

$$\begin{aligned} \ddot{x}_t &= \frac{\ddot{\theta} l}{g} \qquad given \quad \omega_{ph} = \sqrt{\frac{g}{l}} \\ \ddot{x}_t &= \frac{\ddot{\theta}}{\omega_{ph}} \end{aligned} \qquad \textbf{(3.11)}$$

Given the term for tangential acceleration, the transfer function for the tangential acceleration effects on the inclinometer are given in equation 3.12.

$$\frac{e_o}{\theta_c} = \frac{\dfrac{K_i\, s^2}{\omega^2_{ph}}}{\dfrac{s^2}{\omega^2_2} + \dfrac{2\zeta_i}{\omega_2} s + 1} \qquad \textbf{(3.12)}$$

The three transfer functions given compose the complete description for the inclinometer and corresponding effects. These equations represent the general model for inclinometers and have incorporated the anticipated effects that will alter the ideal output of the device.

3.3.2 Determination of Parameters

Considering that the models proposed for the inclinometers apply to the general case, it is necessary to test the actual devices to determine if the salient features of the models are correct and to find values for the parameters. The parameters which must be determined are: K_i, the DC gain, ω_1 and ω_2, the frequency components, and ζ_i, the damping coefficient. This determination will be achieved by first considering the manufacturer data sheets and then collecting and analyzing test data.

The inclinometers provided for this project are Columbia Research Laboratories, Inc., model SI-701-BI. Detail specifications are provided in the appendix. The inclinometers are indicated to have an output range of ± 1 volt for angles of ± 15 degrees. Frequency response data sheets, provided by the manufacturer, indicate a 3 db point of approximately 3 Hz. with a -18 db per octave roll off. This would seem to indicate that one of the frequency components would be located near 3 Hz. Given this information, it was desirable to create a test environment to collect data and estimate the actual model parameters.

A test stand was constructed as shown in figure 3.2. The operation of the test stand involves starting the pendulum at an angle greater than 15 degrees. Then, as the

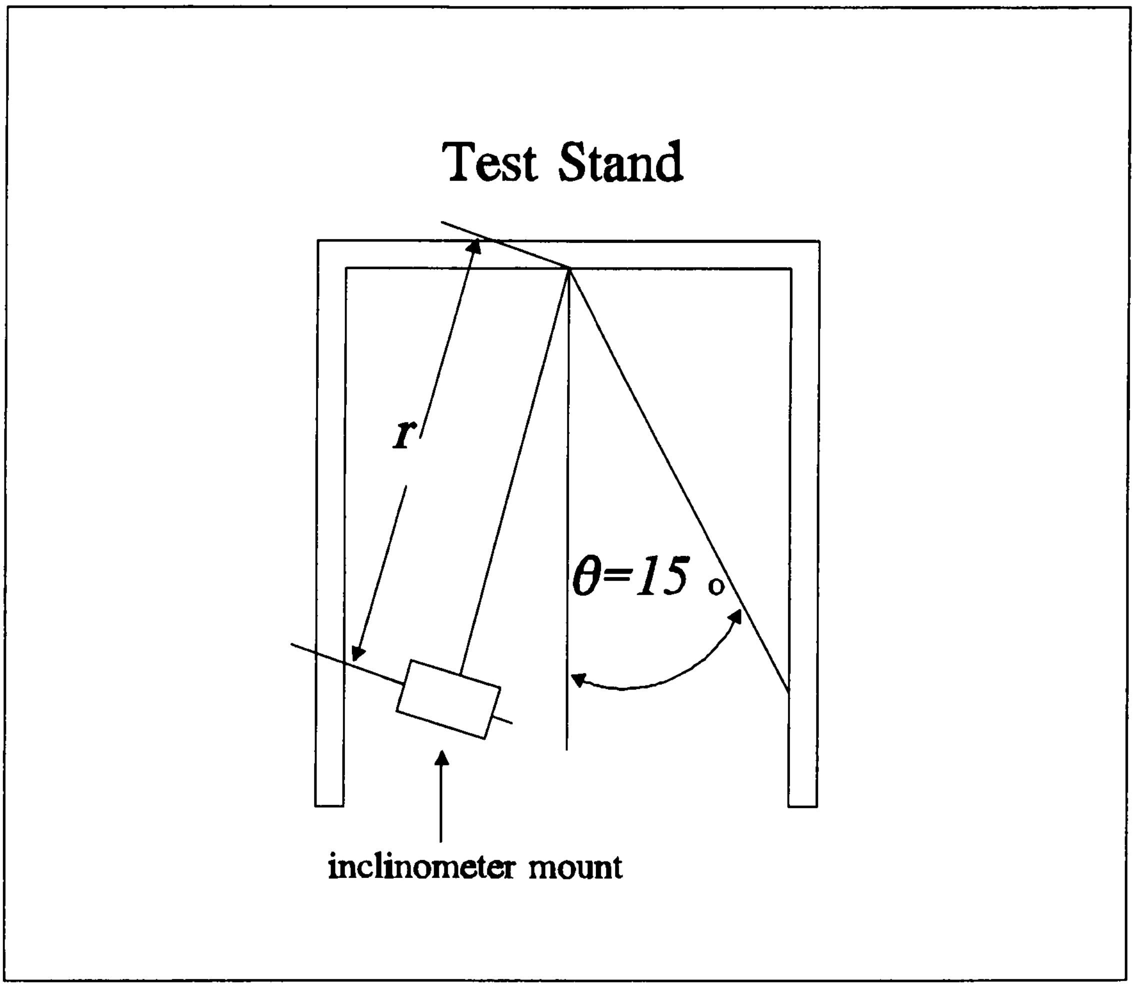

Figure 3.2: *Inclinometer Test Stand.*

amplitude decays to a point measured as being 15 degrees, the period will be estimated by taking multiple readings, while the amplitude of the output signal was recorded by a computer using a 12 bit analog to digital convertor, taking 800 samples at a sampling rate of 50 Hz. In addition, the distance to the location of the inclinometer from the pivot point was measured. These readings provide the period, amplitude, and distance for determination of the tangential acceleration.

The analysis of the collected data is based on the combination of the three transfer functions describing the inclinometer. Because the test stand does not produce any linear acceleration from movement of the pivot point, the term for linear acceleration will be zero. The combination of the other two transfer functions is shown in equation 3.13.

$$H_\theta(s) = \frac{E_o}{\Theta} = \frac{\left[K_i\left(\frac{1}{\omega^2_{ph}} + \frac{1}{\omega^2_1}\right)s^2 + 1\right]}{\frac{s^2}{\omega^2_2} + \frac{2\zeta_i}{\omega_2} + 1} \qquad \textbf{(3.13)}$$

Because information about the phase of the device at the time that any particular amplitude is read is unavailable, it will be necessary to take the magnitude of equation 3.13. This results in

$$|E_o| = \frac{\left|1 - \omega^2 K_i\left(\frac{1}{\omega^2_{ph}} + \frac{1}{\omega^2_1}\right)\right|}{\sqrt{\left(1 + \frac{\omega^2}{\omega^2_2}\right)^2 + \left(\frac{2\zeta_i\omega}{\omega_2}\right)^2}} \ . \qquad \textbf{(3.14)}$$

From the magnitude equation, the test data shown in table 3.1 was analyzed using the Matlab® fmins function, which performs optimization of a multivariable function using a simplex method. The actual samples taken by the analog to digital converter are pictured in figures 3.3 to 3.6. Of particular interest is the noise which is present. The noise has the most effect on the low frequency samples because of the limited amplitude of the inclinometer signal. The period value, listed in the table, is measured in seconds. The counts listed are the output counts from a 12-bit analog to

Table 3.1: *Inclinometer test data.*

Period (sec.)	Max. Counts	Min. Counts	Radius(in.)	Amplification
2.44	2384	1728	59.250	20
2.42	2448	1808	58.000	20
2.35	2448	2064	54.375	20
2.33	2432	1808	52.750	20
2.25	2352	1728	50.500	20
2.25	2320	1888	47.750	20
2.20	2384	1984	47.250	20
2.07	2272	1872	42.875	20
2.03	2352	1872	40.375	20
1.97	2496	1776	35.875	20
1.95	2448	1760	36.625	20
1.93	2448	1616	34.500	20
1.89	2512	1568	33.250	20
1.84	2544	1408	31.875	20
1.80	2800	1280	28.875	20
1.73	3328	848	24.000	20
1.50	4080	0	18.625	20
1.30	2384	1888	16.875	10
1.15	2512	1728	13.000	10
0.95	2864	1184	8.500	10
0.87	3440	576	6.125	10

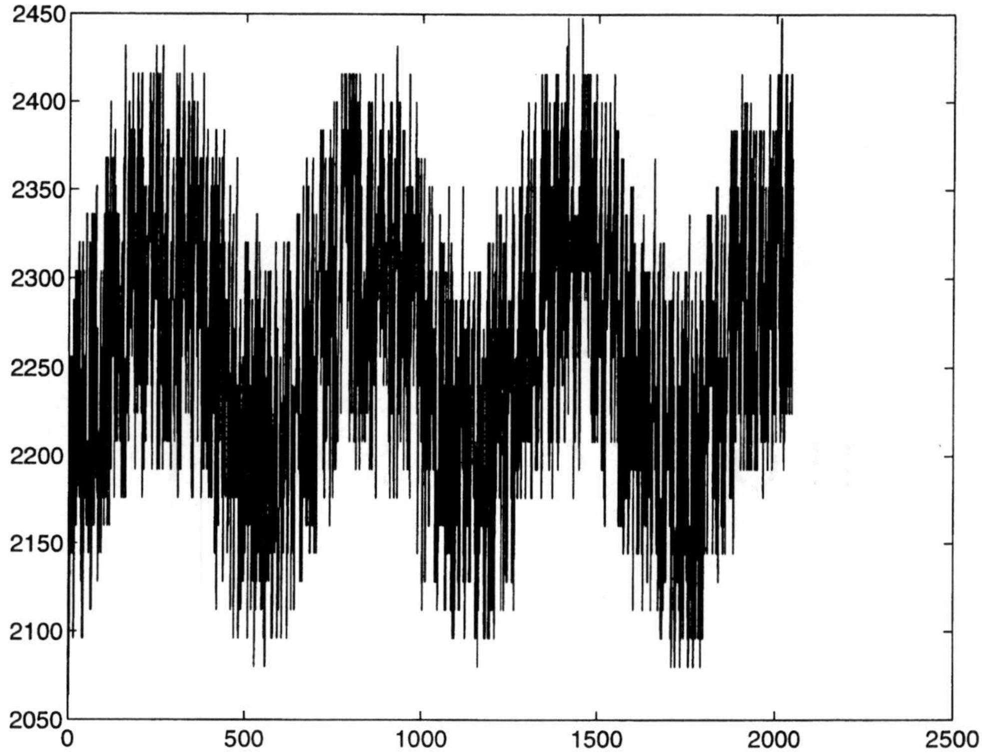

Figure 3.3: *Inclinometer Sample Data 0.41 Hz.*

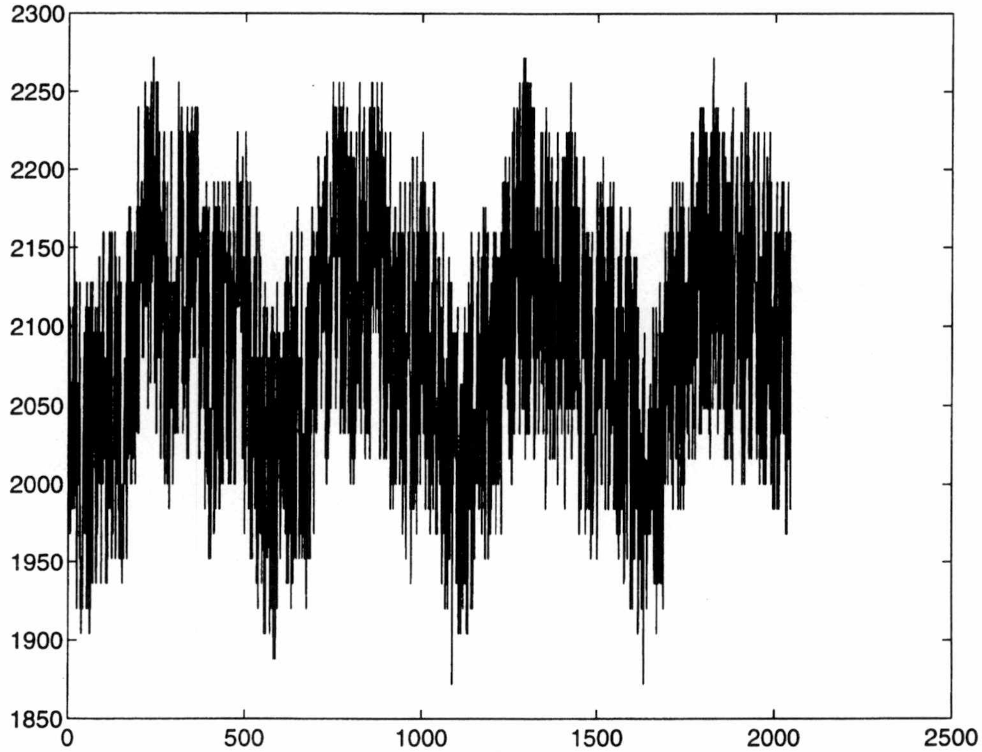

Figure 3.4: *Inclinometer Sample Data 0.44 Hz.*

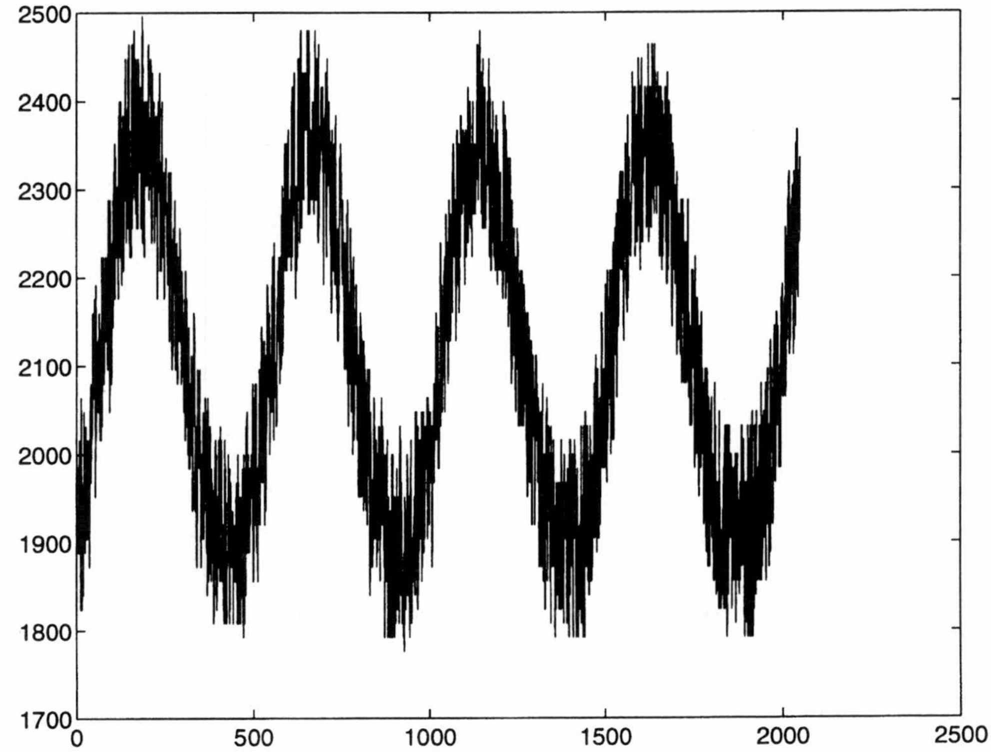

Figure 3.5: *Inclinometer Sample Data, 0.55 Hz.*

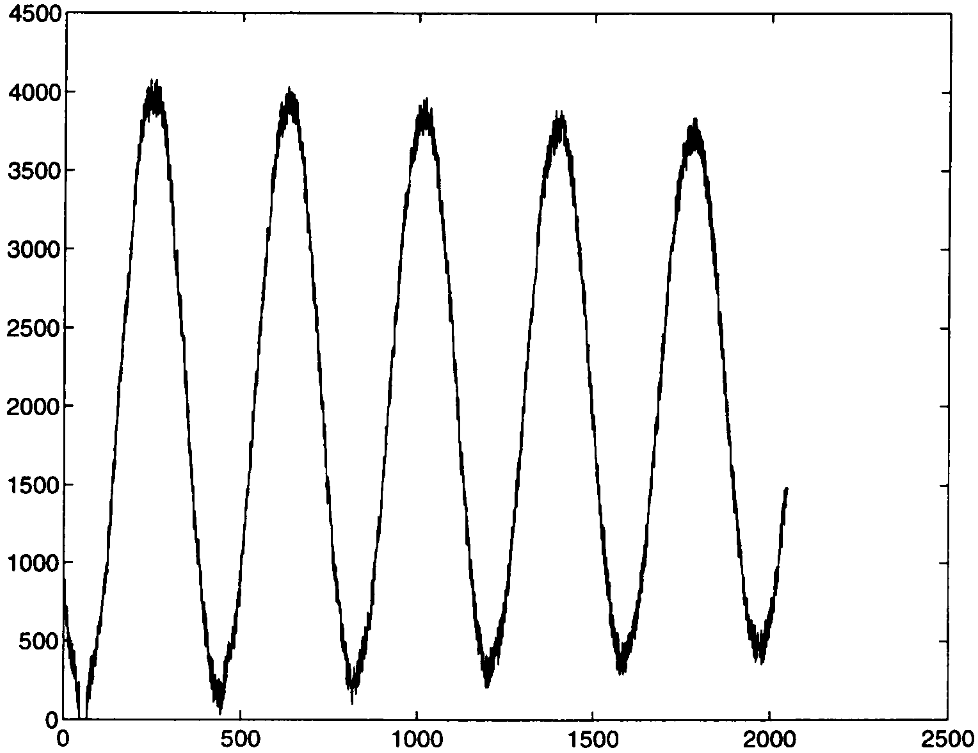

Figure 3.6: *Inclinometer Sample Data, 1.05 Hz.*

digital convertor that ranges over ±5 volts. The radius listed was measured in inches from the pivot point to the location of the inclinometer and was used to calculate the value for ω to provide the value for the input to the system. Finally, the amplification column designates the relative amplification performed by the test equipment to enhance the range of readings.

The results of the Matlab optimization are shown in figure 3.7. The individual data points are shown using the '+' symbol; the calculated values obtained using the parameters estimated are shown as a continuous line. The values obtained are as follows:

ω_l = 4.82052 Hz.

ω_2 = 1.0226 Hz.

K_i = 0.812229

$\zeta_i = 2.0707 \times 10^{-6}$.

Evaluating this data against the information provided by the manufacturer's data sheet highlights three points of difference. The first is the value for ω_l, which is suggested as being 3 Hz. based on the –3 db point specified. The test data indicates a value almost 60% percent higher. This difference may possibly be attributed to the sharp discontinuity in the test data, which is apparent from viewing the plot. This change took place when the test pendulum was replaced with one of shorter overall length to accommodate testing for higher input frequencies. The overall trend was the same, but it provided a sharp decrease in the amplitude values. Second, the –18 db roll-off specified by the manufacturer would indicate a third order pole in the inclinometer

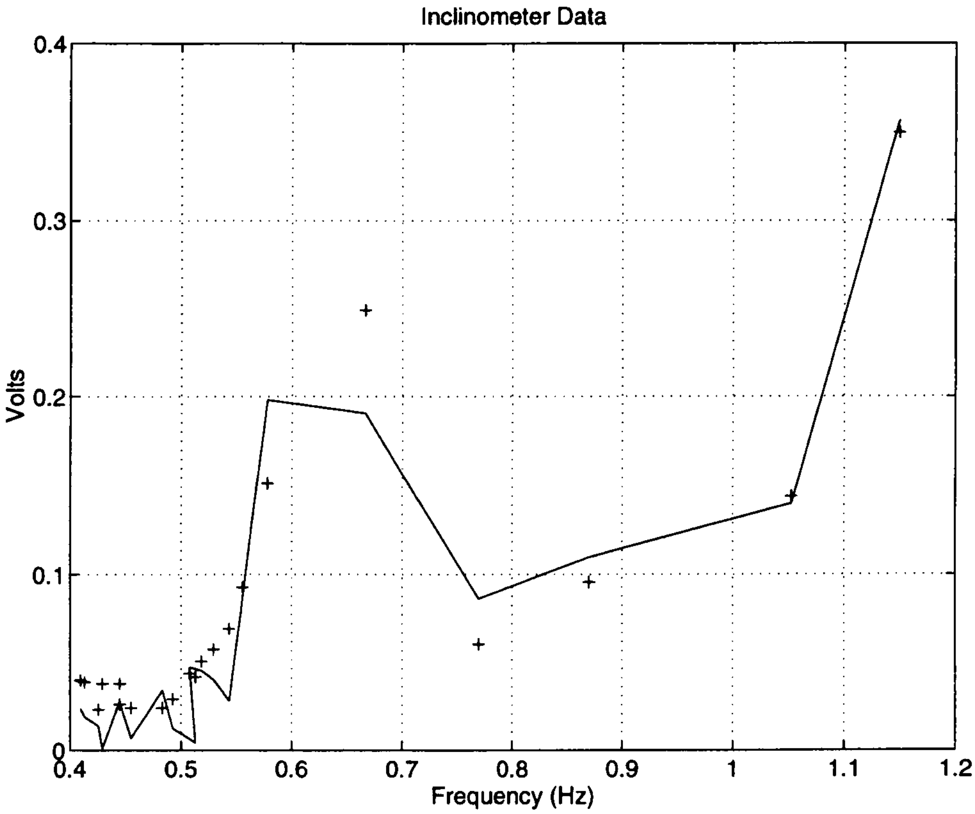

Figure 3.7: *Results of Data Fit for inclinometer, (+) represents sample data, (-) represents values generated with calculated parameters.*

transfer function. It is possible that this difference may be accounted for by the electronic components within the inclinometer. If a simple amplifier is used, it would typically add a first order pole to the transfer function. Finally, the value for the DC gain, K_i, should be close to 1 according to the manufacturer's specifications. The approximate 20% error in that value may be the result of noise on the test data or inaccuracies in the test stand such that the actual angle at which the readings were taken differed from the desired 15 degree.

The values obtained by testing the inclinometer do confirm the agreement between salient features of the theoretical model and the actual device. The close approximation to the sample data by the calculated parameters confirms that the form of the model is correct. Of primary consideration during the design phase will be the DC gain component and the ω_2 values. The DC gain will affect the scaling of the compensator gain during the closed-loop design. The value for ω_2 will be of concern because it is located closest to the range of frequencies which comprise the expected range of operation for the crane.

3.4 Model Gain Values

The next step to be addressed is the determination of the individual gains associated with each model. The values to be determined are K_{cpu}, K_v, and K_i. These address the dimensionless gain through the microprocessor, the gain for the vector drive, and the inclinometer gain expressed in volts per radian. K_{cpu} is the proportional gain through the microprocessor resulting from the conversions made in ranges for the AD input and DAC output. The input command range is a 2.5 volt range while the output is a 20 volt range. The resulting value for K_{cpu} is

$$K_{cpu} = \frac{V_{out}}{V_{\epsilon}} = \left(\frac{4096\ counts}{2.5\ volts}\right)\left(\frac{20\ volts}{4096\ counts}\right) = 8\ . \tag{3.15}$$

The value for K_{cpu} will be multiplied by the gain the filter implemented by the microprocessor. The value for the vector drive is shown in equation 3.16

$$K_{v} = \left(\frac{0.75\ m}{s}\right)\left(\frac{1}{10\ volts}\right) = \frac{1\ m}{15\ volts\ s}\ . \tag{3.16}$$

The values used for the determination of K_v are an estimated velocity of 0.75 meters/second for the maximum input voltage of 10 volts. The value for K_i determined from the test stand needs only to be converted to the proper dimensions to agree with the rest of the models.

$$K_{i} = \left(\frac{1.072\ volts}{15^{\circ}}\right)\left(\frac{180^{\circ}}{\pi\ radians}\right) = 4.0947\ \frac{volts}{radian}\ . \tag{3.17}$$

3.5 Discrete Models

The models previously derived will be used for the design of compensators for the continuous system. However, the actual system will be implemented as a digital controller. Therefore, it is necessary to develop and specify the discrete equivalents for each of the models for this stage of the design process.

The first consideration for determination of the discrete models is selection of the transform to connect the s domain model to the z domain. Discrete equivalents can be obtained by method of numerical integration. The three techniques for numerical integration used are the forward rectangular rule, the backward rectangular rule, and the trapezoidal rule or Tustin's method. Of the three, the most desirable approach is to use Tustin's method because it is the most effective of the three in mapping the stable region of the s-plane into the stable region of the z-plane. The mapping achieved is illustrated in figure 3.8.

A consideration that must be made when using Tustin's method is to correct for distortion of frequencies mapped to the z-plane. From Shahian and Hassul [15] the bandwidth of the discrete filter is given by equation 3.18. When T becomes small in comparison to the value for a, the bandwidth of the discrete equivalent approaches the bandwidth for the continuous model. For the systems under consideration, a sampling rate of 30 Hz. will limit the distortion of the highest frequency components of the system to less than 3%

$$\omega_{BW} = \frac{2}{T} \arctan\left(\frac{aT}{2}\right) . \tag{3.18}$$

Given the use of Tustin's method, the discrete equivalents for the vector drive, crane, and inclinometers are given below. Where the discrete form of the crane

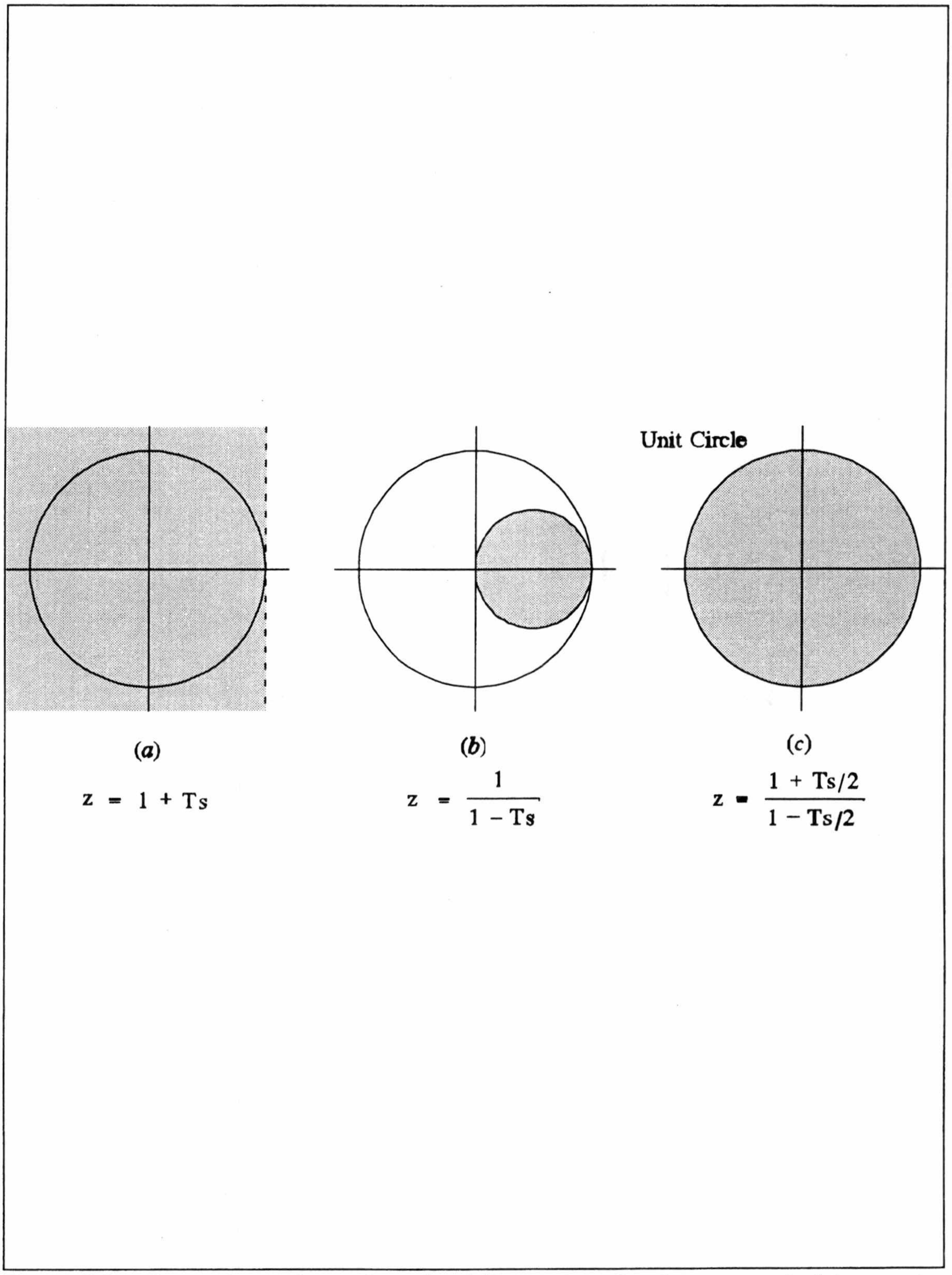

Figure 3.8: *Comparison of mapping of stability regions for three numerical integration methods. (a) forward rectangular rule, (b) backward rectangular rule, (c) trapezoidal rule (Tustin's method).*

transfer function, G_θ, is

$$G_\theta(z) = G_\theta(s)\big|_{s=\frac{2}{T}\frac{z-1}{z+1}} = \frac{\dfrac{-2\omega_p}{gT\left(\omega_p + \dfrac{4}{T^2}\right)} + \dfrac{2\omega_p}{gT\left(\omega_p + \dfrac{4}{T^2}\right)} z^{-2}}{1 + \dfrac{2\left(\omega_p - \dfrac{4}{T^2}\right)}{\left(\omega_p + \dfrac{4}{T^2}\right)} z^{-1} + z^{-2}} . \tag{3.19}$$

The representation for the vector drive transfer function is

$$G_v(z) = G_v(s)\big|_{s=\frac{2}{T}\frac{z-1}{z+1}} = \frac{\left(\dfrac{K_v\omega_v}{\omega_v + \dfrac{2}{T}}\right) + \left(\dfrac{K_v\omega_v}{\omega_v + \dfrac{2}{T}}\right) z^{-1}}{1 + \left(\dfrac{\omega_v - \dfrac{2}{T}}{\omega_v + \dfrac{2}{T}}\right) z^{-1}} . \tag{3.20}$$

Collecting common terms as shown the discrete transfer function for the inclinometer due to effects from the crane cable angles are

$$\text{Let } k_{coeff} = \left[\frac{K_i\omega_2^{\,2} + \dfrac{K_i\omega_2^{\,2}4}{T}\left(\dfrac{1}{\omega_{ph}^{\,2}} + \dfrac{1}{\omega_1^{\,2}}\right)}{\omega_2^{\,2} + \dfrac{4\zeta_i\omega_2}{T} + \dfrac{4}{T^2}}\right]$$

$$H_c(z) = H_\theta(s)\Big|_{s = \frac{2}{T}\frac{z-1}{z+1}} = \frac{k_{coeff} + 2k_{coeff}\,z^{-1} + k_{coeff}\,z^{-2}}{1 + 2\left(\dfrac{\omega_2^{\,2} - \dfrac{4}{T^2}}{\omega_2^{\,2} + \dfrac{4\zeta_i\omega_2}{T} + \dfrac{4}{T^2}}\right)z^{-1} + z^{-2}} \quad . \qquad (3.21)$$

Again, collecting common terms as shown, the discrete transfer function for the inclinometer resulting from effects of movement of the carrier device is

$$\text{Let } q_{coeff} = \frac{K_i\dfrac{2\omega_2^{\,2}}{gT}}{\omega_2^{\,2} + \dfrac{4\zeta_i\omega_2}{T} + \dfrac{4}{T^2}}$$

$$H_L(z) = H_L(s)\Big|_{s = \frac{2}{T}\frac{z-1}{z+1}} = \frac{q_{coeff} - q_{coeff}\,z^{-2}}{1 + 2\left(\dfrac{\omega_2^{\,2} - \dfrac{4}{T^2}}{\omega_2^{\,2} + \dfrac{4\zeta_i\omega_2}{T} + \dfrac{4}{T^2}}\right)z^{-1} + z^{-2}} \quad . \qquad (3.22)$$

The previously presented models of the crane, motor drive system, and inclinometers represent the salient features of the system such that accurate analysis can be performed. Given the models necessary to perform analysis of the crane system, the problems of oscillation avoidance and reduction will be examined. The problems of oscillation avoidance will be presented as an open-loop system. The problem of oscillation reduction will be addressed as a closed-loop system.

4. Open-Loop Solution

The approach taken to the open-loop solution will closely follow the RNF implemented previously by Jansen [11]. This approach provides for creating an IIR filter using frequency-domain techniques. As previously noted, the correlation between a digital implementation of a notch filter and the impulse sequence technique indicates similar performance for the notch filter approach while simplifying the design process.

4.1 Determination of Design Values

From the model for the undamped pendulum developed in chapter 3, the value of significance is the frequency, ω_p, where the subscript p indicates the pendulum's natural frequency. Given that the value for ω_p, for an ideal pendulum is valued as

$$\omega_p = \left(\frac{g}{l}\right)^{\frac{1}{2}} , \tag{4.1}$$

where g is the gravitational constant and l is the length of the pendulum to the center of the payload mass, the determination of frequency values for design must focus on the range of lengths anticipated for normal operation.

The block diagram for the open-loop, input-shaping technique is shown in figure 4.1[1]. The RNF is composed of two second-order notch filters and a second-order lag. The effect of the two successive notch filters is shown in figures 4.2 and 4.3. They show the attenuation of the input signal for a single second-order notch filter and for two second-order notch filters. Figure 4.3 concentrates on the area near the design frequency of the filter. The broadening effect of using two second-order notch filters results in attenuation of the input signal magnitude to less than 5% of the original value at a point 17.89% above and 14.08% below the filter frequency.

The second-order lag filter serves to eliminate unwanted high frequency signals. Although the derivation of design models has focused on the crane as a system with a single vibration mode, the crane actually will have other modes of vibration. Therefore, by setting the lag filter correctly, the RNF will attenuate the signal such that vibration of higher frequency modes will be avoided.

4.2 Simulation of the Open-Loop System

The test simulations for the open-loop system concentrated on evaluating the system response to three types of inputs for variations in the crane frequency from the robust notch filter frequency. The three inputs tested were the step, a 3-second ramp, and a 3-second parabolic signal. Of particular interest is whether the maximum amplitude of the payload oscillations exceeded the imposed limit of 2 inches. The

[1]Figures referenced in chapter 4 are located in Appendix A.

two-inch limit on payload oscillation was previously assigned as an acceptable level of payload swing. For a maximum cable length of 70 feet, the equivalent pendulum angle in radians for the maximum oscillation would be 0.0023. The simulations used the maximum input signal voltage of 2.5 volts to determine if for the extreme limit of operator command, the maximum oscillations could be expected to exceed the 2-inch limit on payload swing.

The values for each of the simulations are shown in table 4.1. In each case the maximum amplitude is shown along with the corresponding radian measure. Also, the input signal type is listed as well as the frequency of the filter stated as a percentage of the crane frequency. The results listed in table 4.1 represent the extreme cases for variation of the design frequency above and below the crane frequency. Also represented are the results for each of the three types of input when the filter frequency equals the crane frequency.

The following figures show the time simulation results for the open loop system. Figures 4.4 through 4.8 show the input, compensator output, crane carrier position, vector drive output, and crane cable angle for a step input to a system where the crane frequency is equal to the robust notch filter frequency. Figures 4.9 through 4.13 show the same responses for a filter frequency equal to 65 percent of the crane frequency. Figures 4.14 through 4.18 show the same responses for a filter frequency equal to 140 percent of the crane frequency. For each of these three simulations, the input was a step of 10 volts. Figures 4.19 through 4.23 show the response of the system to a three-second ramp input where the filter frequency is equal to the crane

Table 4.1: *Open Loop Simulation Results.*

Input Type	**Filter Frequency in % of ω_p**	**Crane Cable Angle: θ (radians)**	**Payload Amplitude (inches)**
step	100	0.00110	0
step	65	0.00230	1.9142
step	140	0.00230	1.9295
ramp	100	0.00067	0
ramp	40	0.0022	1.8594
ramp	240	0.0019	1.6061
parabolic	100	0.00081	0
parabolic	60	0.0023	1.9247
parabolic	170	0.0023	1.9421

frequency. Figures 4.24 through 4.28 show the response for a ramp input where the filter frequency equals 40 percent of the crane frequency. Figures 4.29 through 4.33 show the system response for a ramp input where the filter frequency equals 240 percent of the crane frequency. Figures 4.34 through 4.38 show the system response to a three-second parabolic input where the filter frequency equals the crane frequency. Figures 4.39 through 4.43 show the system response for the parabolic input where the filter frequency is equal to 60 percent of the crane frequency. Finally, figures 4.44 through 4.48 show the system response to the parabolic input where the filter frequency equals 170 percent of the crane frequency.

4.3 Final Design Values

From the results of the system simulations given in figures 4.4 through 4.48 the selection of an appropriate design frequency may be made. Of the three types of inputs, the step input represents the input type most restrictive in the range of values for which an acceptable amplitude is maintained. The results of the simulations indicate that the payload amplitude will remain within the acceptable limit of two inches for a design frequency which deviates either to 35 percent below or 40 percent above the actual crane frequency. The results of the simulations for other types of inputs seem to also indicate that the design frequency may deviate further above than below the crane frequency. Based on these results, the design frequency should be set to the actual crane frequency for the full extension of the cable. Given uncertainty in the value for the crane frequency, the value for the filter should be set to the higher side of the estimated crane frequency. Setting the filter frequency equal to or slightly higher than the crane frequency is preferable also from the perspective that as the crane cable is shortened from full extension, the filter design frequency will become less than the actual crane frequency.

Given that the open-loop system provides adequate avoidance of payload oscillations, the next concern is to address damping of oscillations caused by external disturbance of the system. The damping of oscillations will be addressed by the design of a separate closed-loop controller.

5. Closed-Loop Control

Control of payload oscillation resulting from external disturbance of the payload requires feedback control. The device selected for feedback is the inclinometer previously modeled. The approach taken to produce a controller for oscillations resulting from external disturbance will be to first identify the transfer function of the closed-loop system. Next, the effects of various compensation filters will be tested and results given. Finally, based on the results, a compensator will be recommended.

5.1 Uncompensated System

From the models previously described, the block diagram for the closed-loop system is shown in figure 5.1[1]. In the figure, the block $G_c(s)$ represents the undetermined compensator, $G_v(s)$ is the vector drive, $G_\theta(s)$ is the crane, $H_L(s)$ represents the transfer function for linear acceleration effects on the inclinometer, and $H_C(s)$ represents the effects of the crane cable angle, θ, on the inclinometer. In addition, R is the user input, C is the output of the compensator, X is the output of the vector drive, Θ is the angle of the crane cable, B_θ is the output of the inclinometer because of crane cable angle effects, B_L is the output of the inclinometer because of linear acceleration effects from the carrier device, and B is the combined output of the

[1]Figures referenced in chapter 5 are located in Appendix B.

inclinometer. Replacing the blocks with the appropriate transfer functions, the full block diagram of the closed-loop system is shown in figure 5.2. The compensator is represented in figure 5.2 by the rational expression $N_C(s)/D_C(s)$ where $N_C(s)$ is the numerator polynomial and $D_C(s)$ is the denominator polynomial. The loop gain, L, derived from the block diagram is shown in equation 5.1. The parameters used in the

$$L = \frac{\left(\frac{1}{\omega_p^2} - \frac{1}{\omega_{ph}^2} - \frac{1}{\omega_1^2}\right) s^3}{\left(\frac{1}{\omega_v} s + 1\right)\left(\frac{1}{\omega_p^2} s^2 + 1\right)\left(\frac{1}{\omega_2^2} s^2 + \frac{2\zeta_i}{\omega_2} s + 1\right)} \qquad \mathbf{(5.1)}$$

equation are as follows: ω_p is the frequency of oscillation for the crane, ω_{ph} is the frequency determined by the distance from the pivot point of the crane to the inclinometers, ω_1 is the high frequency zero in the inclinometer angle transfer function, ω_2 is the pole from the inclinometer transfer function, and ω_v is the frequency for the vector drive. As can be seen, the equation has three zeroes at the origin of the s-plane. The poles of the equation are from the vector drive, crane, and inclinometers. From the previously determined parameter values, the most significant poles are those of the crane and the inclinometers. This is because the damping factor for both the crane and inclinometer poles is small enough that the poles are located on the imaginary axis of the s-plane. Also, the poles from the crane and inclinometer are relatively close together compared to the other poles. Given this, it was decided to evaluate the system using root locus techniques.

Root locus techniques are based on an evaluation of the change in the roots of the characteristic equation of a system as parameters in the system are varied. From Kuo [16], if the transfer function for the system may be expressed as in equation 5.2 then the characteristic equation is obtained by setting the denominator of the system

$$\frac{\Theta(s)}{R(s)} = \frac{G(s)}{1 + G(s)H(s)} \tag{5.2}$$

transfer function equal to zero as shown in equation 5.3. Then if *G(s)H(s)*, the loop gain contains a variable parameter, *K*, such that the function may be written as in

$$1 + G(s)H(s) = 0 \tag{5.3}$$

equation 5.4, the characteristic equation may be rewritten in the form of equation 5.5. Of particular interest to the solution of this problem is the determination of departure angles. From Kuo [16] the determination of departure angles, for values of *K*

$$G(s)H(s) = \frac{KQ(s)}{P(s)} \tag{5.4}$$

$$1 + \frac{KQ(s)}{P(s)} = \frac{P(s) + KQ(s)}{P(s)} = 0 \tag{5.5}$$

greater than zero is based on the root locus characteristic that the sum of the angles from the zeros to any point in the s-plane minus the sum of the angles from the poles to the same point equal an integer multiple of π. The equation describing this property is shown in equation 5.6 where s is any point on the s-plane, z is a zero of the characteristic equation, p is a pole of the characteristic equation, and $k = 0, \pm 1, \pm 2, \ldots$ (any integer).

$$\sum_{i=0}^{m} \angle(s + z_i) - \sum_{j=0}^{n} \angle(s + p_i) = (2k + 1)\pi \tag{5.6}$$

The value of this particular property for the crane problem results from the poles of the system being located virtually on the imaginary axis. It is important to ensure that the change in the poles will go toward the left half plane to ensure that stability of the transient response. The root locus plot for the uncompensated closed-loop system is shown in figures 5.3 and 5.4. Figure 5.3 shows the overall plot; figure 5.4 shows the area of the s-plane close to the crane frequency poles. These figures clearly show that the uncompensated system becomes unstable because of departure of the crane frequency poles into the right half of the s-plane.

5.2 Compensator Design

The design of the compensator consists of two considerations. The first consideration is the transient response of the system. The significance of the transient response for the crane system is based on the proximity of the characteristic equation poles to the imaginary axis. This tends to make controlling the transient response the first priority. The second consideration is the steady-state response. This dictates whether the system ultimately performs the desired task. Given that the system is stable, it will be necessary to show that the overall objective of oscillation reduction will be achieved.

5.2.1 Steady-State Response

The steady-state response for the system is characterized by the error as time approaches infinity. Given the error goes to zero or that an acceptable error is achieved, the system is said to have an appropriate steady-state response. For the crane system, the desired response is less than 0.0023 radians amplitude of oscillation.

In evaluating the steady-state response, it is necessary to specify the error function for the system. The general form for a feedback control error function is shown in equation 5.3

$$E = R\left(\frac{1}{1+L}\right), \tag{5.3}$$

where R is the input to the system and L is the loop gain. An acceptable steady-state response will be to make E as close to zero as possible.

There are two basic approaches to predicting the steady-state response of a system. The first is to evaluate the effect of a series of representative inputs when the actual input cannot be known apriori. The typical approach is to evaluate the response to step, ramp, and parabolic inputs to determine the steady-state error. The other approach is to evaluate the error function for a specific signal when it is known what signals the system will be subjected to.

In the case of the crane system, the input to the closed-loop control system is known. Because the purpose of the system is to damp oscillations in the crane payload without effecting overall movement of the payload, the input to the system will be a damped sinusoid with a frequency equal to that of the harmonic frequency of the crane. Therefore, the desired steady-state response will be achieved if the poles of the characteristic equation equal the frequency of the crane. This may be shown by the association where the value of L approaches ∞ as ω_R, the frequency of the sinusoidal input, approaches ω, the frequency of the poles of L. Therefore, as L approaches ∞, E approaches zero.

5.2.2 Transient Response

The evaluation of compensation of the transient response may be approached by several means. The method employed was that of the root locus. As mentioned previously, the greatest value of root locus analysis for the system being studied is its depiction of the departure angles for the characteristic equation poles. This evaluation varies a number of parameters to determine a range of values which satisfy the conditions of stability. This is necessary because the actual system will vary from the models. Therefore, it will be necessary to evaluate sensitivity of the change in response of the system for the variation in parameters.

The overall form of the compensator to be used will be similar to the one used for the open-loop solution. Two biquads will be made available as well as a second-order lag filter. The biquads will have the same frequency in the numerator and denominator because using different frequencies can have undesirable transient effects in actual implementation. The lag filter is made available to provide filtering of unwanted high frequencies.

5.2.2.1 Qualitative Selection of Values

Examining the uncompensated system, it is desirable to place the poles and zeroes of the compensator such that the departure angles for the crane poles are changed by some value greater than 90 degrees and ideally near 180 degrees. At the same time, minimal change should be made in the inclinometer pole departure angles because they are already within the desirable range. Qualitatively, this may be achieved by placing the zeros of one filter at a value slightly greater than that of the inclinometer pole. These zeros should be on the imaginary axis. The result will be that the effects of the zeros on the departure angle of both the inclinometer and the crane poles will cancel to a net change of zero degrees. The poles for the first filter may be placed on the real axis by assigning a damping factor of one. This will have a detrimental effect on the departure angle of the inclinometer poles while improving the departure angles for the crane poles. The next filter could be placed at or near the same frequency value as the first filter, causing the departure angles for the inclinometer poles, as well as the crane poles, to improve. The advantage in placing at least one filter in close proximity to the inclinometer poles will be to reduce feedback of the inclinometer response to the compensator.

Use of the lag filter will reduce unwanted high frequency components. Considering the requirements for steady-state response, it is desirable to place the frequency of the lag filter close to the crane frequency without causing unnecessary attenuation of the compensator output for the crane frequency. This will dictate as low a value for the lag frequency as possible while hopefully maintaining an approximate factor of five above the crane frequency. The transfer function for the proposed compensator is shown in figure 5.5.

5.2.2.2 Simulation of Parameter Effects

To evaluate the possible effects of the suggested parameters, it is necessary to simulate the system in an effort to identify valid ranges. The use of root locus contours provides both an indication as to the stability of the parameters being evaluated and some indication of the effect of changing those parameters. A root locus contour is obtained by varying two parameters of the characteristic equation to produce multiple root locus plots which indicate change in the overall plot for the two parameters being changed.

For the evaluation of the crane system it was decided to investigate the variation of ω_L, the frequency of the second order lag filter, ω_{c2}, the frequency of the second biquad compensation filter, and ξ_{c2}, the damping coefficient for the second compensation filter. The following values for the previously mentioned parameters will be used:

ω_L — for values ranging from 0.35 to 0.40 Hz.,

ω_{c2} — for values ranging from 1.3 to 2.4 Hz.,

ζ_{c2} — for values ranging from 0.78 to 1.0.

The reasoning for these values is based upon the previous qualitative discussion and the likely range of values which will yield acceptable results. Each possible range is represented by a root locus contour of four values over the range. This provides some indication of the effects of the change without producing such a small change that the individual loci are obscured.

The first set of figures shows the effects of varying ω_{c2}. These are shown in figures 5.6 through 5.9. The accompanying data from the simulation is given in table 5.1. Figure 5.6 shows the full view of the root locus. Figure 5.7 illustrates a detailed view of the response of the inclinometer poles to the change in ω_{c2}. The higher the frequency for ω_{c2}, the further the loci departs from the imaginary axis. In all cases, the inclinometer poles terminate on the zeros of the first compensator filter. Figure 5.8 shows details of the response of the crane poles. The higher the frequency for ω_{c2}, the less the crane poles depart from the imaginary axis and the lower the stable gain limit. Finally, figure 5.9 shows a close up overall view of the root locus contour. The largest variation in loci for the range of ω_{c2} is that of the poles contributed by the second compensator filter, which is specified by ω_{c2}.

The next variation of parameters investigated is values for ω_L ranging from 0.35 to 0.37 Hz. The results are shown in figures 5.10 through 5.13. The results shown in figure 5.10 show the full-view root-locus contour for variation of ω_L. The general view shows less overall change than the contour for ω_{c2}. Figure 5.11 shows the detail of the inclinometer pole response for variation of ω_L. The inclinometer poles show no significant change for the variation of the lag filter frequency. The change in response of the crane poles is shown in figure 5.12. The changes show the relatively narrow range for which the system is stable. Finally, figure 5.13 shows the overall root-locus contour at a range which covers the response of the compensator filters.

The last simulation covered variation in values for ζ_{c2} from 0.78 to 1. This variation in the second filter-damping factor was intended to help evaluate the reduction of damping in the compensator filter to allow for faster response to input. Figure 5.14 shows the overall root locus contour for variations in ζ_{c2}. Figure 5.15 shows detail of the inclinometer pole response. Performance of the inclinometer poles does not change significantly for the variation in ζ_{c2}. Detail of the response of the crane poles to variation in ζ_{c2} is shown in figure 5.16. The crane poles respond similarly to previous simulations in that they show little departure from the imaginary axis before crossing into the right half plane. Finally, figure 5.17 shows the overall root-locus contour in a view which covers the response of the compensator filters. The change of significance is that of the change in loci direction as damping for the filter based on ω_{c2} varies.

The actual values for the above simulations are shown in table 5.1. Included in the table are departure angles for the crane and inclinometer poles, denoted ω_{p1} and ω_{p3} respectively. Also included are the values for the crane frequency, ω_p, inclinometer pole frequency, ω_2, crane pole damping, ζ_p, first filter frequency, ω_{c1}, second filter frequency, ω_{c2}, second filter pole damping, ζ_{c2}, and the maximum stable compensator gain for the values listed.

5.3 Selection of Compensator Parameters

From the simulations performed and the information obtained in evaluating an appropriate steady state and transient response, the values for closed-loop compensation may be selected. Given the selection of values within the ranges indicated, the system was simulated to determine the expected response.

The values for the compensator, where the following parameters are ω_{c1}, the frequency of the first quadratic binomial filter; ζ_{c1}, the damping coefficient for the first filter; ω_{c2}, the frequency for the second filter; ζ_{c2}, the damping coefficient for the second filter; and ω_L, the frequency of the second order lag filter; were selected within the following ranges:

Table 5.1: *Results of Root Locus contours to determine transient response.*

ω_{p1}	ω_{p3}	ω_p	ω_2	ω_{c1}	ω_{c2}	ω_l	ζ_{c2}	K_m
97.04	-152.62	1.10	8.03	8.11	8.17	2.20	1.00	46.20
93.70	-166.68	1.10	8.03	8.11	10.47	2.20	1.00	34.86
91.55	-177.34	1.10	8.03	8.11	12.78	2.20	1.00	10.38
90.05	-174.43	1.10	8.03	8.11	15.08	2.20	1.00	0.56
93.47	-167.77	1.10	8.03	8.11	10.68	2.20	1.00	21.46
92.61	-168.33	1.10	8.03	8.11	10.68	2.24	1.00	22.92
91.77	-168.88	1.10	8.03	8.11	10.68	2.28	1.00	11.03
90.96	-169.43	1.10	8.03	8.11	10.68	2.32	1.00	6.21
90.93	-171.99	1.10	8.03	8.11	10.68	2.20	0.78	7.17
91.78	-170.37	1.10	8.03	8.11	10.68	2.20	0.85	11.98
92.62	-168.97	1.10	8.03	8.11	10.68	2.20	0.93	20.32
93.47	-167.77	1.10	8.03	8.11	10.68	2.20	1.00	21.46

ω_{c1} — 8.1 radians, of 1 % over the value for the inclinometer pole frequency

ω_{c2} — 1.3 to 2.0 Hz.

ζ_{c1} — damping of 1

ζ_{c2} — damping of 0.85 to 1

ω_L — 0.35 Hz.

The selected values are within the ranges which the simulations suggest will provide adequate response. Also, the values are such that changes may be made to allow for deviations between the design models and the actual system.

To determine the probable response of the system, it was necessary to perform time simulations with the selected values and determine the predicted performance. The simulations were based on the discrete models derived in chapter 3. The simulation incorporated the effects of a zero order hold circuit to account for the final solution being implemented as a digital control system. Given the simulation model, it was determined that the simulations would be performed for values of ω_p varying from 85% to 115% of the expected base value.

The results of the time simulations are shown in figures 5.18 through 5.26. Figures 5.18 through 5.20 show the results for ω_p equal to 85% of the base model value. Figure 5.18 depicts the output of the crane. Superimposed on this figure is the approximated envelope of decay for the output. The simulation shows an expected decay to less than 5% of initial amplitude within 4 periods of the crane. Figure 5.19 shows the feedback signal from the inclinometers. The predominant characteristic is the frequency of oscillation for the inclinometer. Figure 5.20 shows the output of the compensator. It can be clearly seen that the signals at the inclinometer frequency have been eliminated.

Figures 5.21 through 5.23 show the results for ω_p equal to the base model value. The output of the crane is shown in figure 5.21. The response is similar to those obtained for the simulation at 85% of base model value. The inclinometer feedback signal is shown in figure 5.22. Finally the output of the compensator is shown in figure 5.23.

The final set of simulation figures are for ω_p equal to 115% of the base model value. These figures are 5.24 through 5.26. The results for this simulation are practically identical to the previous two simulations. The values for the simulations are shown in table 5.2. From the values shown, it can be seen that the actual gain required to damp oscillations is much less than the maximum possible. This is a result of the need to minimize the steady-state error. As previously stated, the steady-state error is zero if the characteristic equation of the system has poles at the frequency of the crane. Therefore, increasing the gain too much would result in a less desirable response by shifting the value of the characteristic equation pole further from the frequency of the crane.

Given the previously discussed open- and closed-loop solutions, it is necessary to discuss the hardware and software systems required for implementation. The focus for the implementation of the control systems is on the use of low-cost components to make the solution more attractive to private companies which manufacture cranes similar to the IPD crane.

Table 5.2: *Results of Time Simulations.*

ω_p	ω_{c1}	ω_{c2}	ζ_{c2}	ω_l	ζ_{sys}	ω_{sys}	Gain
0.93	8.10	10.68	0.85	0.35	0.17	0.83	3
1.10	8.10	10.68	0.85	0.35	0.17	0.99	3
1.15	8.10	10.68	0.85	0.35	0.17	1.16	3

6. System Overview

The system used to implement the project consisted of an eight-bit microcontroller, the AC motor drives, and interface hardware. The microcontroller also had associated peripheral boards containing 12-bit analog to digital(A/D), and digital to analog, DAC, converters. The motor drives were Thor Technologies AC Vector Drives. The motor drives provided a means of controlling the crane's AC motors with a voltage signal like that which would be used with a DC motor. The interface hardware consisted of an operator pendant and circuitry to interface the microcontroller to the Vector drives. The operator pendant used a joystick for position control and incorporated a series of buttons to activate the closed-loop system and to provide safety kill switches for the crane.

6.1 System Hardware

As mentioned, the hardware consisted of a microcontroller, motor drives, and interface circuitry. The microcontroller was selected as representative of the inexpensive programmable controllers which have gained popularity for industrial use. The motor drives were installed for work previously done on the IPD crane by ORNL. The purpose behind the use of these drives was to illustrate the use of AC drives because of their lower associated maintenance and wider acceptance for industrial application. Finally, the interface circuitry was designed to present a controller similar in appearance to those operator pendants typically employed to operate cranes of this type. Figure 6.1 shows an overall diagram of the hardware used. Actual pictures of the crane structure, inclinometer mount, and controller hardware are shown in figures 6.2 through 6.4. Figure 6.2 shows the bridge and trolley structure from below. Figure 6.3 shows how the inclinometers were mounted on the payload lifting hook. Figure 6.4 shows the cabinet which housed the microcontroller and interface hardware.

6.1.1 Microcontroller

The microcontroller used was based on the eight-bit Z180 microcontroller manufactured by Zilog. The particular product used was made by Z-World, Inc. The controller consisted of a microcontroller board, an A/D, and a DAC board. The A/D and DAC boards both provided 12-bit resolution.

The microcontroller board consisted of the microprocessor, eight digital inputs, eight digital outputs, and two serial communications ports. The microprocessor was a Z180 microcontroller running on a 9 Mhz. clock. The digital inputs provided an interface for TTL level signals. The digital outputs were high current outputs capable of driving relays and switching devices with operating voltages of up to 50 volts. The two serial communications ports provide RS-485 protocol communications.

The A/D convertor board was also a product of Z-World, Inc. The convertor board connected to the microcontroller board by means of an expansion bus. The bus connection was made by ribbon cable. The convertor provided 8 differential input channels at 12-bit resolution. The input range was ±2.5 volts or 0 to 2.5 volts. The

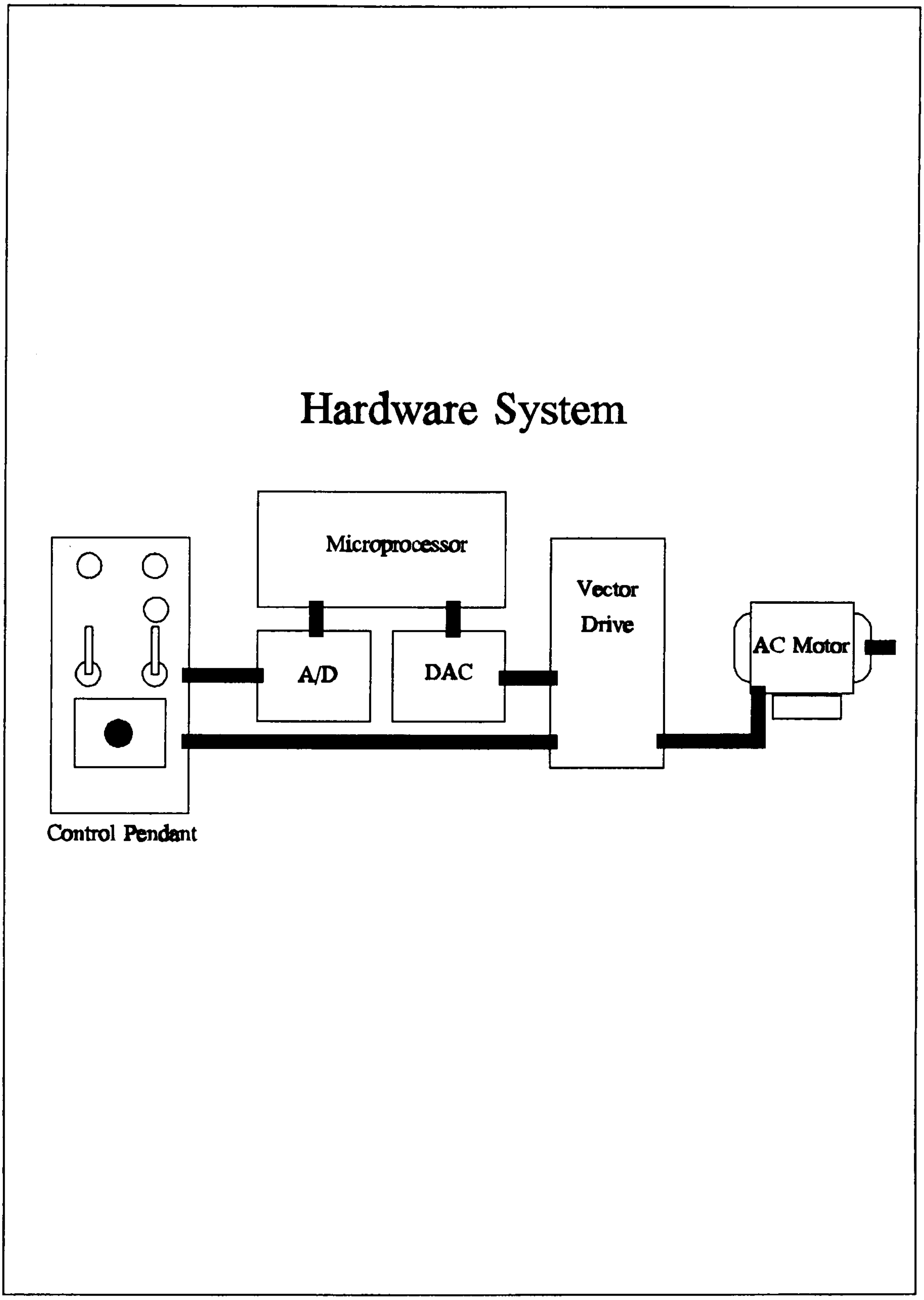

Figure 6.1: *Block diagram of hardware system components.*

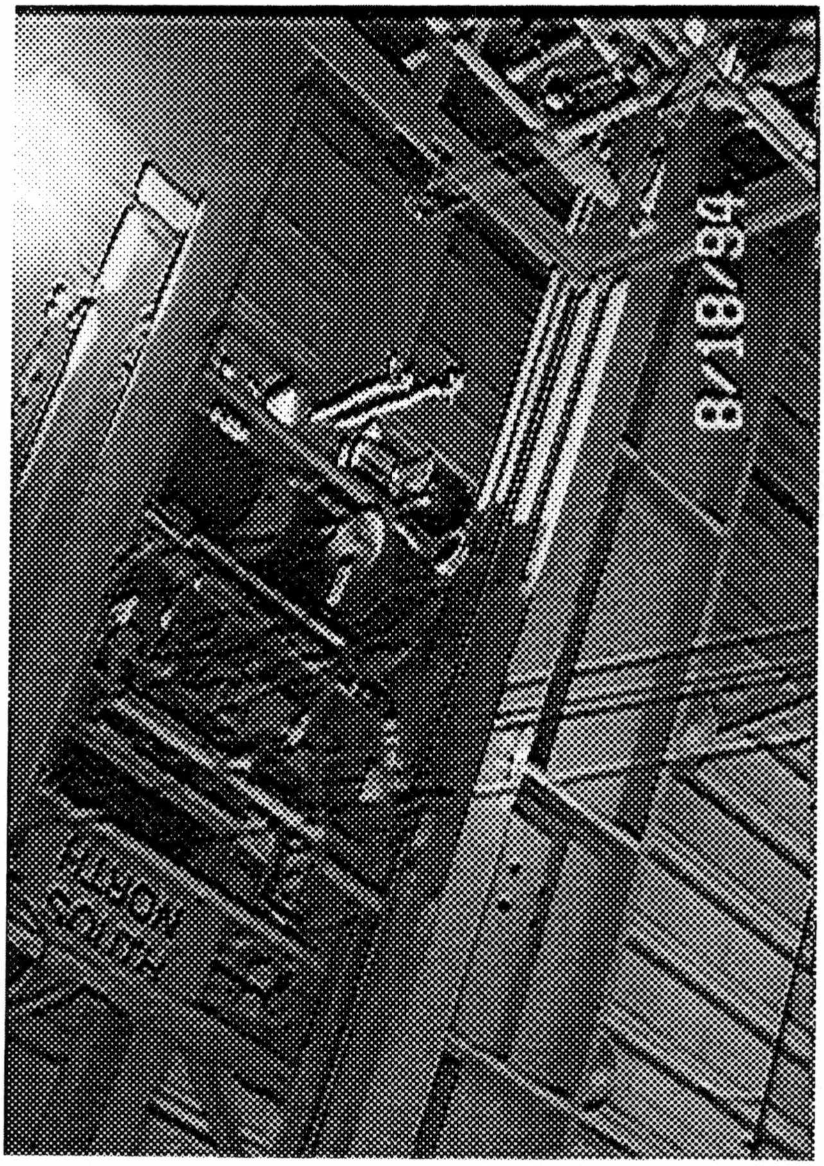

Figure 6.2: *Picture of bridge and trolley structure from 70 feet below.*

Figure 6.3: *Picture of inclinometer mounting to the side of the payload lifting hook.*

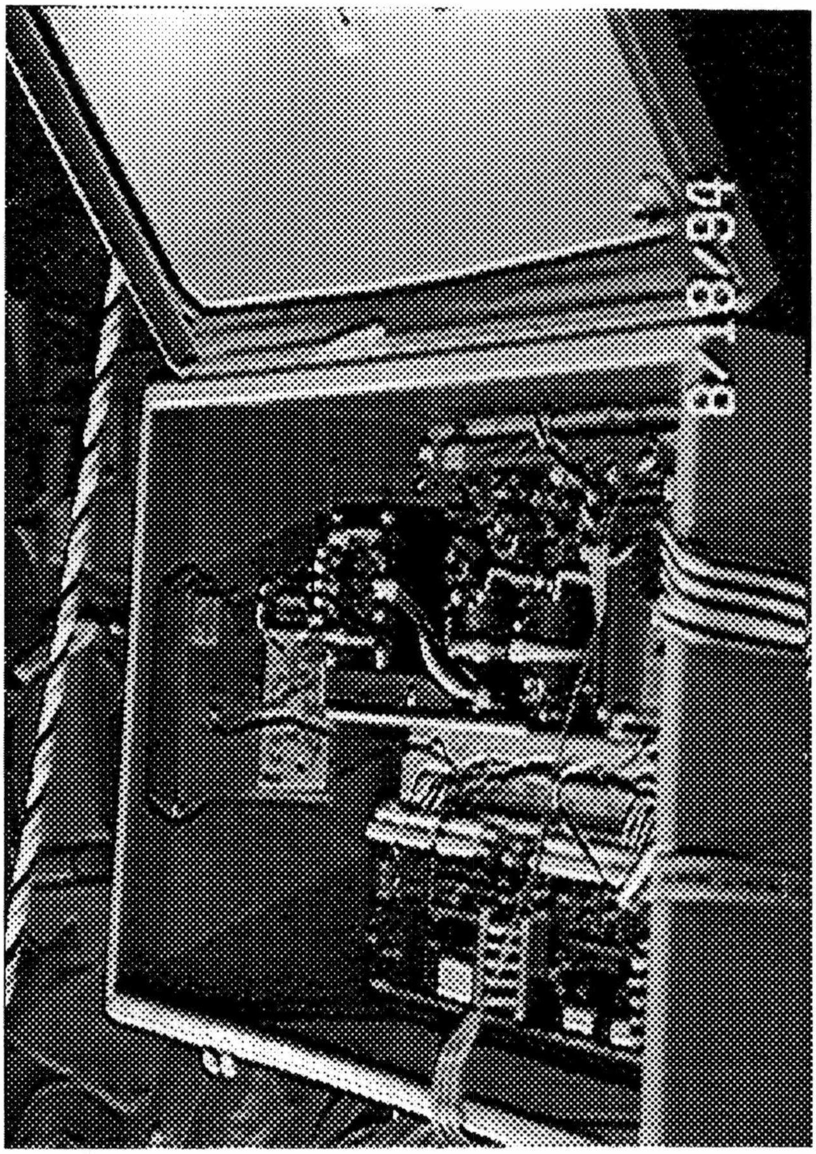

Figure 6.4: *Picture of electrical cabinet containing the microprocessor and associated interface hardware.*

ranges could additionally be decreased by means of programmable gains. The time required to complete one conversion at a gain of one is one millisecond.

The DAC convertor board, also from Z-World, Inc., connected to the microcontroller board by means of the same expansion bus used for the A/D convertor board. The DAC provided two 12-bit resolution ports. The voltage range output was software selectable as 0 to 2.5, 0 to 5, or 0 to 10 volts. The time required to output a voltage was four milliseconds.

6.1.2 AC Motor Drives

The AC motor drives were manufactured by Thor Technologies. The motor drives incorporate pulse width modulated invertors for producing the AC motor control. The drives use shaft encoders to provide precise velocity control. Control inputs for the drives use a ±10 volt signal to indicate motor speed and direction. The drives also include setting for maximum speed and acceleration as well as motor disable. Each crane motor was equipped with a separate drive which was tuned for the motor.

6.1.3 Interface Circuitry

The interface circuitry consisted of two parts. The first part was the operator control pendant. The second was the circuitry required to interface the microcontroller to both the motor drives and the operator pendant. Each part was constructed with attention paid to the simplicity of operation and minimization of expense. Circuit diagrams for the components are shown in figure 6.5.

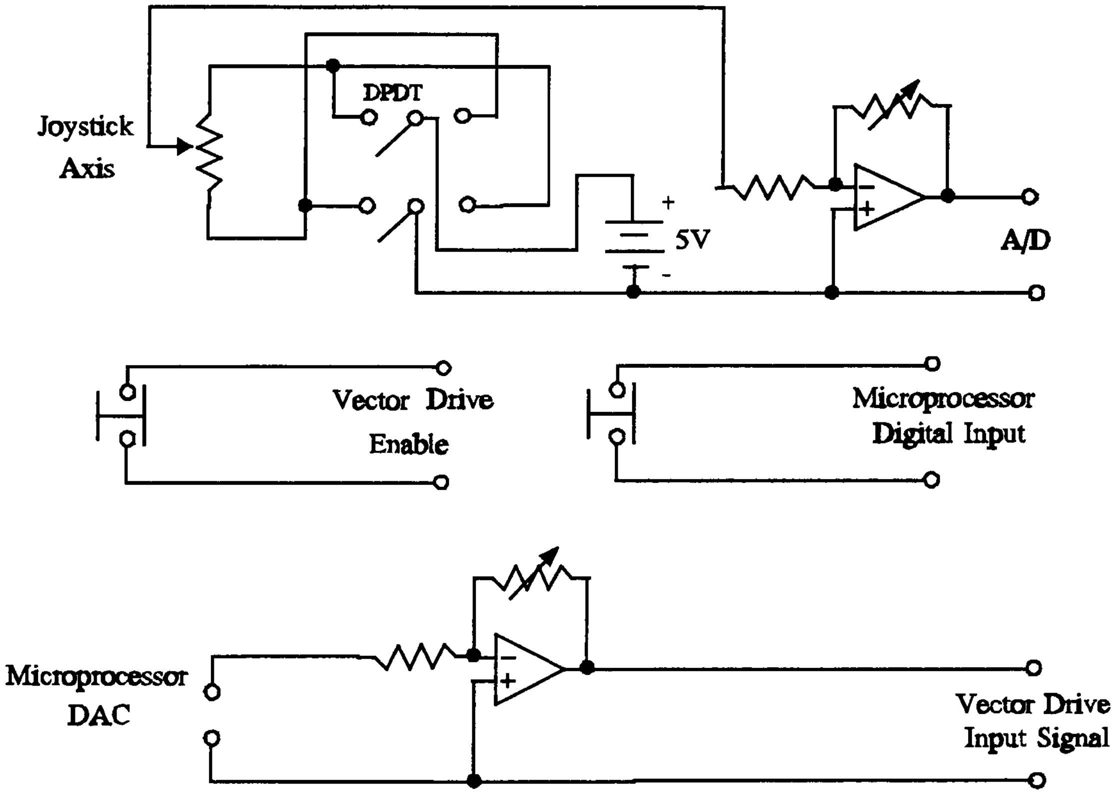

Figure 6.5: *Circuit diagrams representing the interface between the control pendant, microprocessor, and vector drives.*

The operator pendant consisted of a joystick and buttons for controlling the crane's operation. The joystick was of a simple x-y type similar to those used with computer games. Each axis was controlled by a connected potentiometer for which the center position value can be adjusted. The signal was read from the potentiometer wiper and compared against a reference of five volts. Additionally, there were two double-pole double-throw switches provided to allow reversal of the directional sense for each axis. This permitted greater freedom in selecting operator orientation to the crane.

The other buttons on the operator pendant were for disabling individual motor drives and for activating the closed-loop control system. The drive disable buttons were directly connected to the drive enable lines on the motor drives. The experimental nature of the system dictated that the operator should be able to stop the operation of the crane quickly should a problem develop. The closed-loop control button served to activate feedback damping of payload oscillations. When the button was pressed, the joystick input was disabled and the microcontroller operated based on the signals from the inclinometers. Then, when any oscillations had been damped, the button could be released and normal crane movement resumed.

6.2 Software System

The software for this project was developed using the Dynamic C Compiler from Z-World, Inc. This compiler is provided with libraries intended for use with products sold by Z-World, Inc. The major components of the software system were the real-time control routines and the implementation of the control filters.

The real-time control was achieved through the use of a real-time software kernel provided with the Z-World Dynamic C Compiler. The structure of the scheduler for this real-time system is based upon defining routines as tasks and specifying under what conditions they should be executed. The scheduler is then controlled by specifying the rate at which a scheduler "tick" occurs. The tick rate is the maximum frequency at which any task may occur. Also, the assignment of the task number controls the priority order in which tasks are executed. The approach taken to the crane system was to specify the filter function as the single task to be executed. This prevented any concerns over priority scheduling. All other routines for initializing the system were run at start time.

The software implementation of the filters focused on minimizing the amount of storage required and the number of calculations required for each current filter value to be generated. In an effort to minimize the storage and number of multiplications, the filters were implemented using the canonic direct form taken from Oppenheim and Schafer [17]. The canonic direct form requires two memory storage values for each filter per axis. The direct form I shown by Oppenheim and Schafer require four memory storage values for filter per axis. The number of multipliers for each implementation is the same:

$$2N + 1 \,, \tag{6.1}$$

where N is the order of the filter being implemented. Figures 6.6 and 6.7 show the signal flow graphs for both the direct I form and the canonic direct form respectively. For figure 6.3 the values used are taken from equation 6.1.

$$\begin{aligned} y[n] &= \sum_{k=1}^{N} a_k \, y[n-k] + \sum_{k=0}^{M} b_k \, x[n-k] \\ v[n] &= \sum_{k=0}^{M} b_k \, x[n-k] \end{aligned} \qquad \textbf{(6.2)}$$

The values used in figure 6.4 are taken from the revised form of equation 6.2 shown in equation 6.3.

$$\begin{aligned} y[n] &= \sum_{k=0}^{M} b_k \, w[n-k] \\ w[n] &= \sum_{k=1}^{N} a_k \, w[n-k] + x[n] \end{aligned} \qquad \textbf{(6.3)}$$

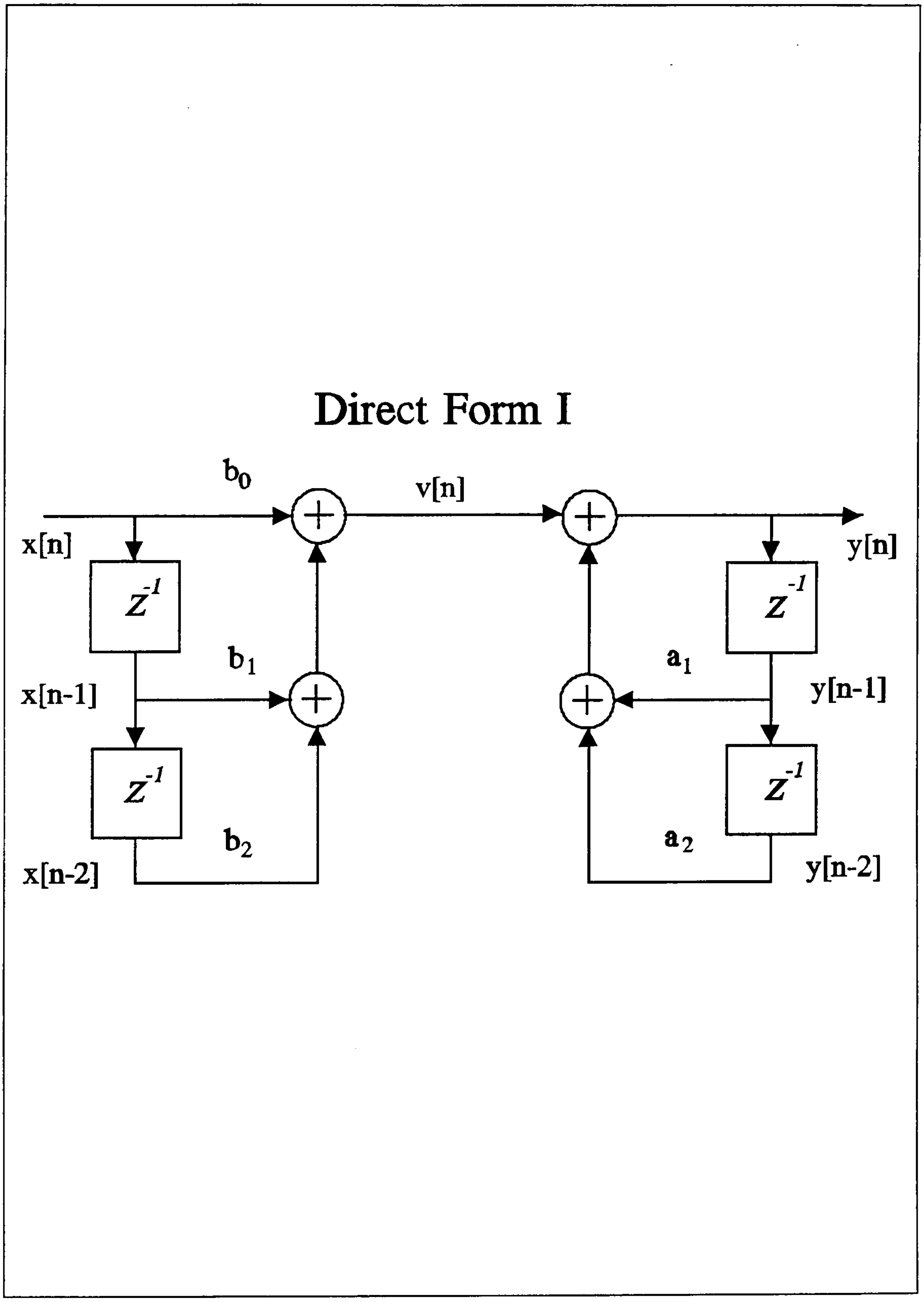

Figure 6.6: *Signal flow diagram for the Direct I form for a difference equation.*

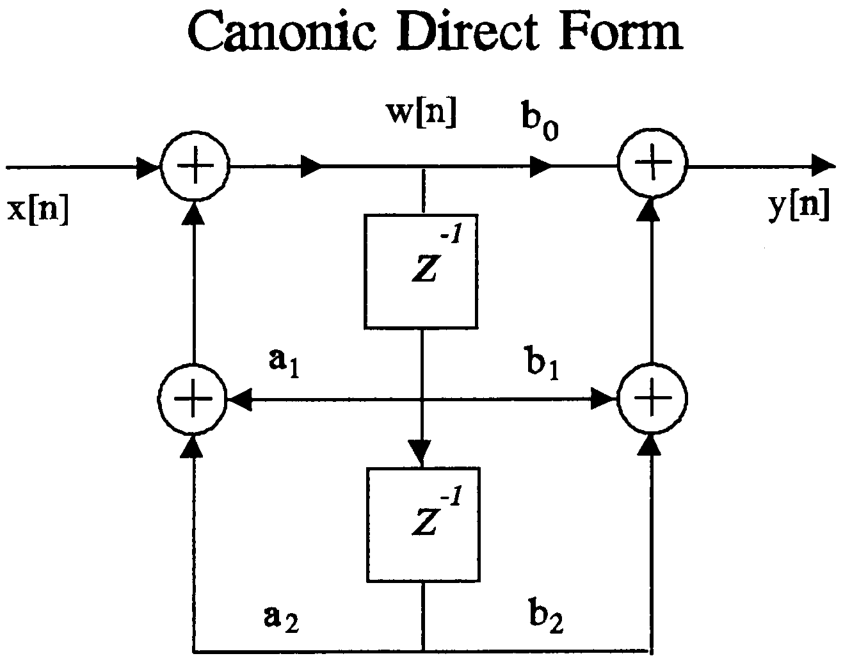

Figure 6.7: *Signal Flow diagram for Canonic Direct form for a difference equation.*

7. Experimental Results

The experimental results for the crane examine the two solutions separately. First, the open-loop compensation is examined. Of particular significance are the observed oscillations, delay in command response, and other observed characteristics of the system's performance. Second, the closed-loop system is examined. The examination of the closed-loop system concentrates first on the response for each axis individually and then on both axes simultaneously.The points considered include the number of cycles to damp and the characteristics of the combined system.

In both systems, the tests were performed in an actual working environment. The working space, as well as the time, were at a premium. Therefore, the results were obtained by crude measurement based on a ruler graduated in inches and visual approximation. The compromise of precise measurement was considered a reasonable one to allow the opportunity to test the system on working equipment.

7.1 Open-Loop System

The open-loop system was tested using the values specified in the design shown in chapter 4. As stated, the compensator consisted of a robust notch filter and a second-order lag filter. The robust notch filter frequency was set to the value approximated for the crane, $\omega_p = 1.1$ radians. The frequency for the crane was estimated based on observation of the period of oscillation. The frequency for the lag filter was set to 25.13 radians.

The open-loop system was operated at the full extension of the crane cable, which was approximated at 70 feet. Also, the system was operated with the cable length reduced to 60 feet. Although it would have been preferable to try even shorter cable length, the test area limited this possibility. The observed operation for both cable lengths was the same. In both cases, no discernable oscillations were apparent. The payload was moved in each individual axis of motion as well as in directions which would cause motion in both axes. In no case was any significant oscillation observed.

The one aspect of the open loop which presented measurable information was the delay in response to operator input. The system required approximately 2 to 3 seconds to respond to any input. This corresponds to the results predicted by previous work by Jansen [11]. It was stated in the review of the robust notch filter that a delay approximately equal to half the period of the filter frequency was expected. The corresponding value based on the measured frequency of the crane was 2.86 seconds.

The other observed performance for the open-loop system included an observation that the payload tended to vibrate in an up and down motion. The apparent frequency of this vibration was above 4 Hz. This would most likely be a result of vibration of the cable. Because the original model for the system treated the cable as a rigid body, no predictions of this response were made.

The overall results for the open-loop system corresponded to those expected from the design. The nature of the observations restricted the evaluation of the results to a predominantly qualitative discussion, but the performance on an actual system provided important confirmation of the applicability of the system to working hardware.

7.2 Closed-Loop System

Testing of the closed-loop system was based more on quantitative measurements than was the open-loop system. The system was tested first for the individual axes and then for the combined response. The values used for the closed-loop system were adjusted as a part of the equipment installation. The values used are listed for the crane bridge and trolley separately. This was necessary because of the difference in the components for the two directions. The values for the system are shown in table 7.1. The results of the tests for the closed-loop system include observation of the number of cycles required for oscillations to cease. Also, observations of differences in performance between tests of individual axis compensation and both axes were made.

The results of the observations of the number of cycles to damp an initial 48-inch amplitude oscillation to two inches are listed in table 7.2. This table also includes the number of cycles required for the uncompensated system to damp. The entries in the table are prefixed "Un." to indicated uncompensated and "Cmp." to indicate compensated.

The results show an increase in damping equal to almost one order of magnitude. The results for the bridge in single axis control closely correspond to the values predicted by the design simulations. The trolley showed slightly worse performance; the combined system achieved an increase of only six times over the uncompensated system.

Table 7.1: *Compensator parameters.*

	bridge single	trolley single	bridge combined	trolley combined
ω_{c1}	8.10	8.10	8.10	8.10
ζ_{c1}	1.0	1.0	1.0	1.0
ω_{c2}	12.57	12.57	12.57	12.57
ζ_{c2}	0.4	0.3	0.4	0.4
ω_{l}	5.03	5.03	5.03	5.03
ζ_{l}	1.0	1.0	1.0	1.0
gain	2.7	3.1	1.7	1.8

Table 7.2: *Test results for closed-loop system.*

	Starting Amplitude	Ending Amplitude	Number of Cycles	Approximate Damping
Un. Bridge	48	12	18	0.02
Un. Trolley	48	13	18	0.02
Un. Both	48	12	18	0.02
Cmp. Bridge	48	3	3	0.17
Cmp. Trolley	48	3	3.5	0.15
Cmp. Both	48	3	4	0.13

Another observation concerning the combined system was that the motion of the bridge direction was reduced quicker than the motion of the trolley. In fact, the greater time required to damp the motion along the axis of the trolley seemed to introduce oscillation back into the bridge axis. This was most likely the result of some coupling of the axes. The mounting bracket for the inclinometers could not be perfectly aligned along the individual axes. Therefore, motion in one axis would produce some feedback signal in the inclinometer for the other axis. Also, and rotation of the crane cables tended to add to this coupling. This activity leads to the observation that the combined system performed best at gains which were lower than the single-axis compensators. This would tend to minimize the lower value signals resulting from the coupling of the inclinometer signals.

8. Conclusions

The task of oscillation avoidance through the technique of input shaping verified previous work with the RNF [11]. The closed-loop control for damping existing oscillations performed well. The hardware required to implement the systems was inexpensive and potentially appealing to potential manufacturers.

In the case of the RNF, its performance was such that refinements would seem unnecessary. The RNF's insensitivity to change in cable length make it a technology which is immediately ready for implementation on commercially manufactured cranes. One area which bears further testing would be transport of payloads whose vertical size is such that the cable length is equal to or less than the vertical measure of the payload. For such instances, the situation might be addressed by cascading multiple RNFs.

For the closed-loop control system to damp payload oscillations, the problem might be better addressed through the use of another type of feedback sensor. The inclinometers, used for the work reported in this thesis, were selected primarily for the ease with which they could be installed. Consideration was given to the use of sensors to directly measure the angle of deflection for the crane cable. It was determined that the measurement would be inconvenient to take directly from the crane cable. Also, the installation of an auxiliary cable to take the measurement would be expensive and time consuming to fabricate. Had direct cable angle measure been available, the closed-loop system would probably have been able to sustain higher gains and subsequently able to damp system oscillations more quickly. Another factor in the direct measure of the crane angle versus the use of the inclinometers is that the inclinometers were found to be sensitive to twisting of the payload hook. Twisting of the payload hook resulted in coupling of the axes of motion and increased the time required to damp the payload oscillations. Direct measurement of crane cable angle would not be sensitive to twisting of the payload hook.

Finally, the hardware used to implement the control systems would benefit from being constructed for the specific purpose of running the controllers. The processor and interface hardware were selected for the flexibility which they would afford during the design process. However, the functions of the interface circuits and the A/D and DAC function could be incorporated into less space once the final design for the controller had been specified. Also, the size of processor board itself could be reduced by specifying an application-specific version of the processor for production by the manufacturer of the processor. Given these refinements, the entire controller, excluding the motor drive system, could be constrained in the pendant control.

The results of the work to control vibrations of the payload for the IPD crane were very successful. The overall response of the system does suggest some potential future work.

Bibliography

Bibliography

[1] Neil C. Singer and Warren P. Seering, "Using Acausal Shaping Techniques to Reduce Robot Vibration," *Proceedings of the 1988 International Conference on Robotics and Automation, Philadelphia, PA. April 25-29, 1988.*

[2] Neil C. Singer and Warren P. Seering, "Preshaping Command Inputs to Reduce System Vibration," *ASME Journal of Dynamic Systems Measurement and Control, March 1990, pp. 76-82.*

[3] Neil C. Singer and Warren P. Seering, "Design and Comparison of Command Shaping Methods for Controlling Residual Vibration," *Proceedings of the 1989 IEEE International Conference on Robotics and Automation, Scottsdale, AZ. May 14-19, 1989.*

[4] William E. Singhose, Warren P. Seering, and Neil C. Singer, "Shaping Inputs to Reduce Vibration: A Vector Diagram Approach," *Proceedings of the 1990 IEEE International Conference on Robotics and Automation.*

[5] James M. Hyde and Warren P. Seering, "Using Input Command Pre-Shaping to Suppress Multiple Mode Vibration," *Proceedings of the 1991 IEEE International Conference on Robotics and Automation, Sacramento, CA. April 1991.*

[6] Neil C. Singer and Warren P. Seering, "An Extension of Command Shaping Methods for Controlling Residual Vibration Using Frequency Sampling," *Proceedings of the 1992 IEEE International Conference on Robotics and Automation, Nice France, May 1992.*

[7] James F. Jones and Ben J. Petterson, "Oscillation Damped Movement of Suspended Objects," *Proceedings of the IEEE International Conference on Robotics and Automation, Philadelphia, PA. April 25-29, 1988.*

[8] Ben J. Petterson, Rush D. Robinett, and Jill C. Werner, "Parameter Scheduled Trajectory Planning for Suppression of Coupled Horizontal and Vertical Vibrations in a Flexible Rod," 1990.

[9] Mark W. Noakes, Ben J. Petterson, and Jill C. Werner, "An Application of Oscillation Damped Motion for Suspended Payloads to the Advanced Integrated Maintenance System," *Proceedings of the 38th Conference on Remote System Technology, 1990, vol. 1.*

[10] Mark W. Noakes and John F. Jansen, "Shaping Inputs to Reduce Vibration for Suspended Payloads," *Proceedings of the 1991 American Nuclear Society Conference, Feb. 24-28, 1991.*

[11] John F. Jansen, "Control and Analysis of a Single-Link Flexible Beam With Experimental Verification," *ORNL/TM-12198, Dec. 1992.*

[12] Brett R. Murphy and Ichiro Watanabe, "Digital Shaping Filters for Reducing Machine Vibration," *IEEE Transactions on Robotics and Automation, April 1992, vol. 8, No. 2, pp. 285-289.*

[13] Adel S. Sedra and Kenneth C. Smith, "*Microelectronic Circuits*", Holt, Rinehart and Wilson, Fort Worth, Texas 1987.

[14] Ernest O. Doebelin, "*Measurement Systems: Application and Design*," Fourth Edition, McGraw-Hill, Inc., New York, pp 341–344.

[15] Bahram Shahian and Michael Hassul, *Control System Design Using MATLAB®*, Prentice-Hall, Inc., Englewood Cliffs, New Jersey, 1993.

[16] Benjamin C. Kuo, *Automatic Control Systems.* Prentice Hall, Englewood Cliffs, New Jersey, 1991.

[17] Alan V. Oppenheim and Ronald W. Schafer. *Discrete-Time Signal Processing.* Prentice Hall, Englewood Cliffs, New Jersey, 1989.

Appendices

Appendix A

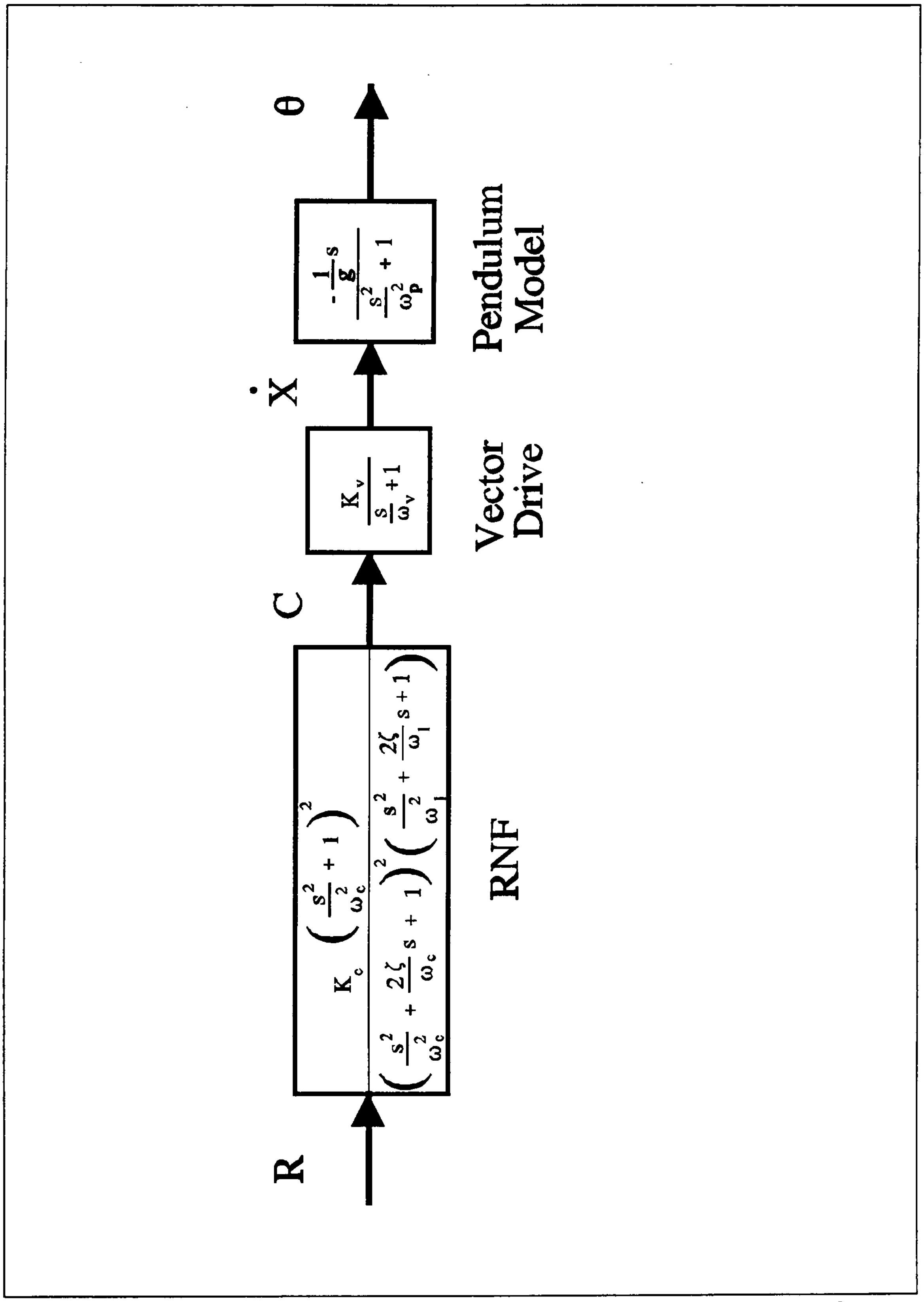

Figure 4.1: *Block Diagram for open-loop input shaping using Robust Notch Filter.*

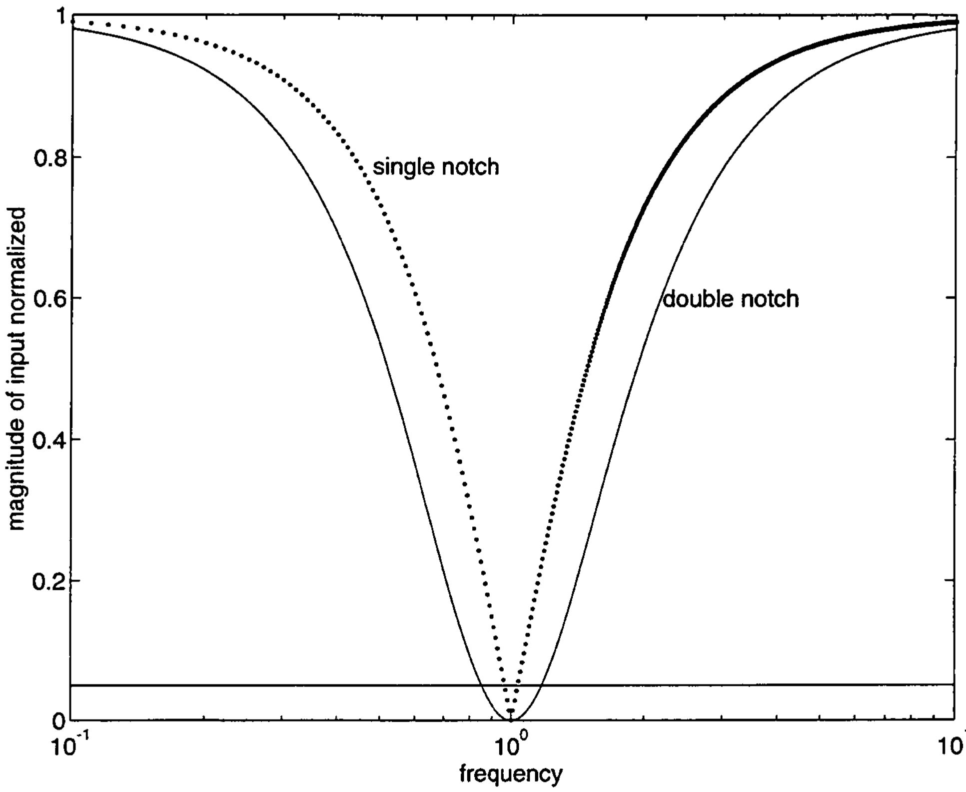

Figure 4.2: *Input signal attenuation by a single (dotted line) and double (continuous line) second-order notch filter.*

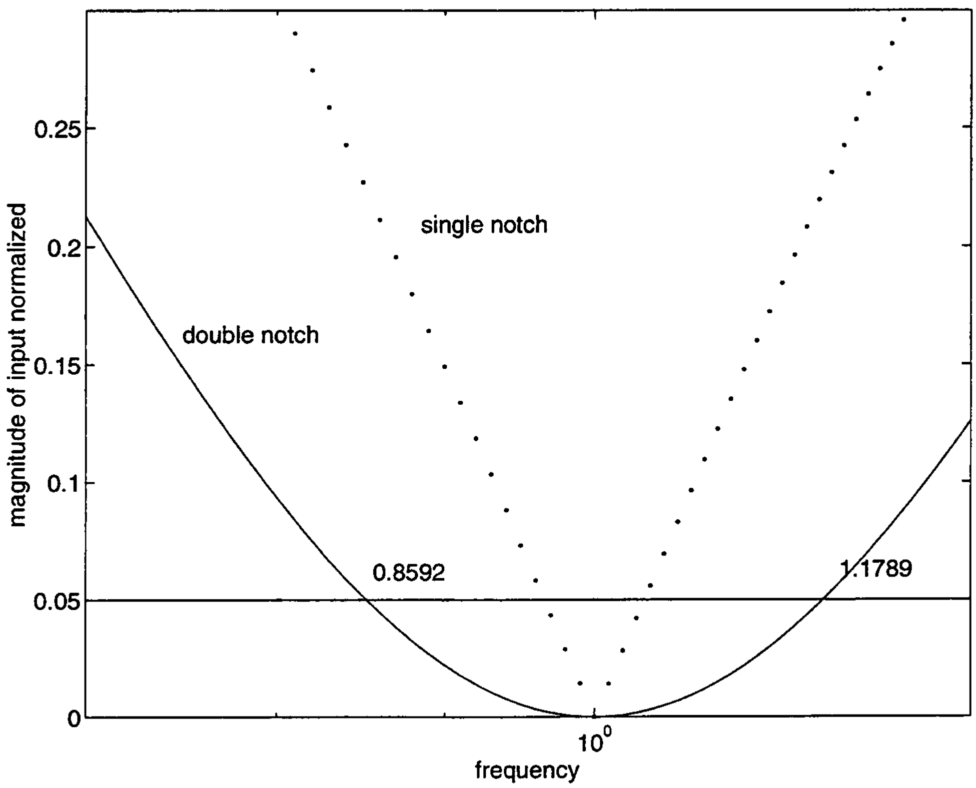

Figure 4.3: *Detail of single and double second-order notch filter attenuation: Horizontal line indicates 5% of initial magnitude.*

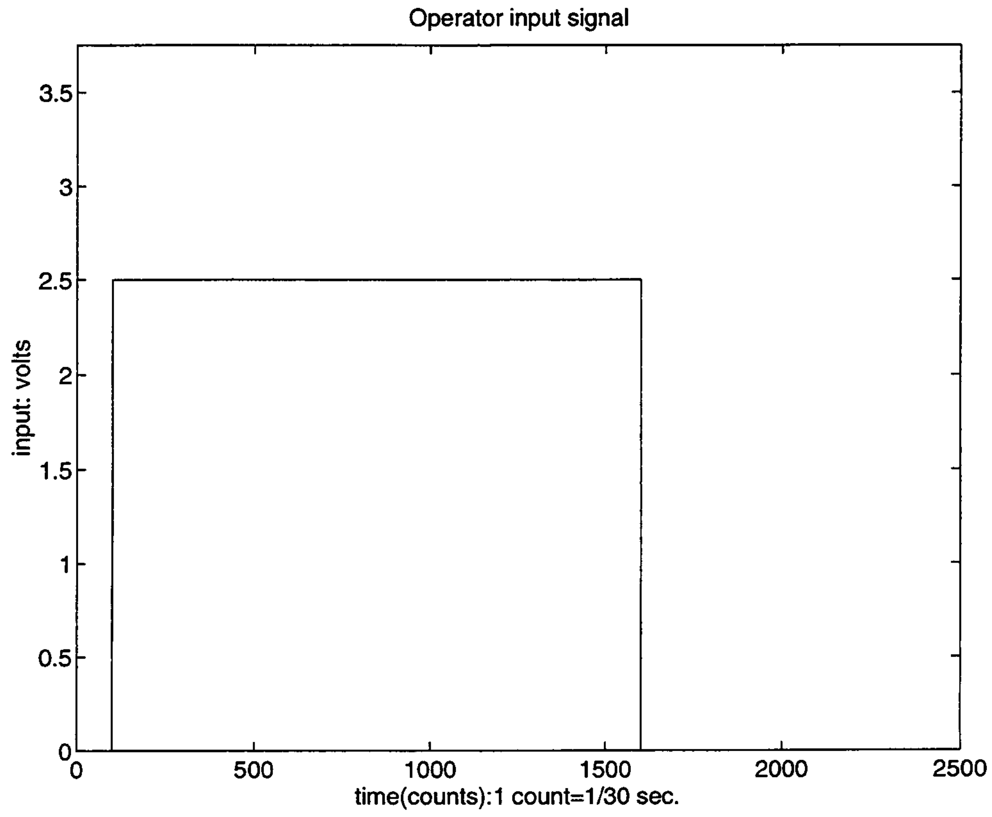

Figure 4.4: *Open loop system step input to system where* $\omega_{filter} = \omega_{crane}$.

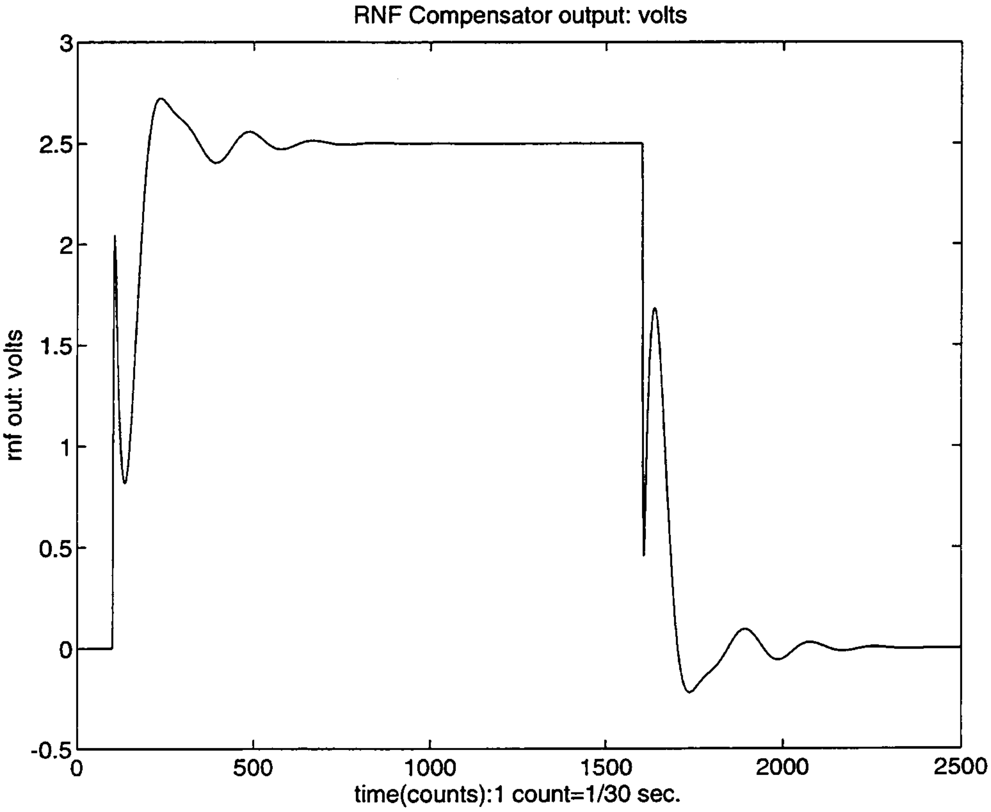

Figure 4.5: *Open loop system compensator output for step input where* $\omega_{filter} = \omega_{crane}$.

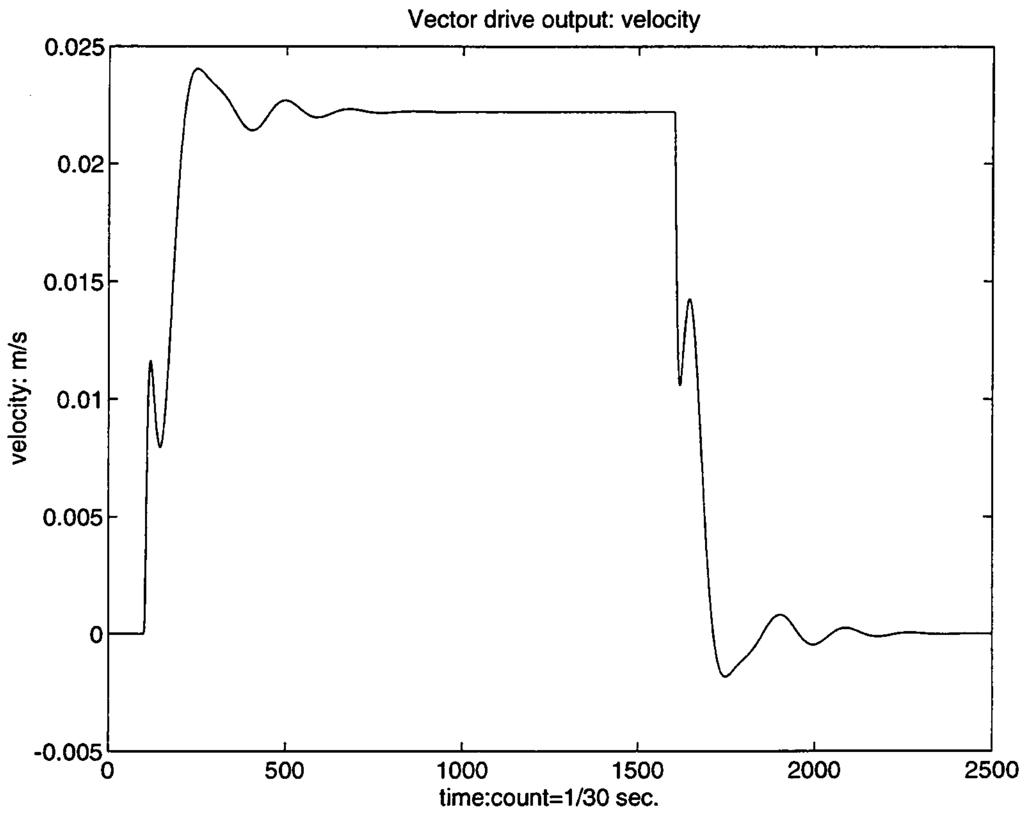

Figure 4.6: *Open loop system vector drive output for step input where* $\omega_{filter} = \omega_{crane}$.

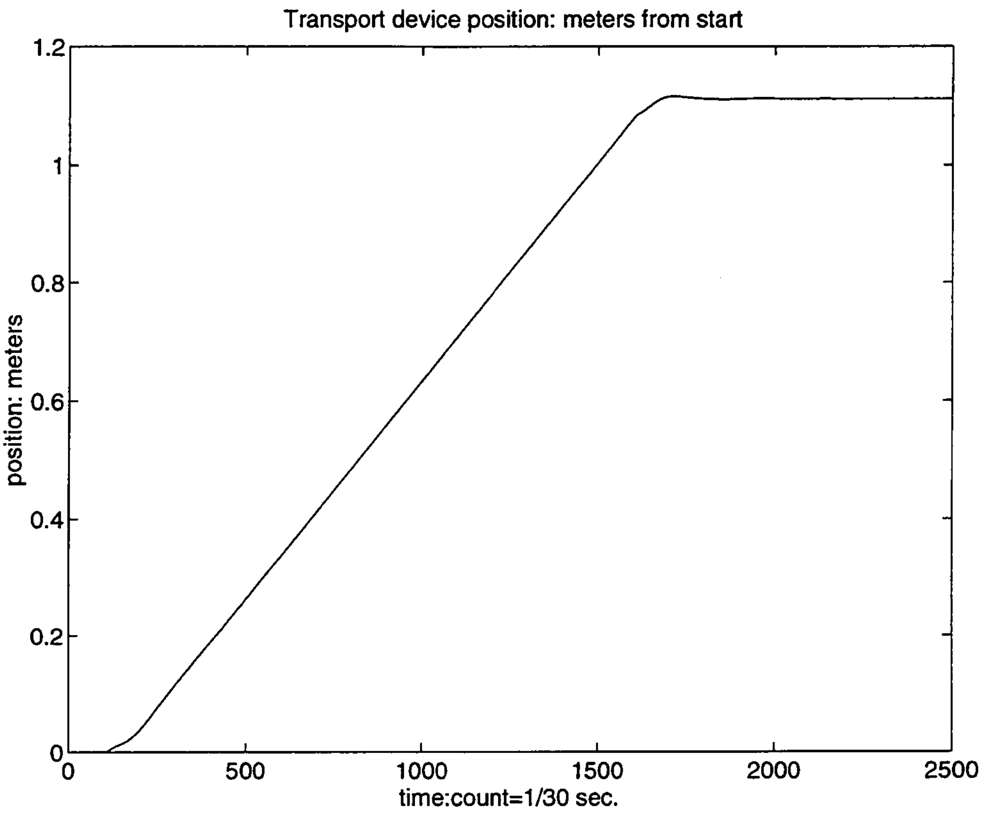

Figure 4.7: *Open loop system carrier position for step input where* $\omega_{filter} = \omega_{crane}$.

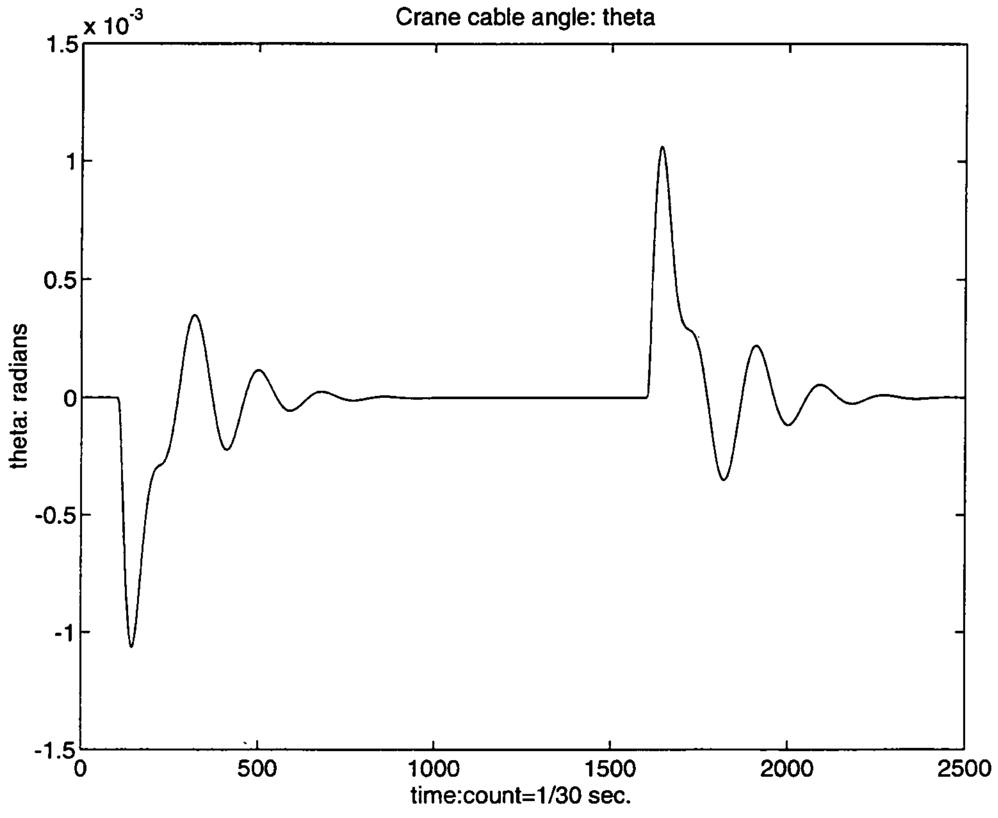

Figure 4.8: *Open loop system crane theta for step input where* $\omega_{filter} = \omega_{crane}$.

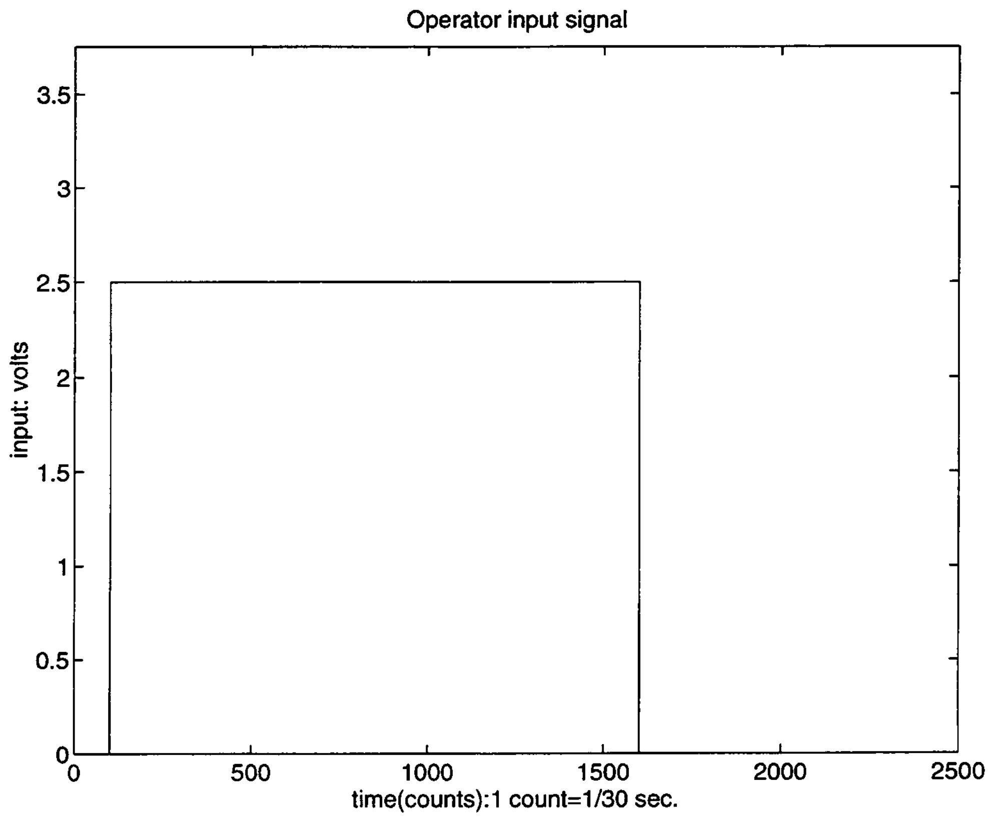

Figure 4.9: *Open loop system step input where* $\omega_{filter} = 0.65\omega_{crane}$.

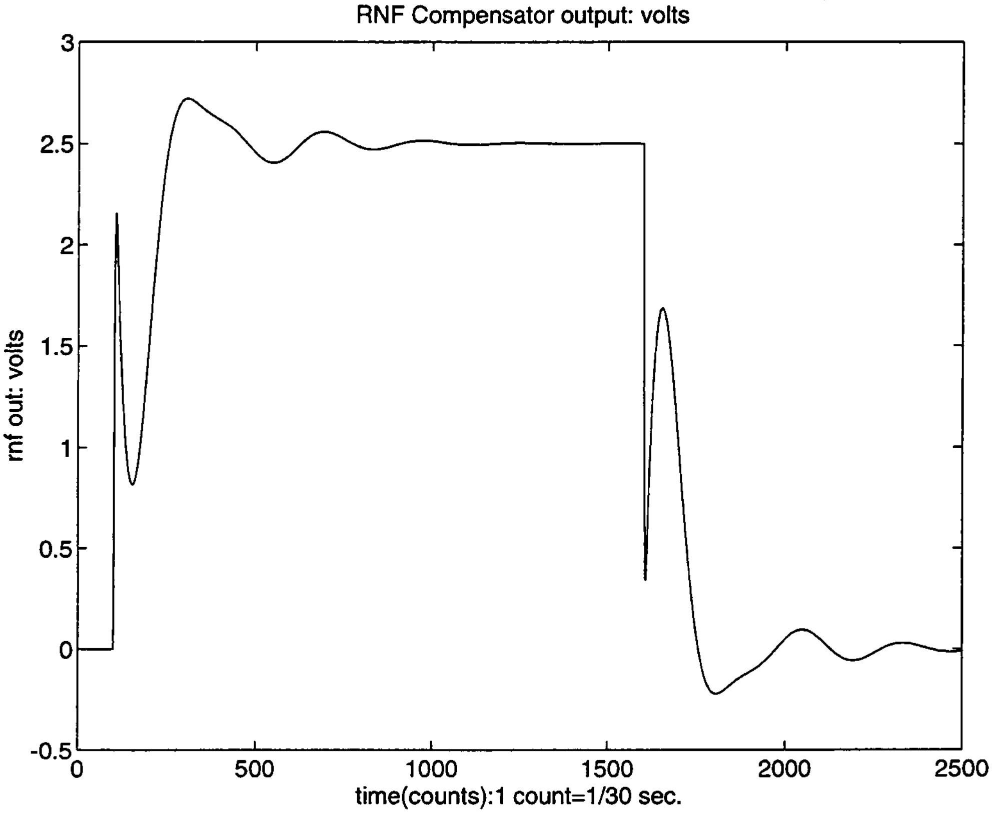

Figure 4.10: *Open loop system compensator output for step input where* $\omega_{filter} = 0.65\omega_{crane}$.

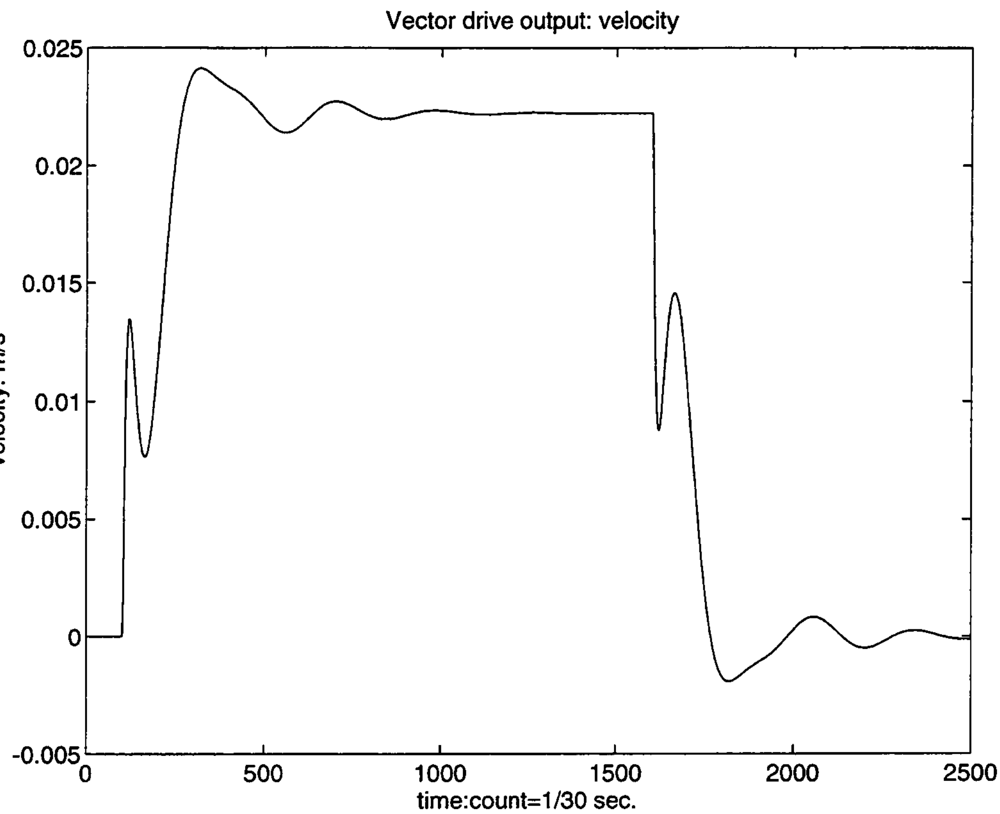

Figure 4.11: *Open loop system vector drive output for step input where*

$\omega_{filter} = 0.65\omega_{crane}$.

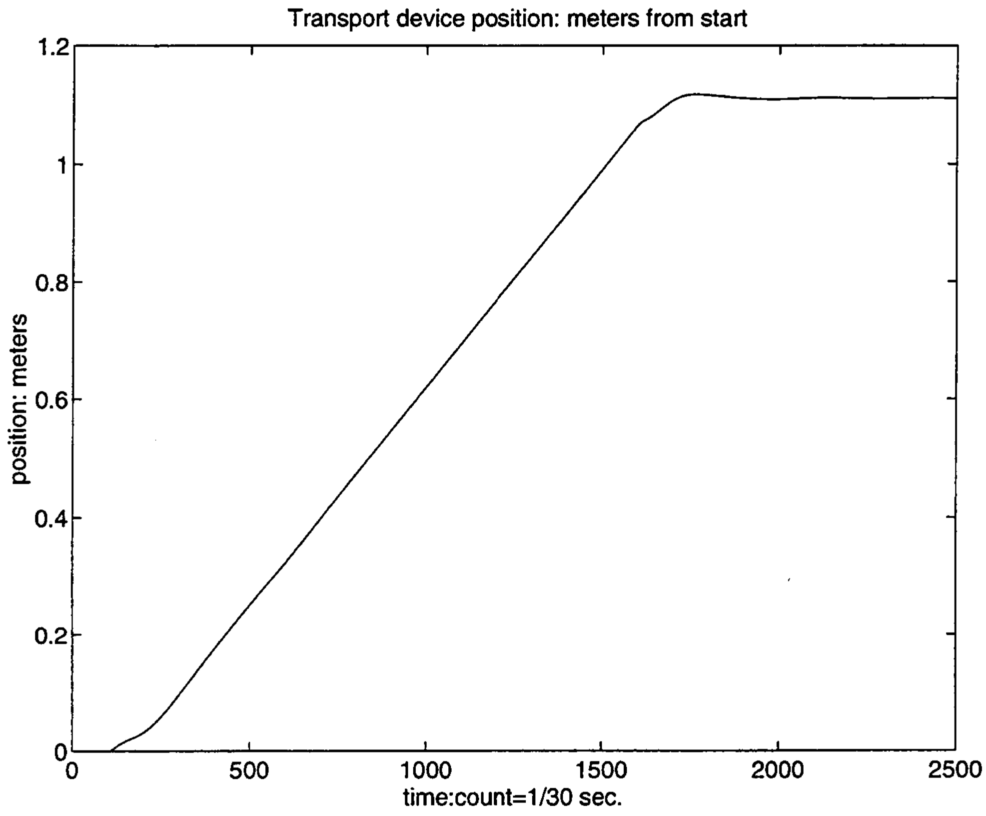

Figure 4.12: *Open loop system carrier position for step input where* $\omega_{filter} = 0.65\omega_{crane}$.

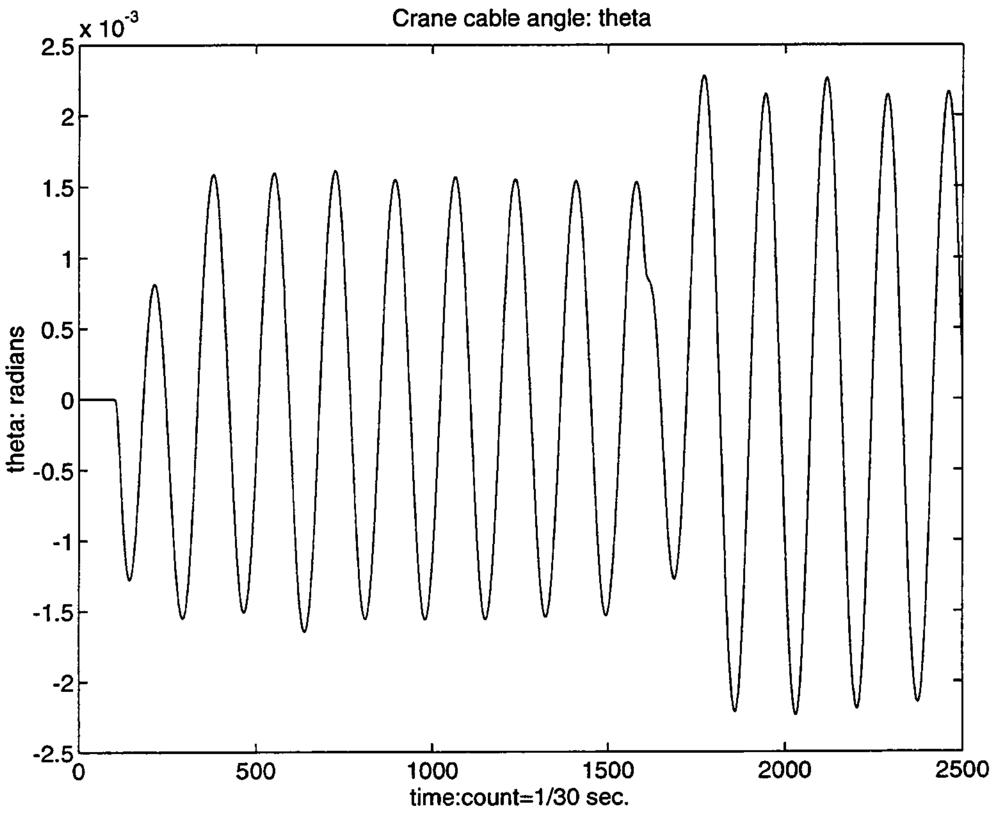

Figure 4.13: *Open loop system crane theta for step input where* $\omega_{filter} = 0.65\omega_{crane}$.

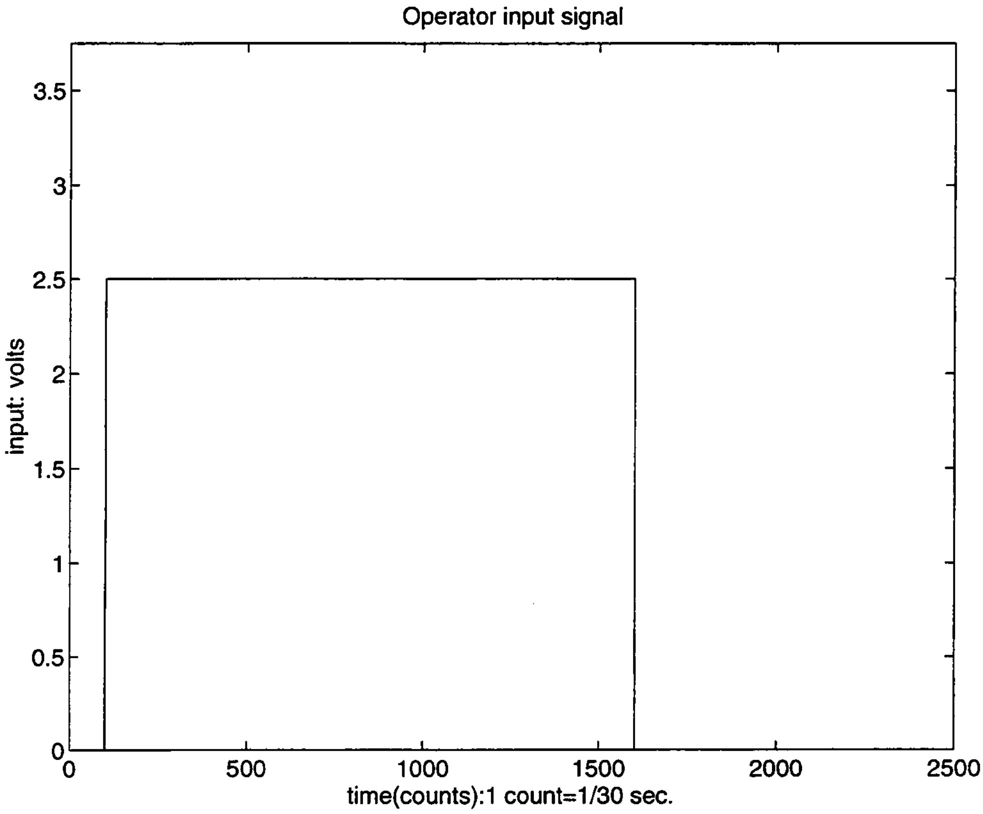

Figure 4.14: *Open loop system step input where* $\omega_{filter} = 1.40\omega_{crane}$.

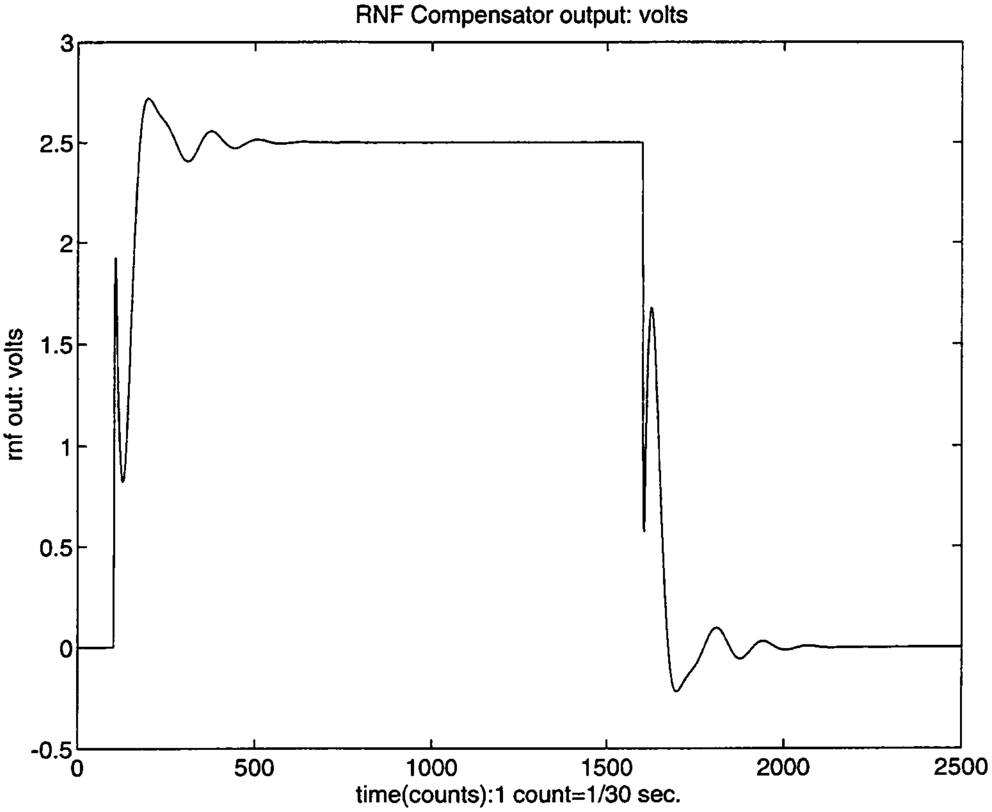

Figure 4.15: *Open loop system compensator output for step input where*

$\omega_{filter} = 1.40\omega_{crane}$.

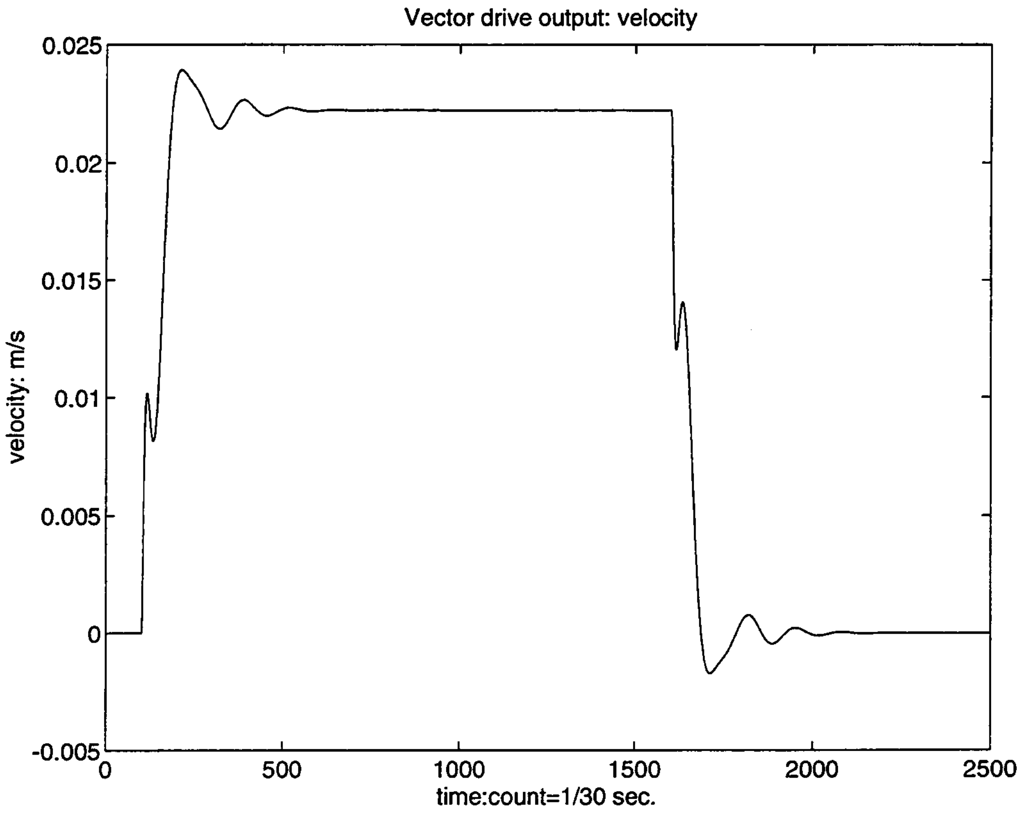

Figure 4.16: *Open loop system vector drive output for step input where* $\omega_{filter} = 1.40\omega_{crane}$.

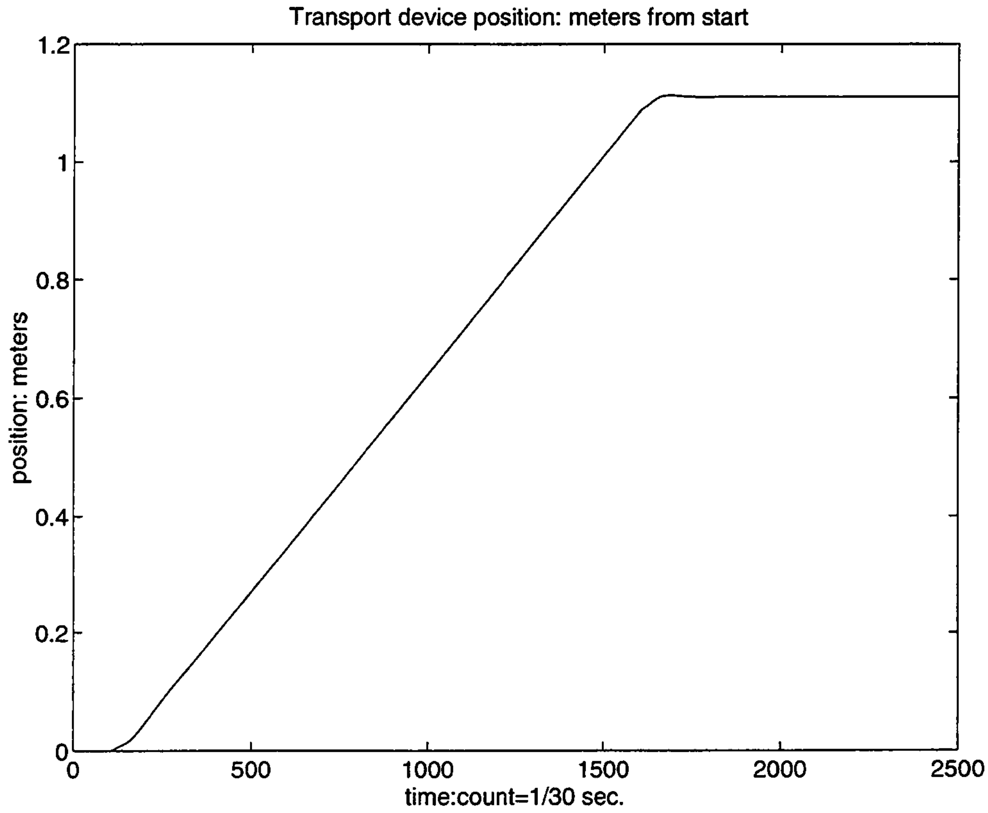

Figure 4.17: *Open loop system carrier position for step input where* $\omega_{filter} = 1.40\omega_{crane}$.

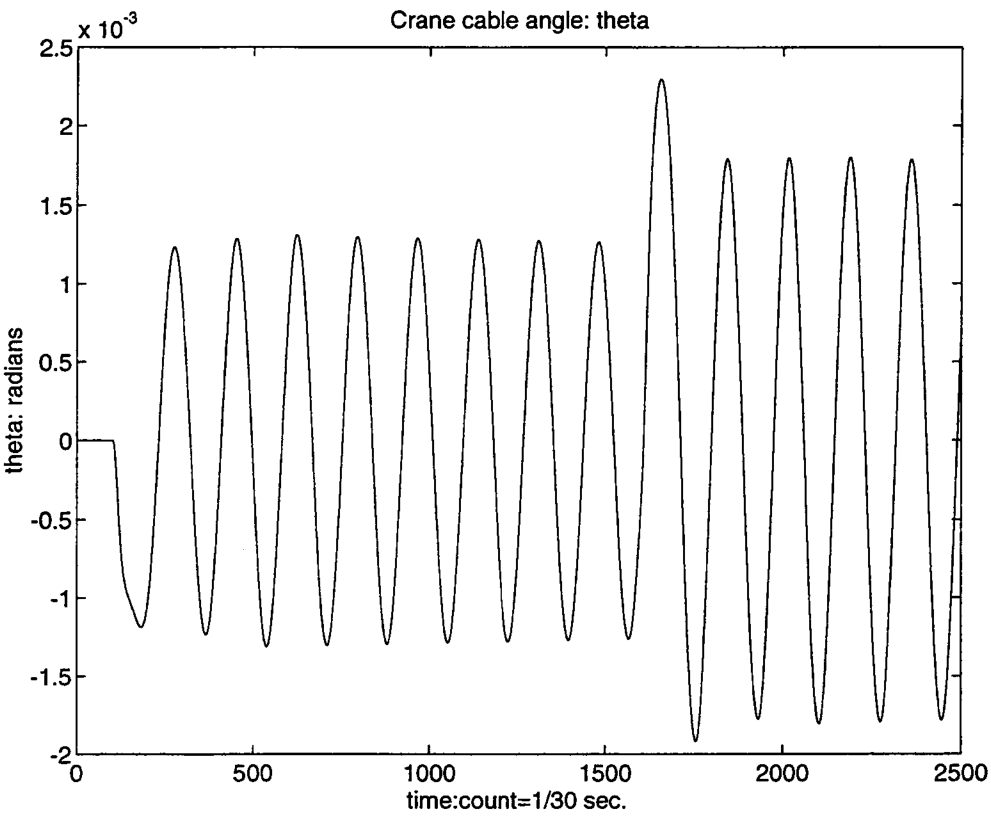

Figure 4.18: *Open loop system crane theta for step input where* $\omega_{filter} = 1.40\omega_{crane}$.

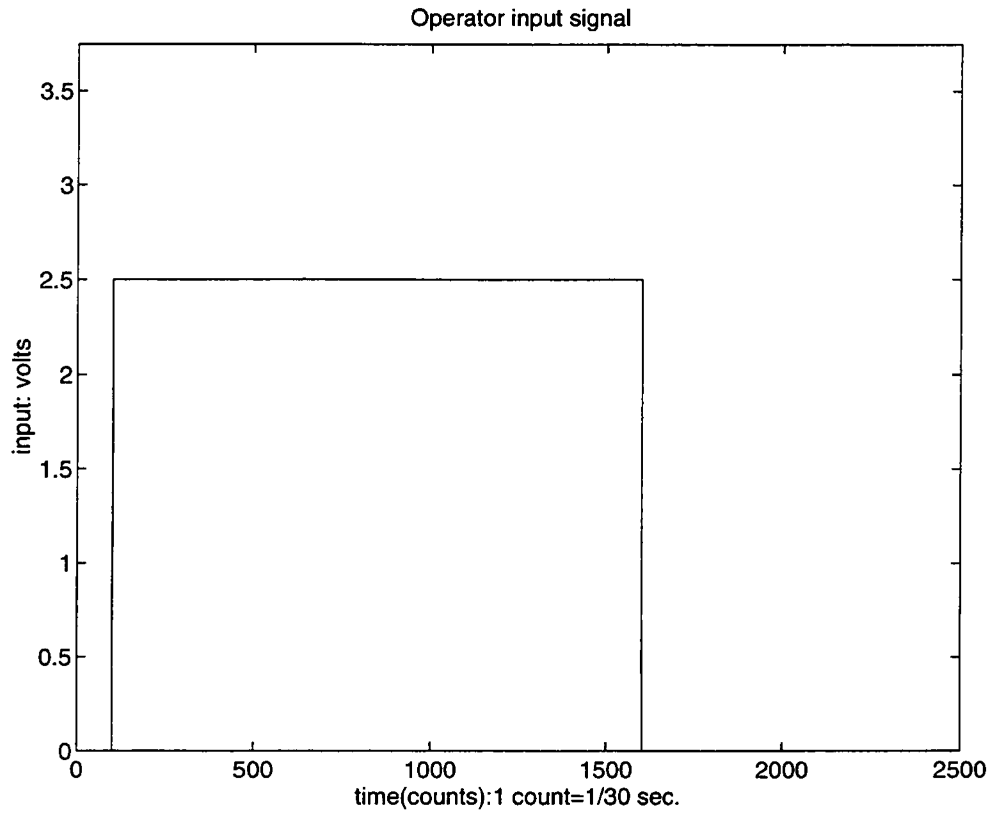

Figure 4.19: *Open loop system ramp input where* $\omega_{filter} = \omega_{crane}$.

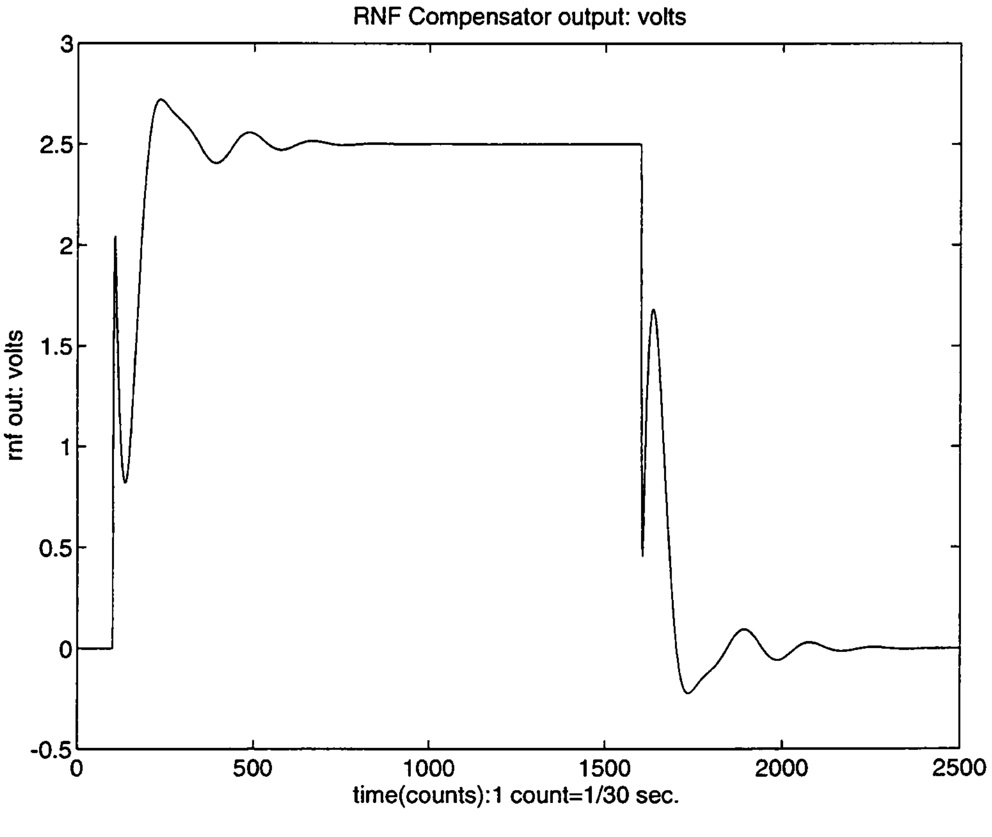

Figure 4.20: *Open loop system compensator output for ramp input where* $\omega_{filter} = \omega_{crane}$.

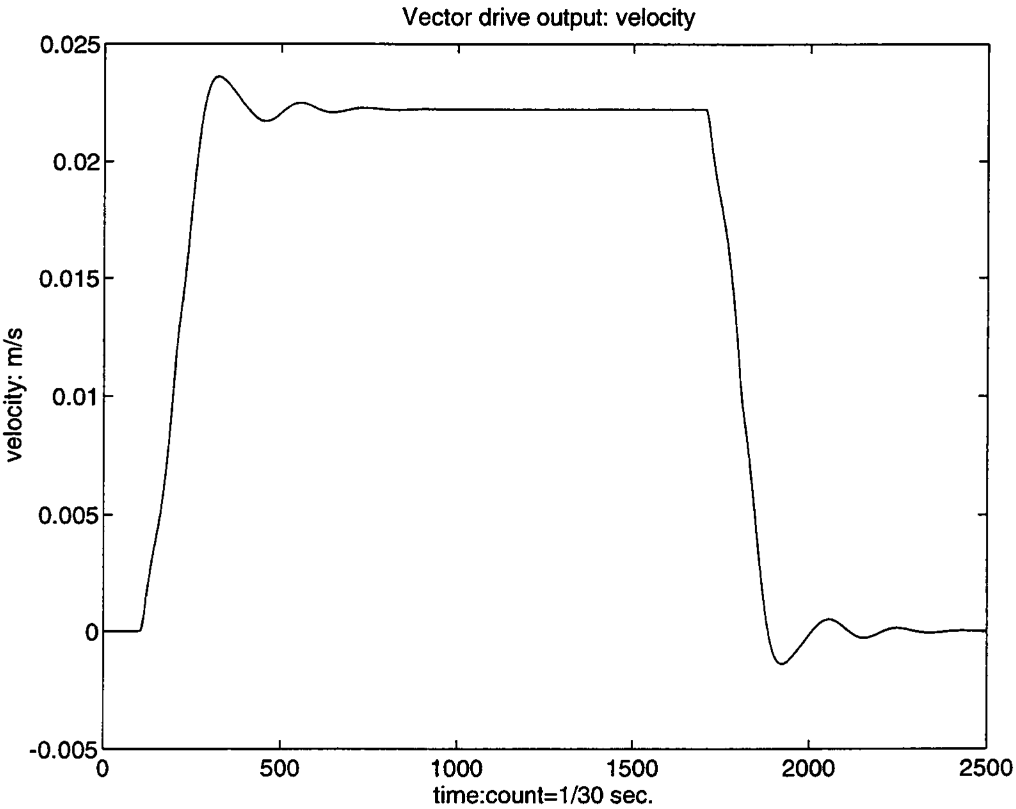

Figure 4.21: *Open loop system vector drive output for ramp input where*

$\omega_{filter} = \omega_{crane}$.

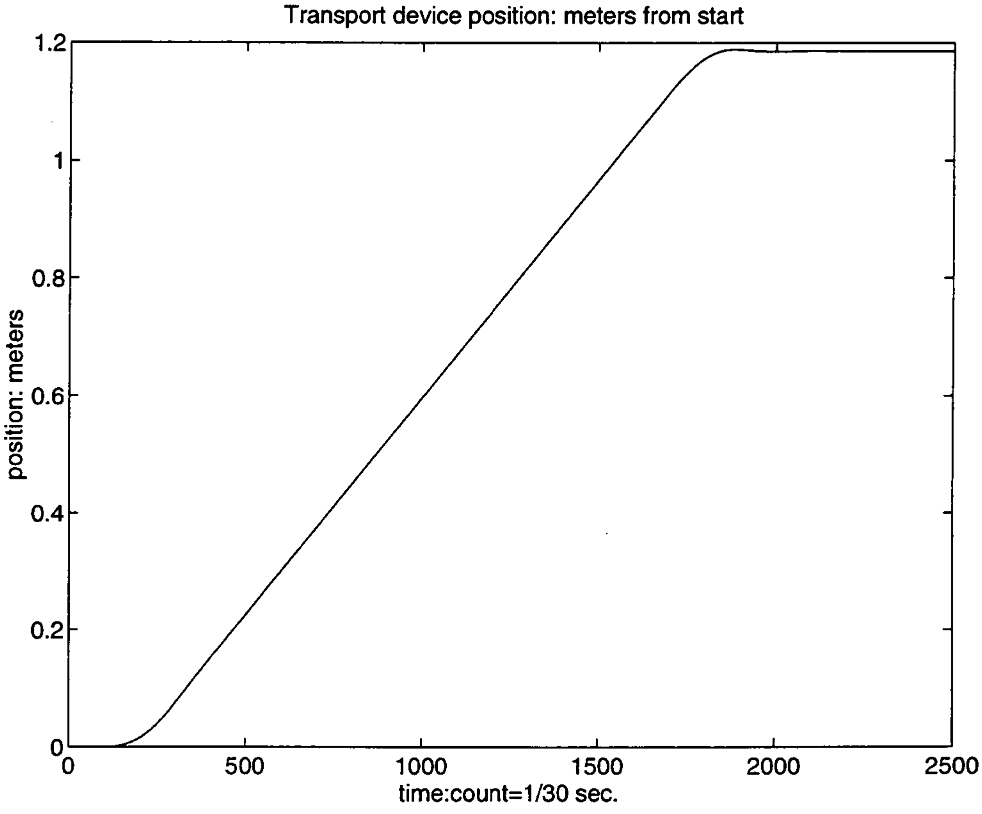

Figure 4.22: *Open-loop system carrier position for ramp input where* $\omega_{filter} = \omega_{crane}$.

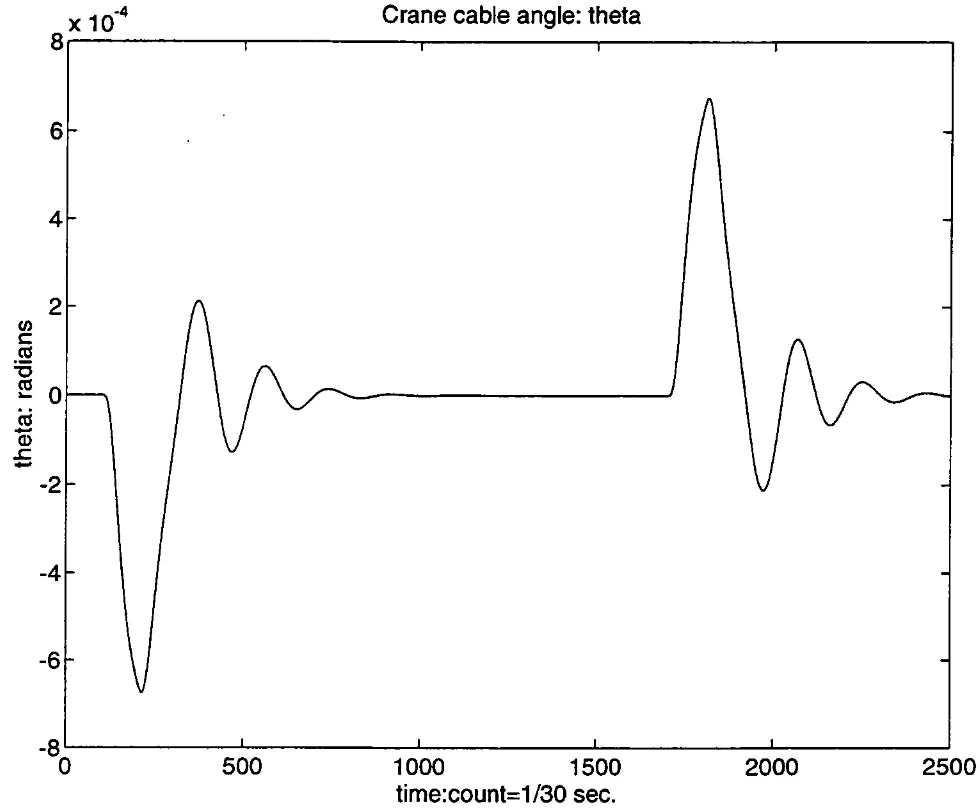

Figure 4.23: *Open-loop system crane theta for ramp input where* $\omega_{filter} = \omega_{crane}$.

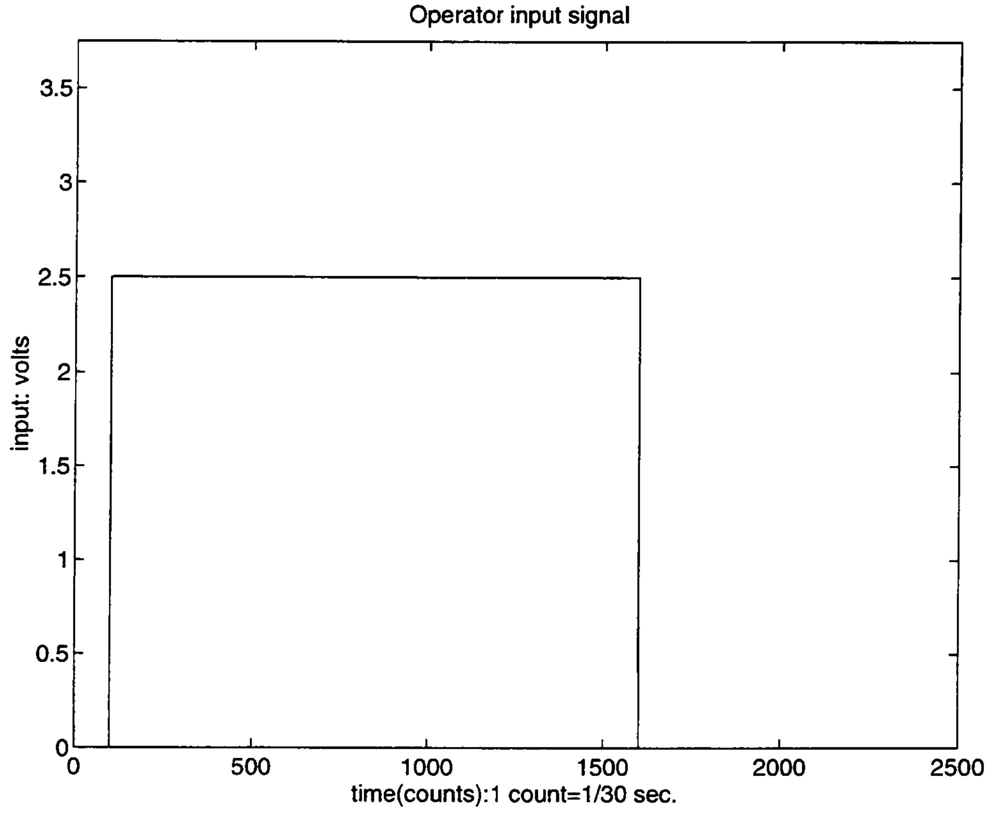

Figure 4.24: *Open-loop system ramp input where* $\omega_{filter} = 0.40\omega_{crane}$.

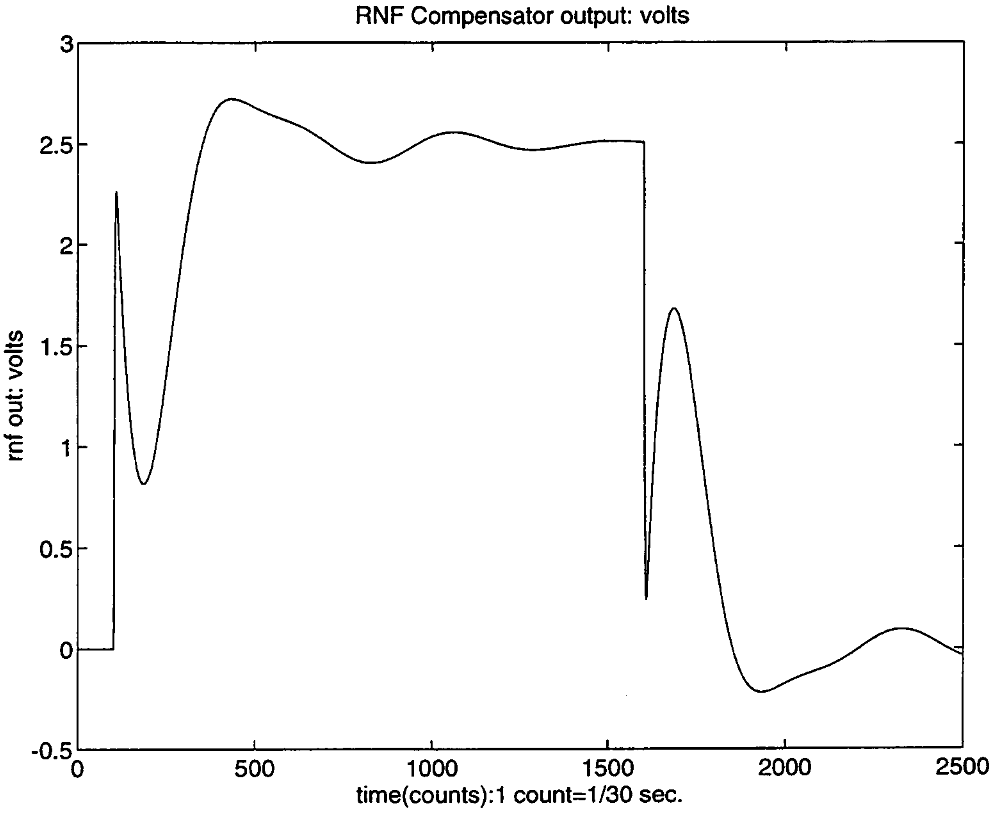

Figure 4.25: *Open-loop system compensator output for ramp input where* $\omega_{filter} = 0.40\omega_{crane}$.

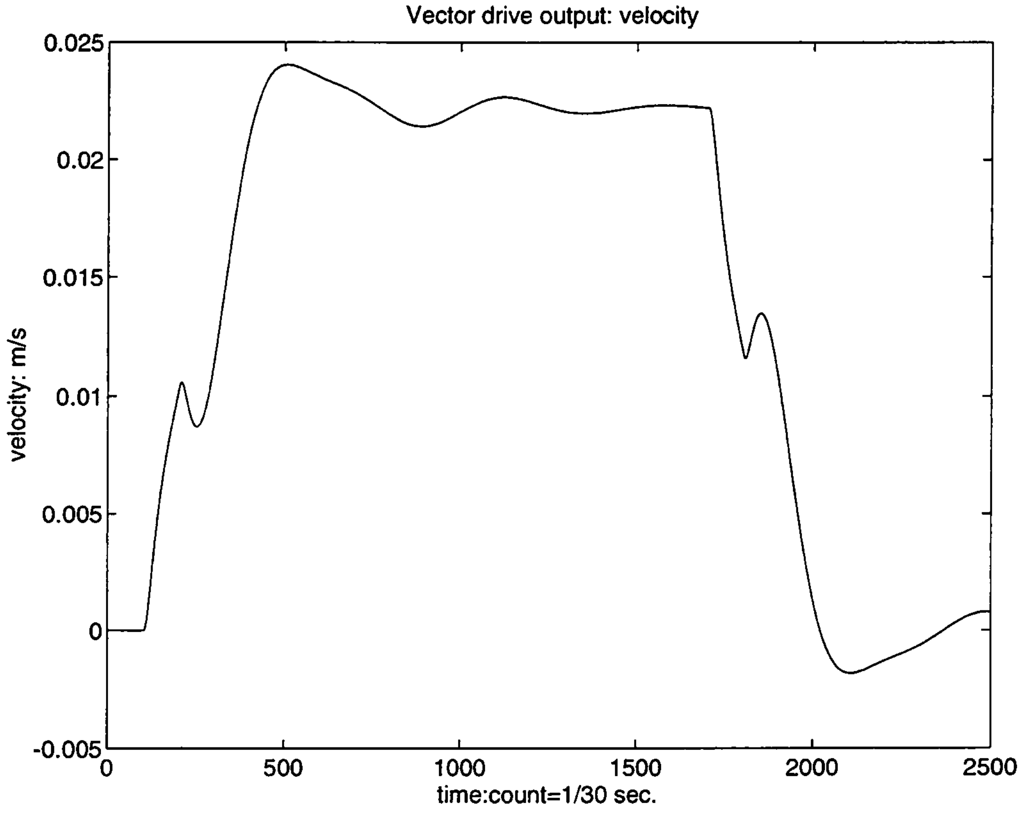

Figure 4.26: *Open-loop system vector drive output for ramp input where* $\omega_{filter} = 0.40\omega_{crane}$.

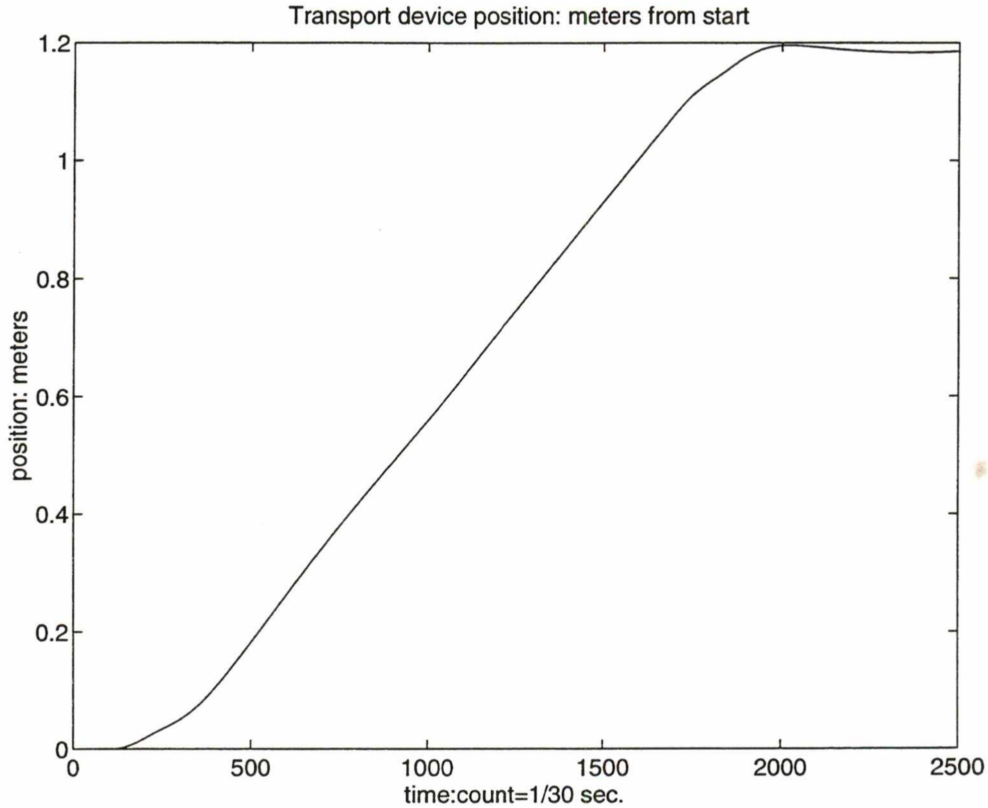

Figure 4.27: *Open-loop system carrier position for ramp input where*

$\omega_{filter} = 0.40\omega_{crane}$.

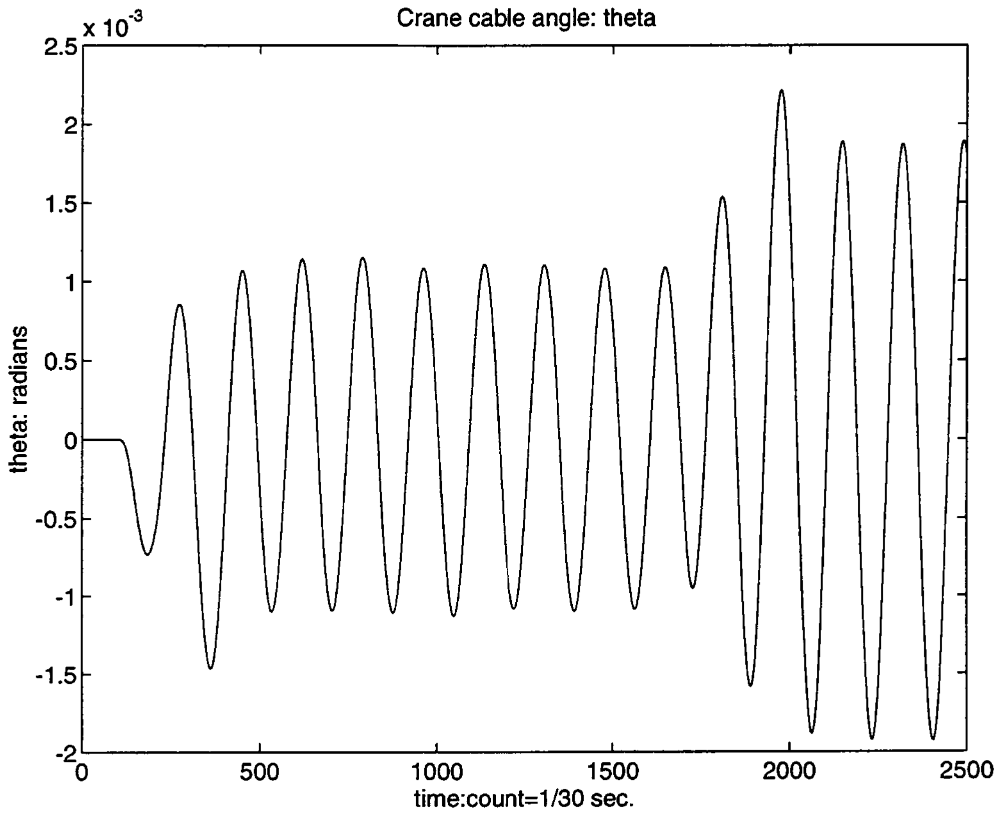

Figure 4.28: *Open-loop system crane theta for ramp input where* $\omega_{filter} = 0.40\ \omega_{crane}$.

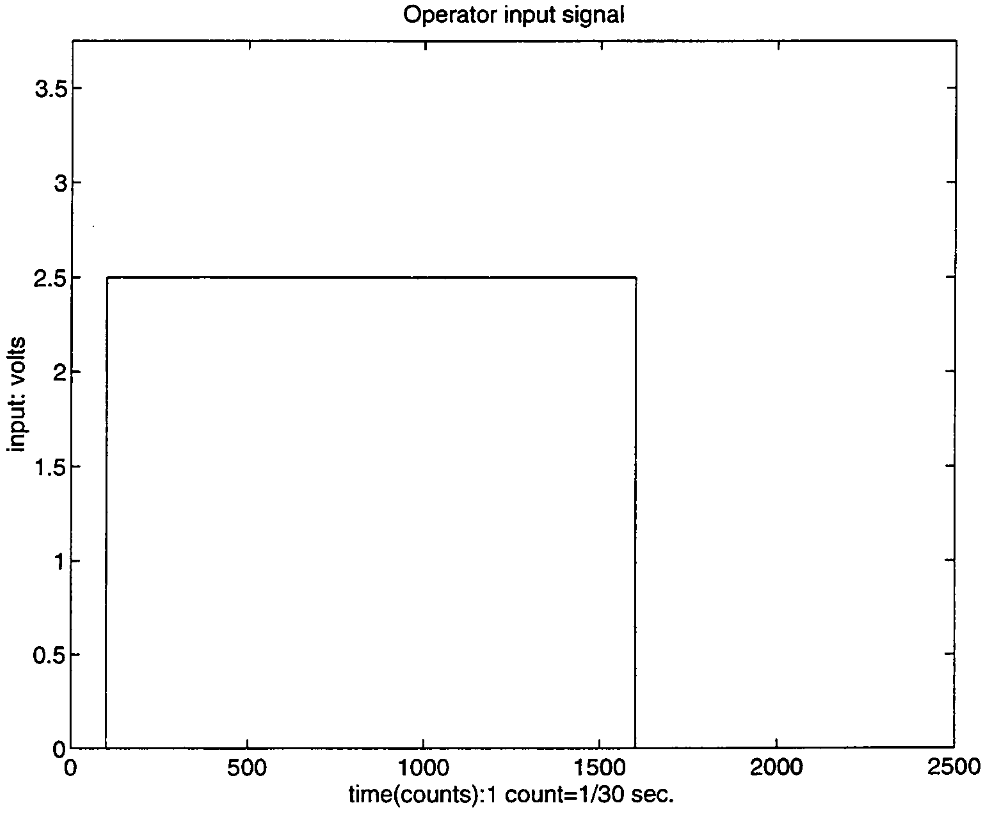

Figure 4.29: *Open-loop ramp input where* $\omega_{filter} = 2.40\omega_{crane}$.

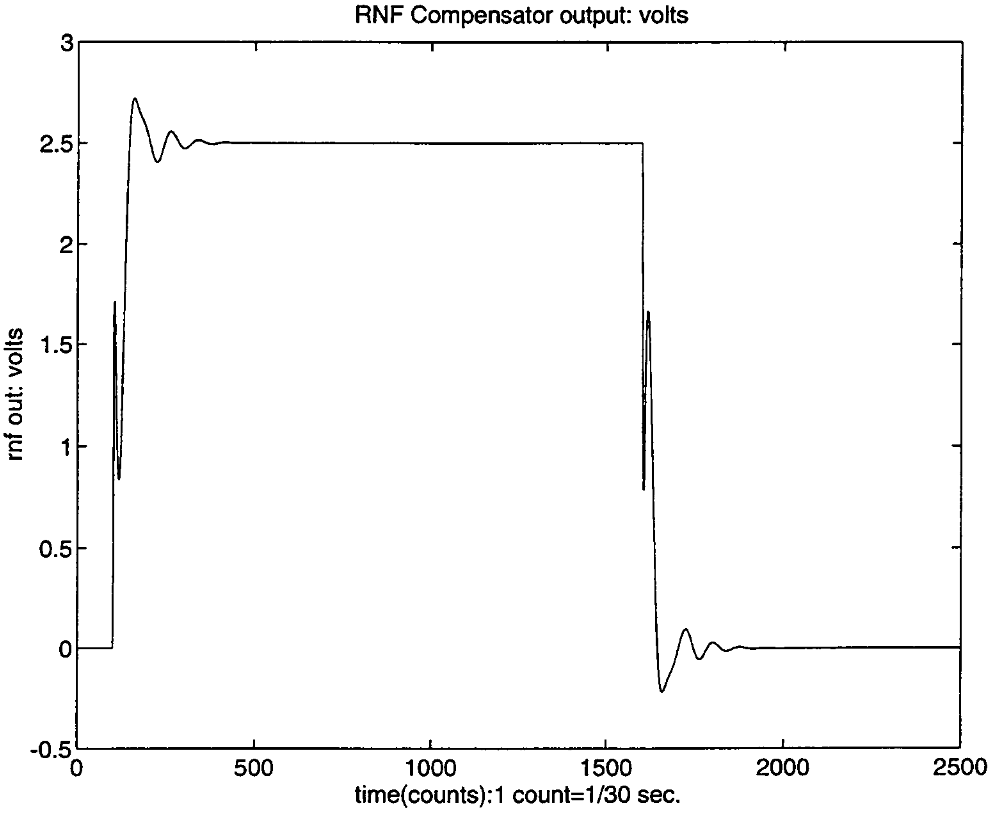

Figure 4.30: *Open-loop compensator output for ramp input where* $\omega_{filter} = 2.40\omega_{crane}$.

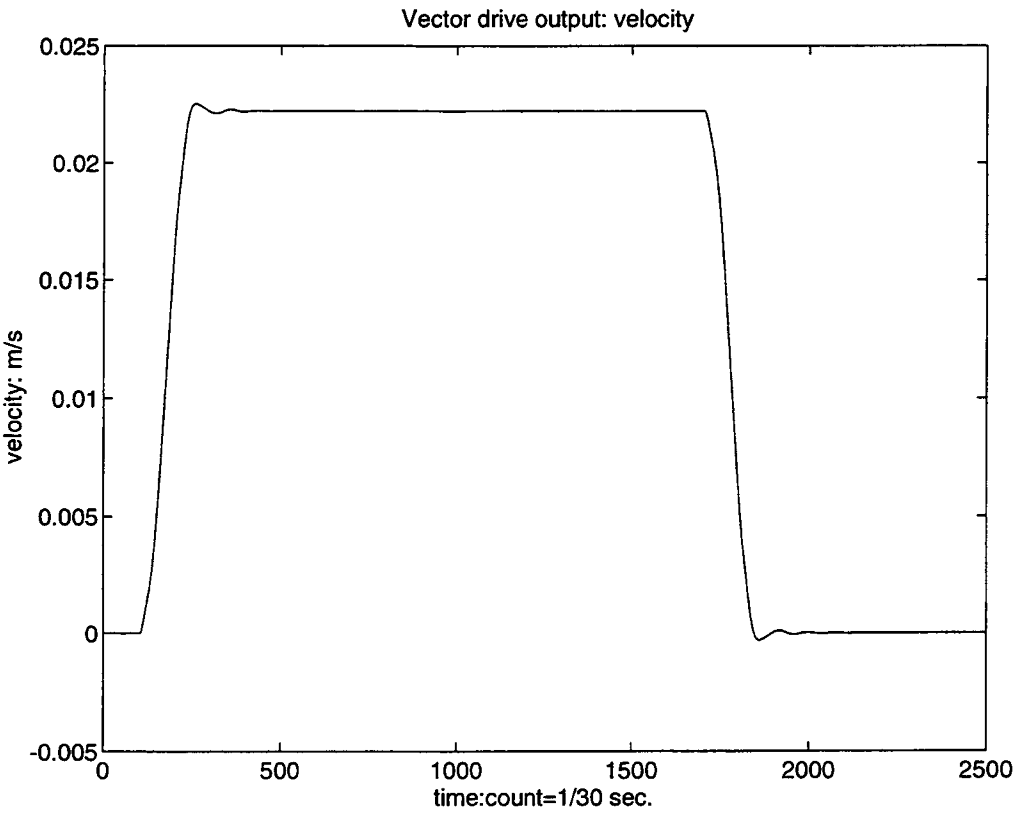

Figure 4.31: *Open-loop system vector drive output for ramp input where*

$\omega_{filter} = 2.40\omega_{crane}$.

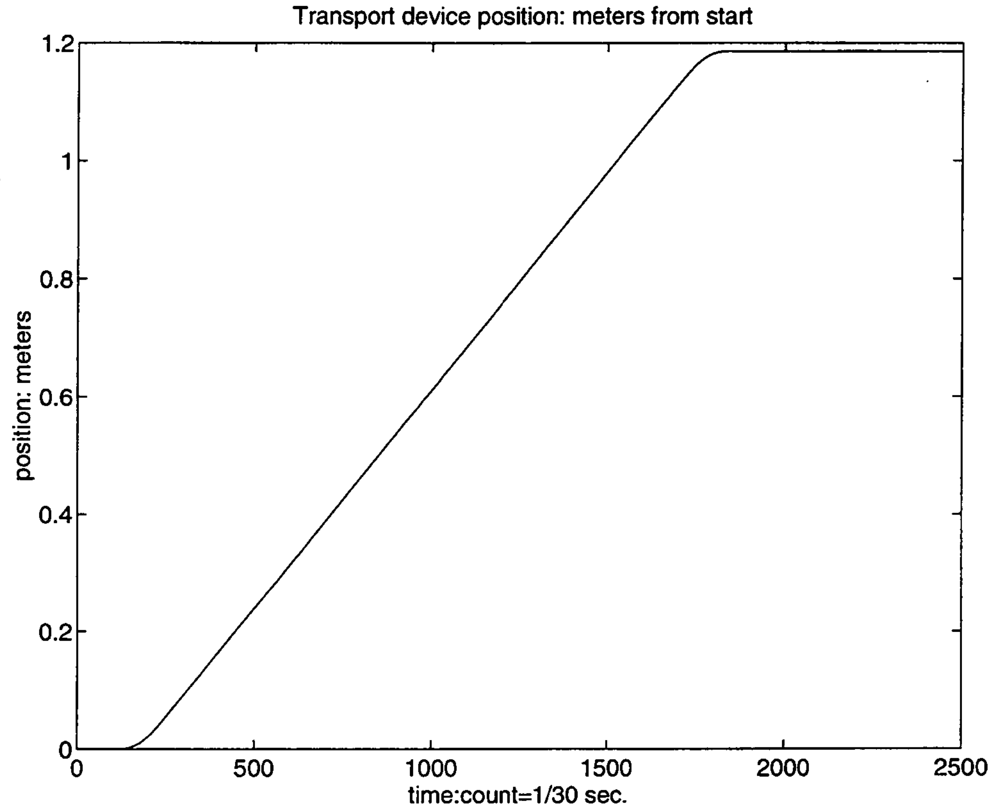

Figure 4.32: *Open-loop system crane carrier position for ramp input where* $\omega_{filter} = 2.40\omega_{crane}$.

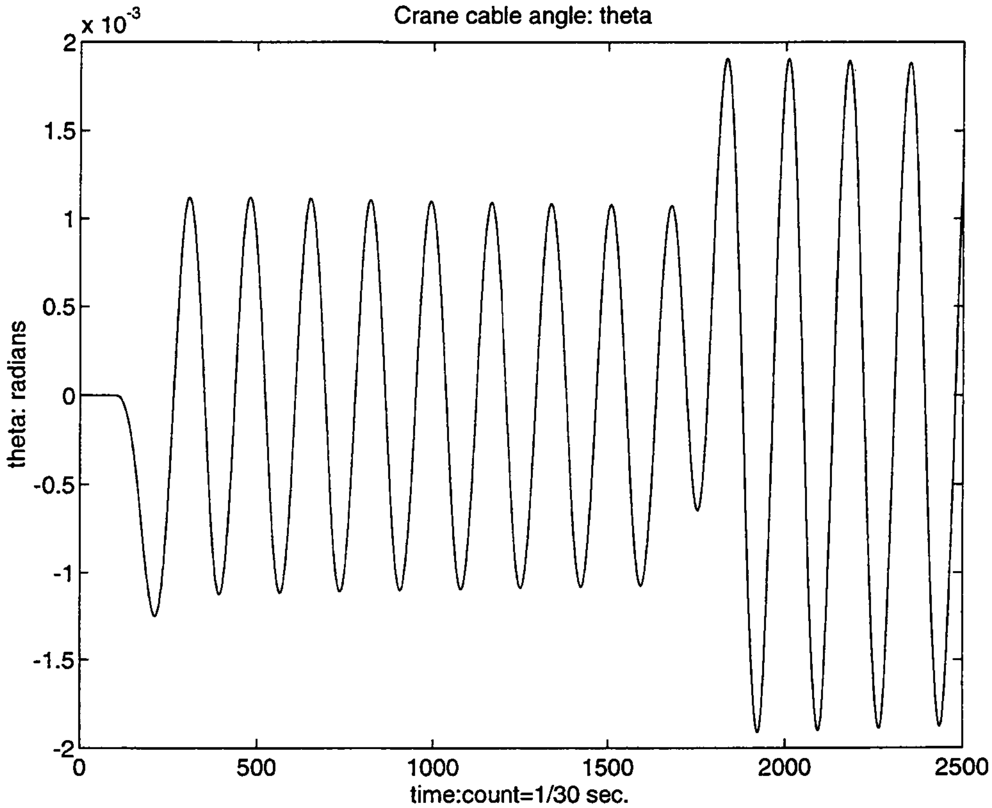

Figure 4.33: *Open-loop system crane cable angle for ramp input where* $\omega_{filter} = 2.40\omega_{crane}$.

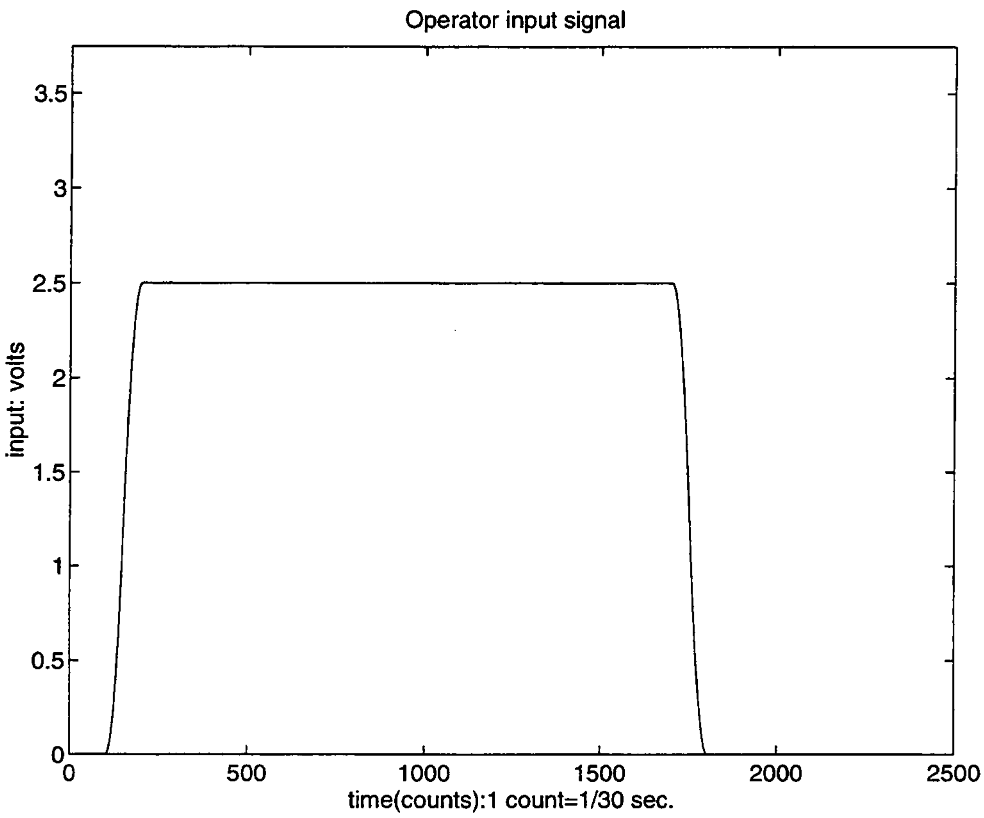

Figure 4.34: *Open-loop system parabolic input where* $\omega_{filter} = \omega_{crane}$.

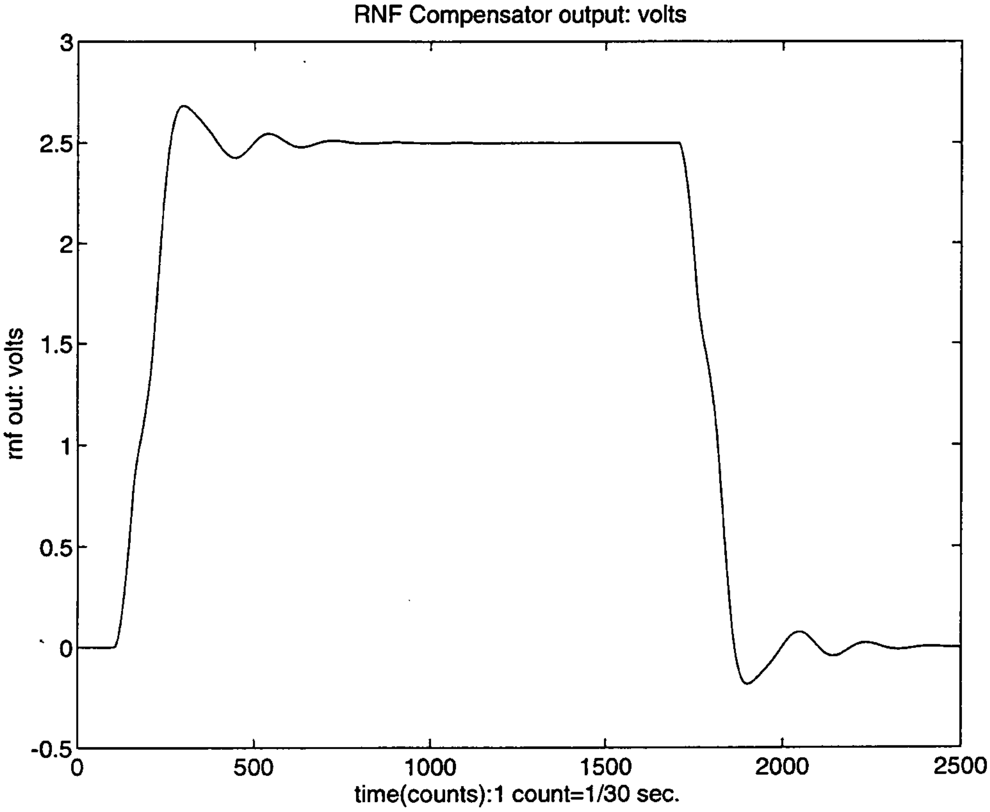

Figure 4.35: *Open-loop system compensator output for parabolic input where* $\omega_{filter} = \omega_{crane}$.

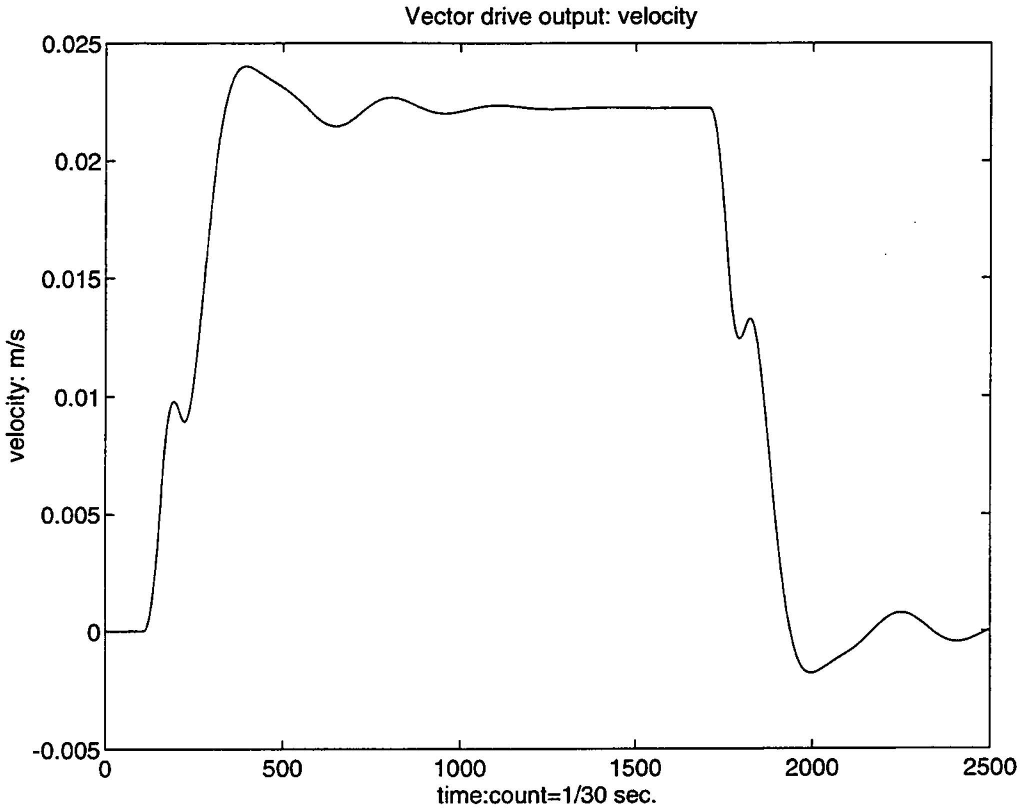

Figure 4.36: *Open-loop system vector drive output for parabolic input where*

$\omega_{filter} = \omega_{crane}$.

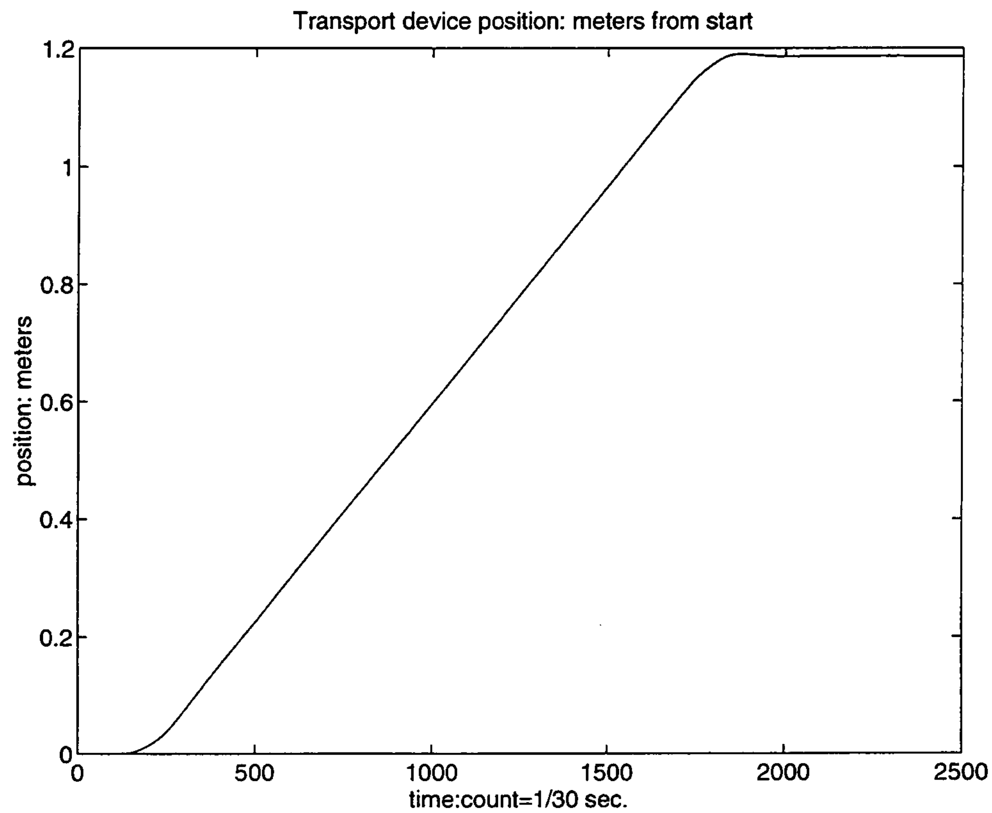

Figure 4.37: *Open-loop system crane carrier position for parabolic input where* $\omega_{filter} = \omega_{crane}$.

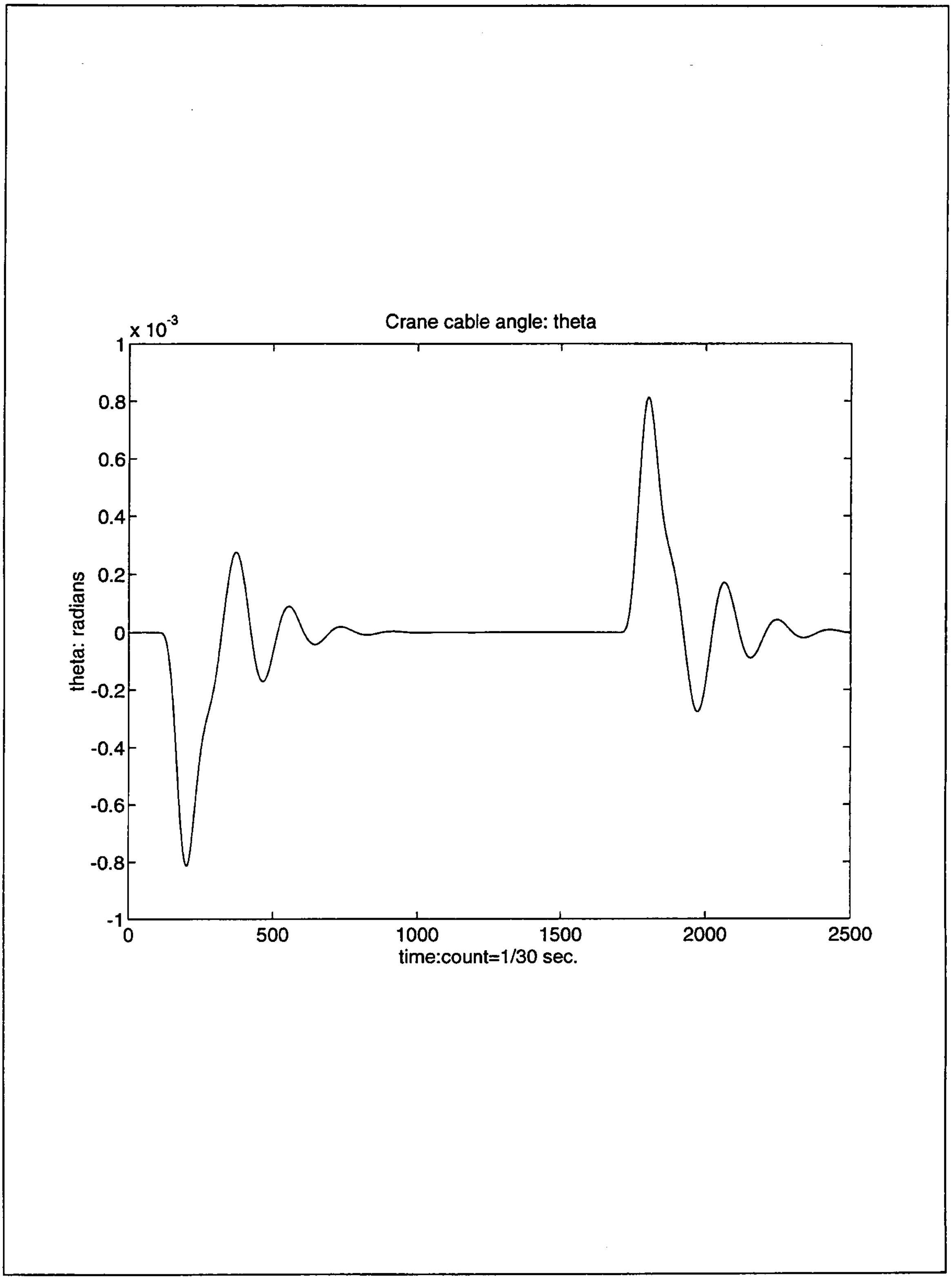

Figure 4.38: *Open-loop system crane cable angle for parabolic input where*

$\omega_{filter} = \omega_{crane}$.

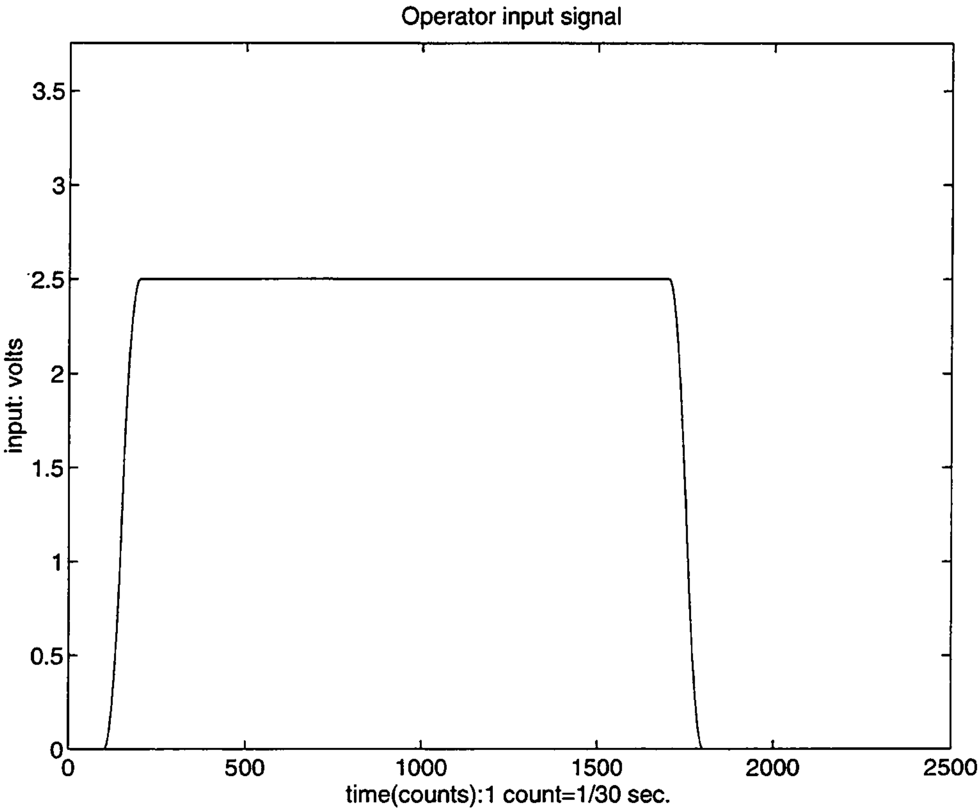

Figure 4.39: *Open-loop system parabolic input where* $\omega_{filter} = 0.60\omega_{crane}$.

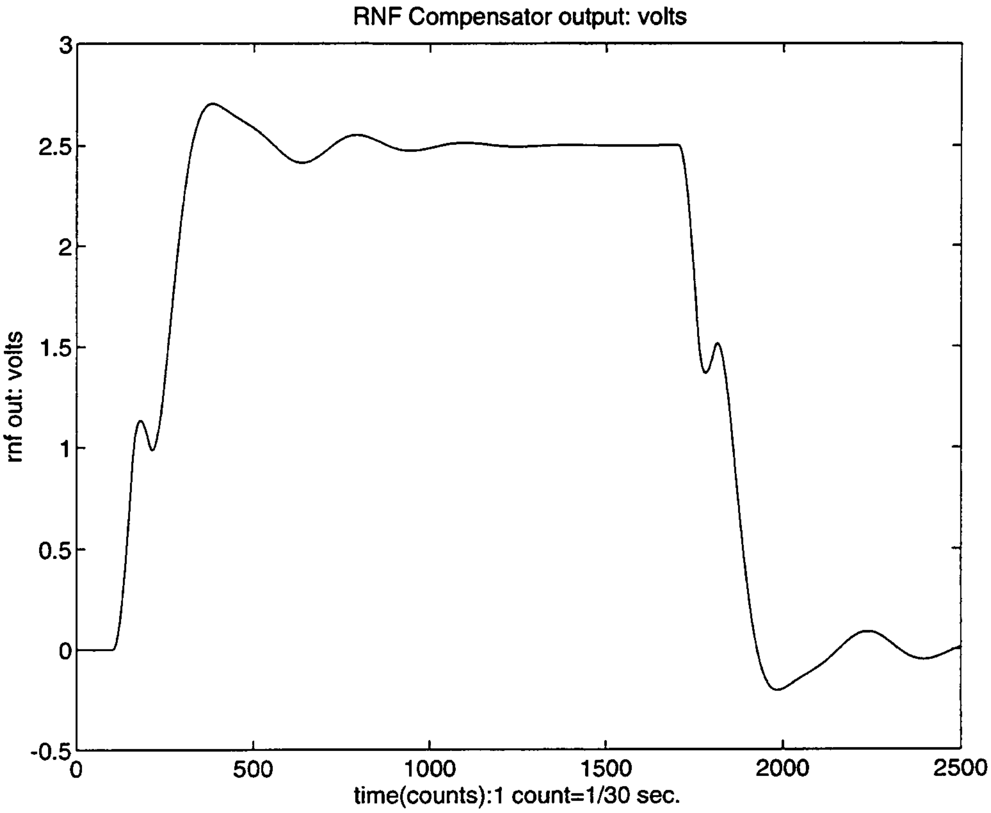

Figure 4.40: *Open-loop system compensator output for parabolic input where* $\omega_{filter} = 0.60\omega_{crane}$.

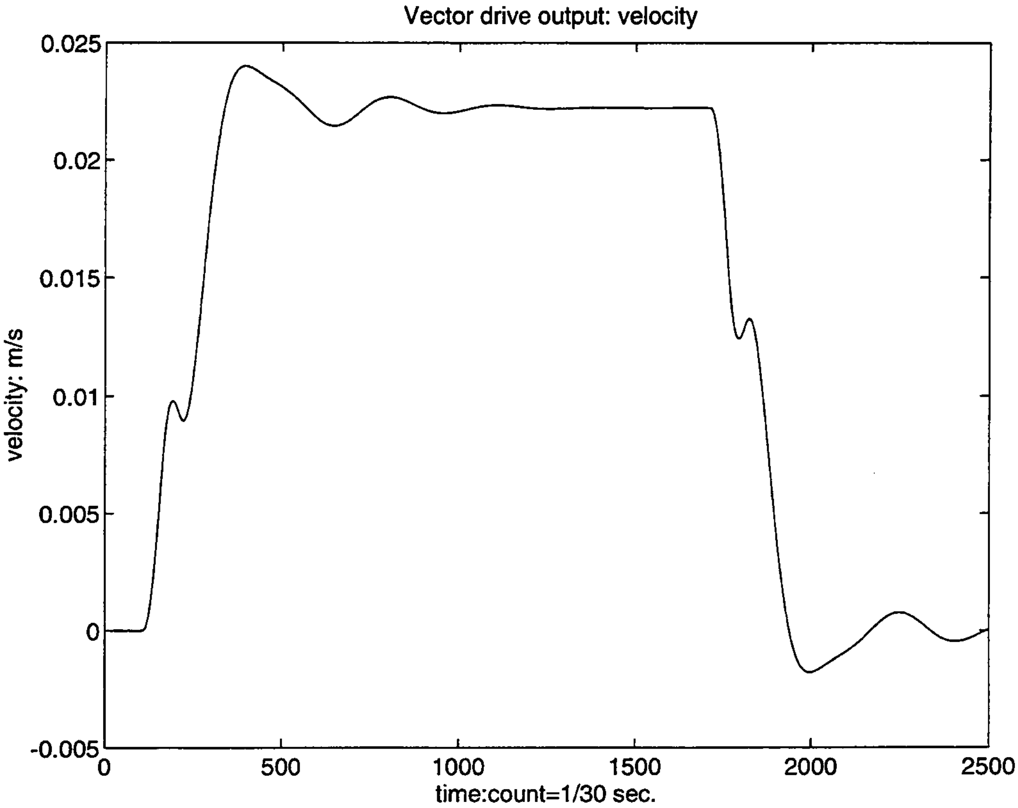

Figure 4.41: *Open-loop system vector drive output for parabolic input where*

$\omega_{filter} = 0.60\omega_{crane}$.

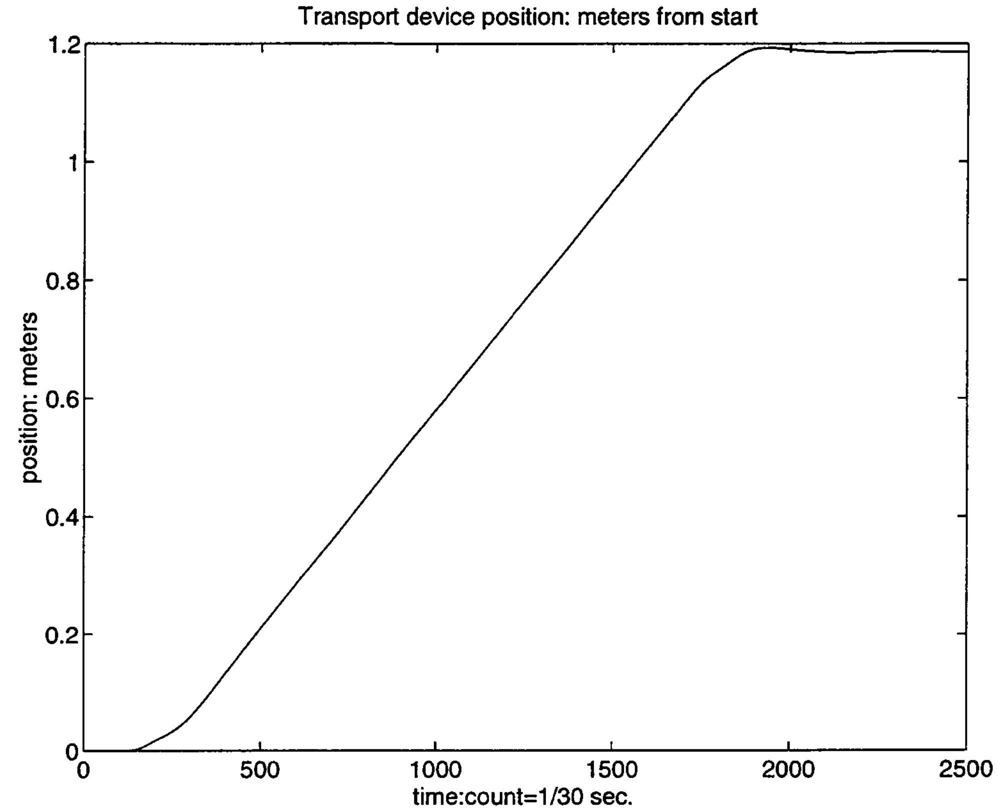

Figure 4.42: *Open-loop system crane carrier position for parabolic input where* $\omega_{filter} = 0.60\omega_{crane}$.

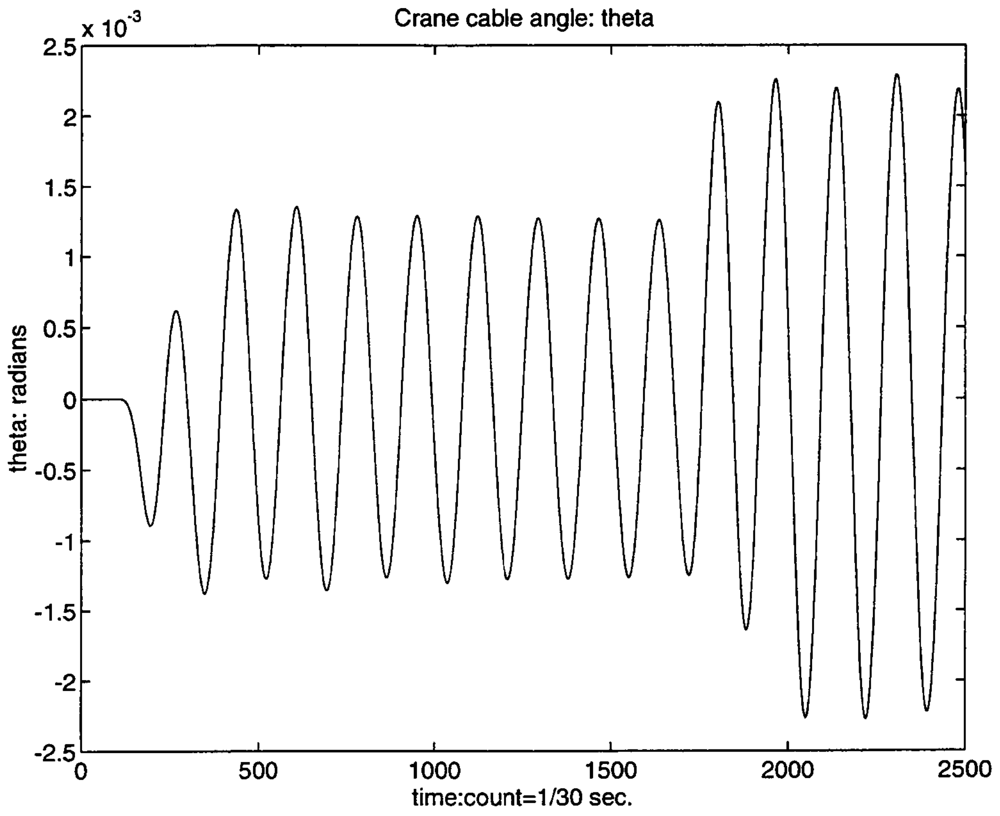

Figure 4.43: *Open-loop system crane cable angle for parabolic input where*

$\omega_{filter} = 0.60\omega_{crane}$.

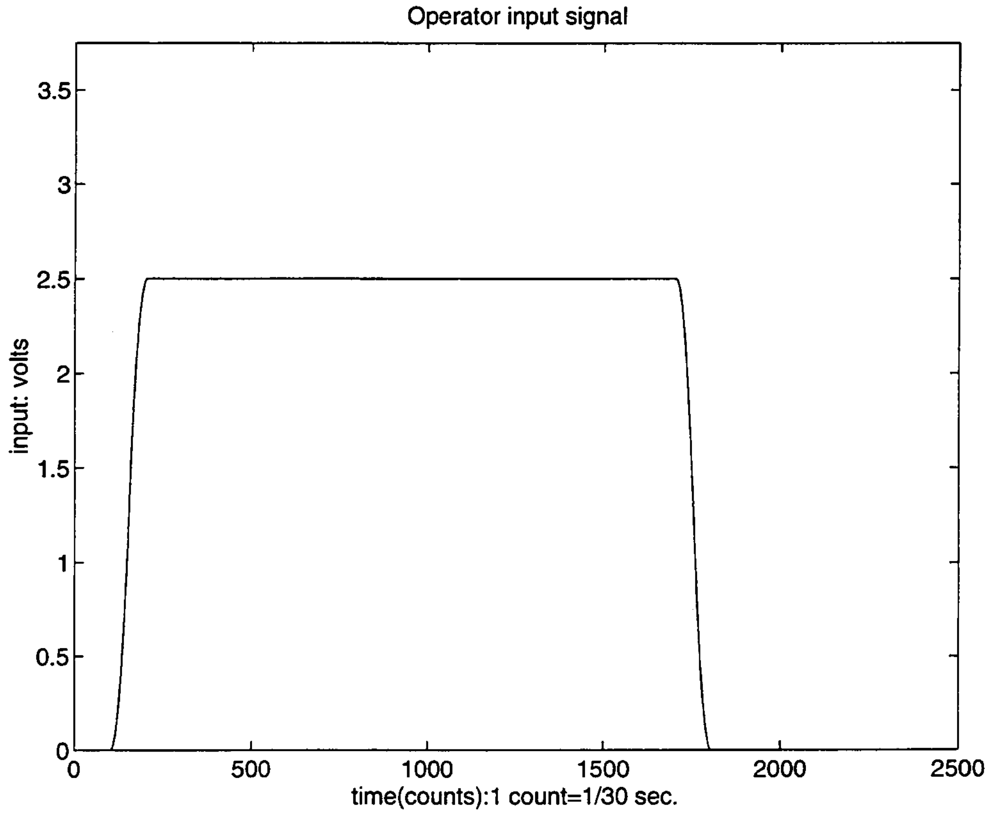

Figure 4.44: *Open-loop system parabolic input where* $\omega_{filter} = 1.70\omega_{crane}$.

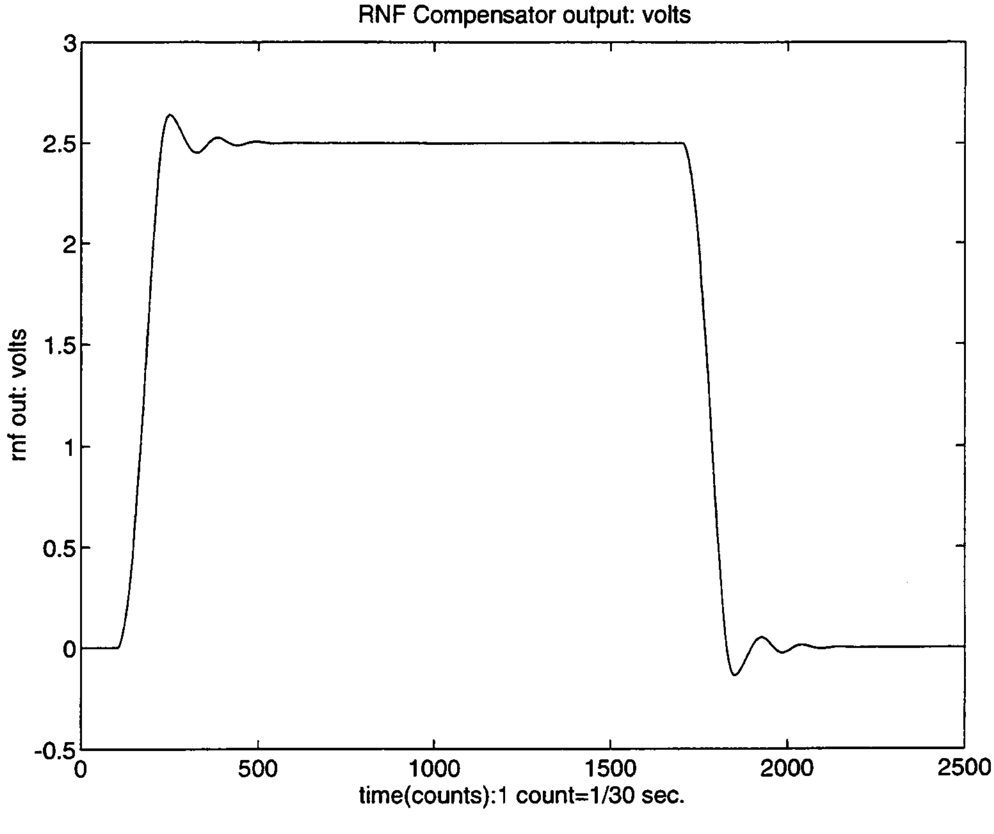

Figure 4.45: *Open-loop system compensator output for parabolic input where* $\omega_{filter} = 1.70\omega_{crane}$.

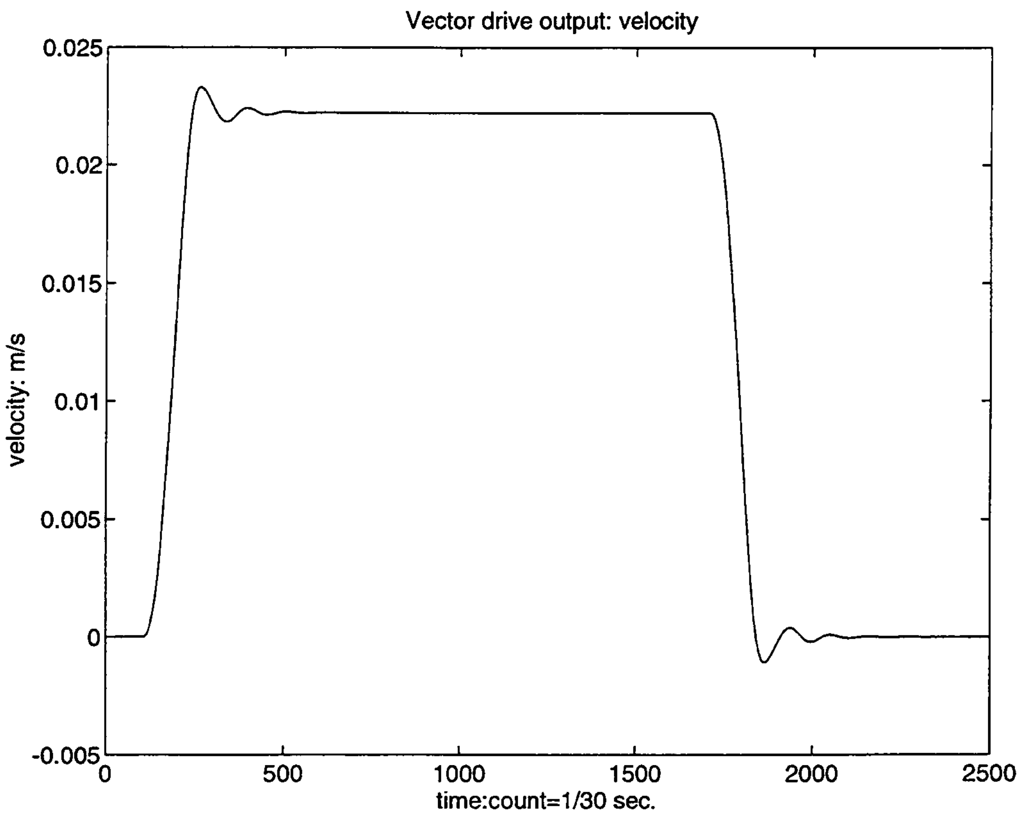

Figure 4.46: *Open-loop system vector drive output for parabolic input where* $\omega_{filter} = 1.70\omega_{crane}$.

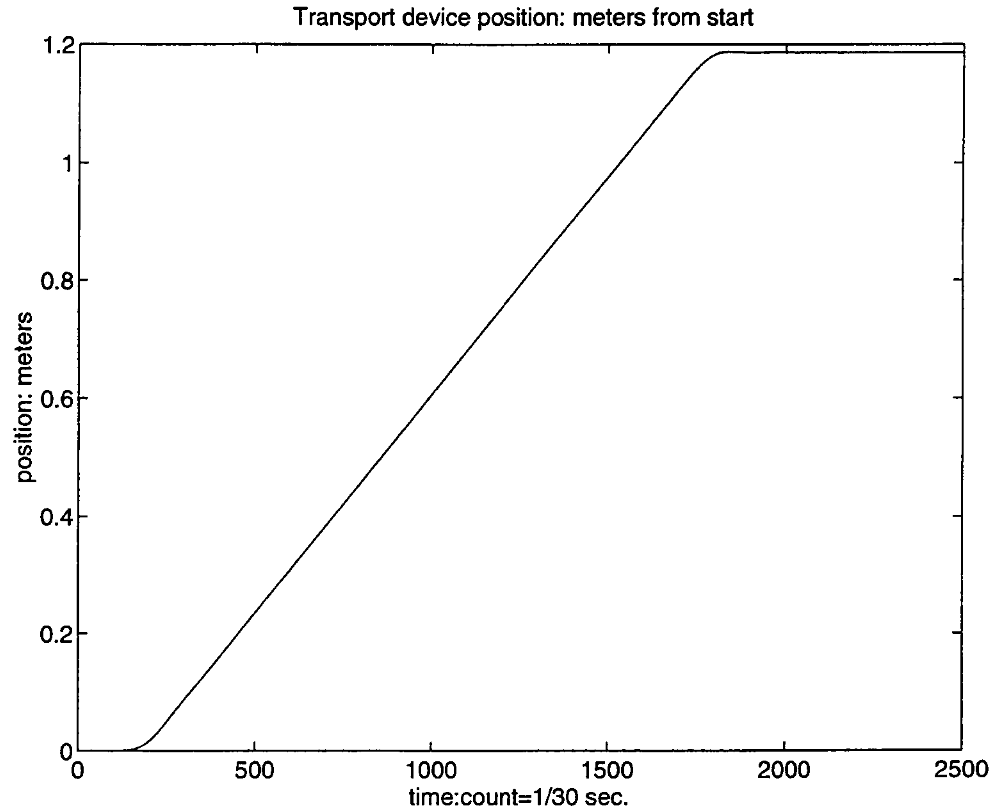

Figure 4.47: *Open-loop system crane carrier position for parabolic input where*

$\omega_{filter} = 1.70\omega_{crane}$.

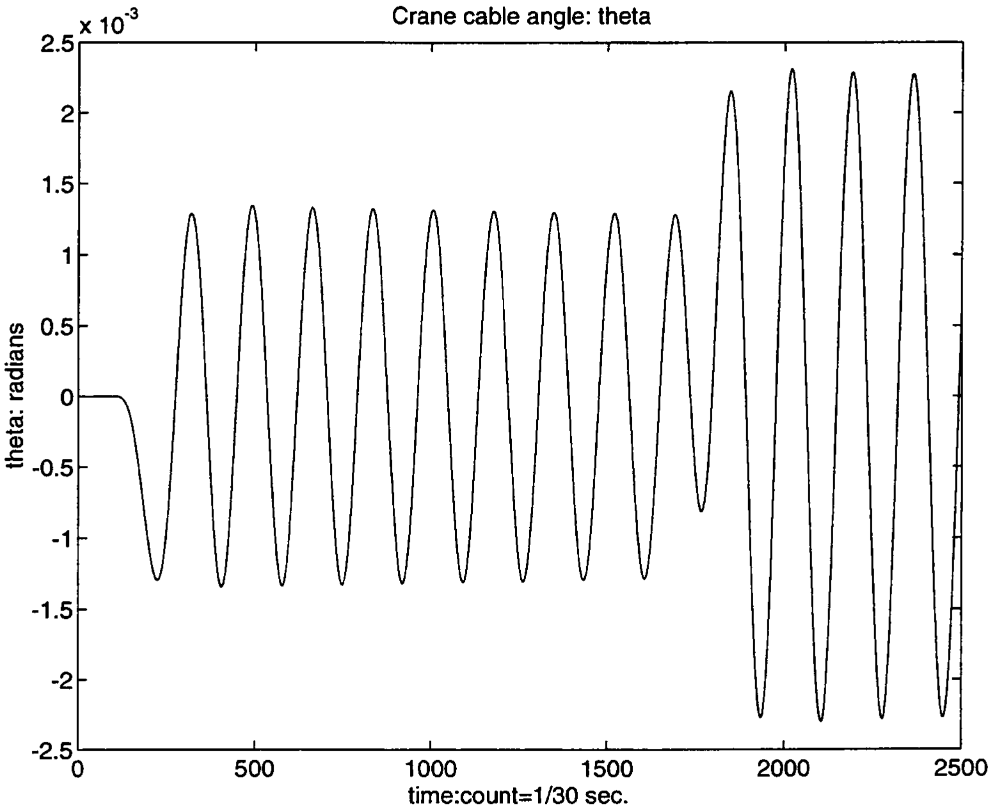

Figure 4.48: *Open-loop system crane cable angle for parabolic input where*

$\omega_{filter} = 1.70\omega_{crane}$.

Appendix B

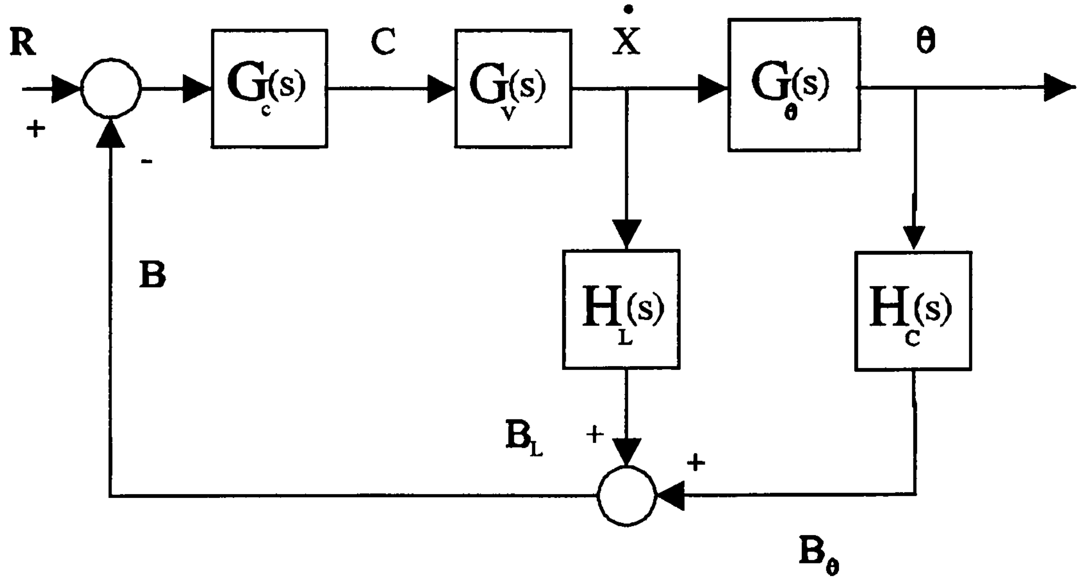

Figure 5.1: *General block diagram for closed loop system.*

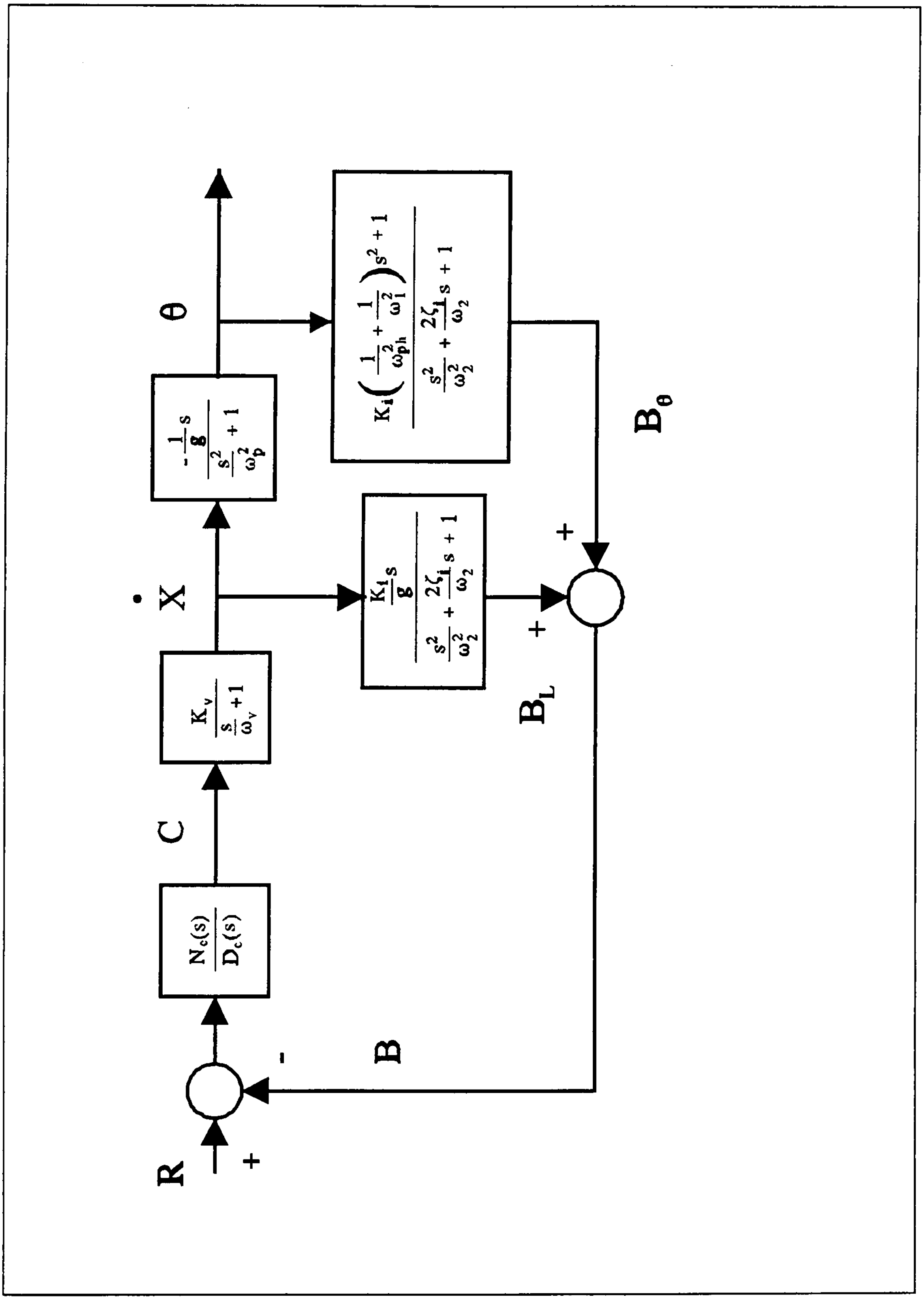

Figure 5.2: *Closed Loop system block diagram with transfer functions.*

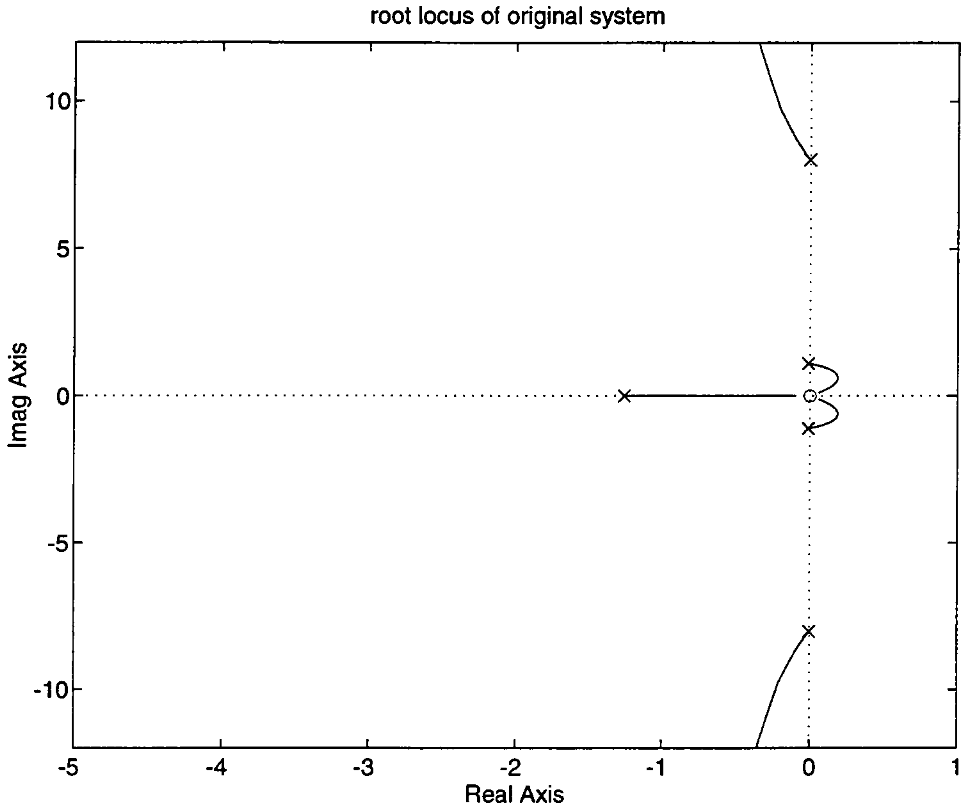

Figure 5.3: *Root locus plot for uncompensated closed-loop system.*

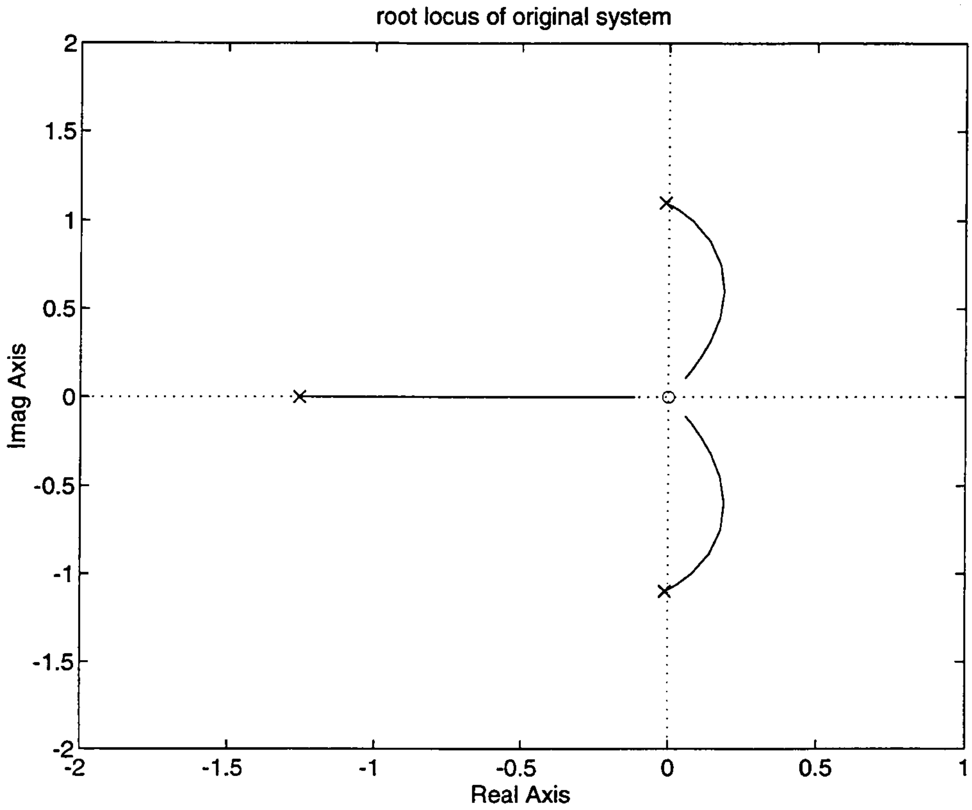

Figure 5.4: *Root locus plot for uncompensated closed loop system. Detail of crane pole response.*

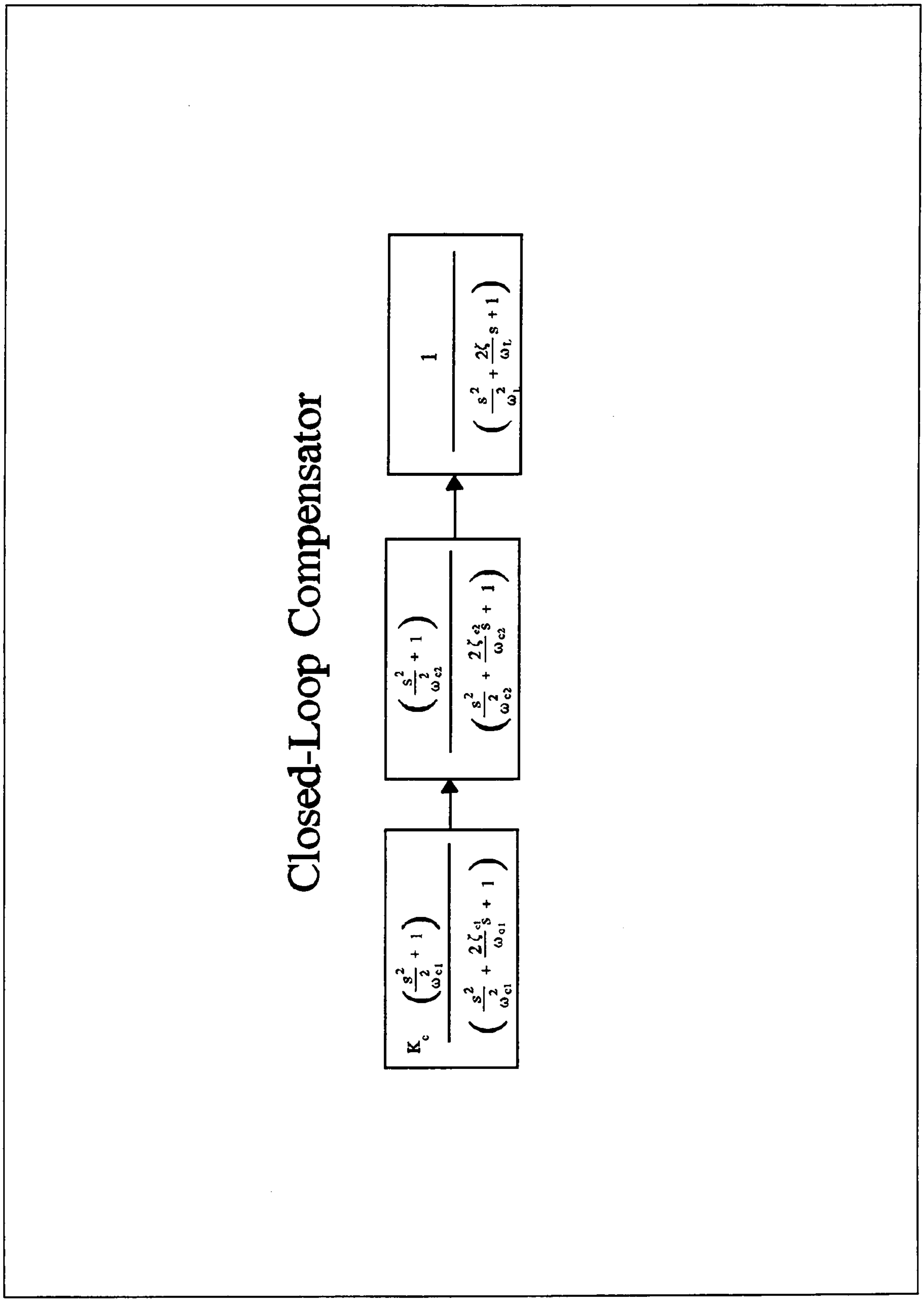

Figure 5.5: *Block diagram of closed-loop compensator.*

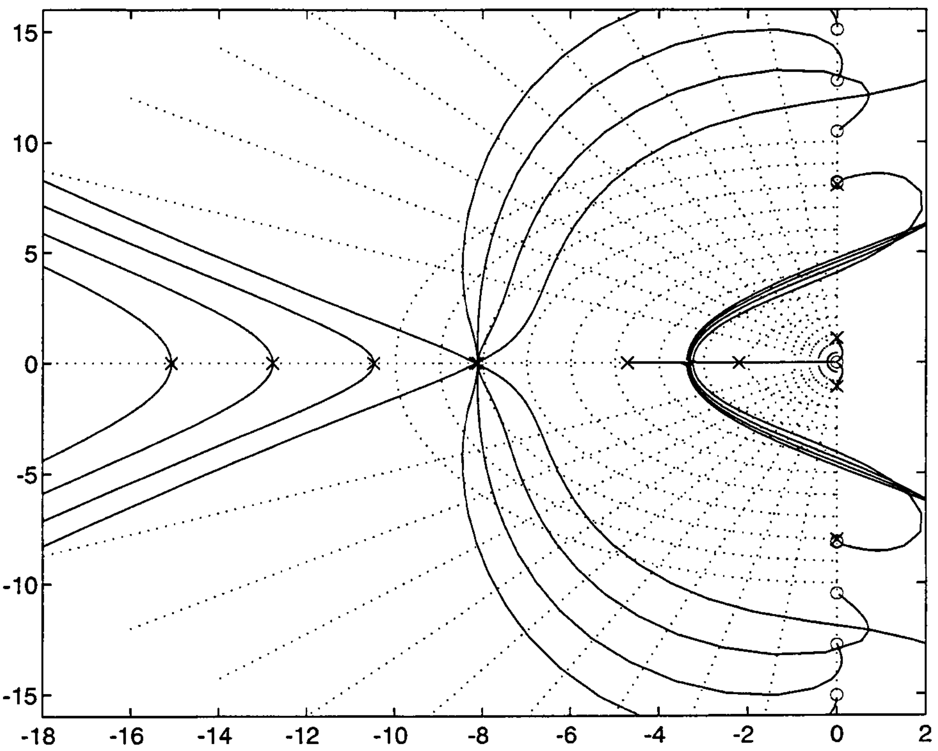

Figure 5.6: *Root locus contour for ω_{c2} ranging from 1.3 to 2.4 Hz.: inclinometer pole detail.*

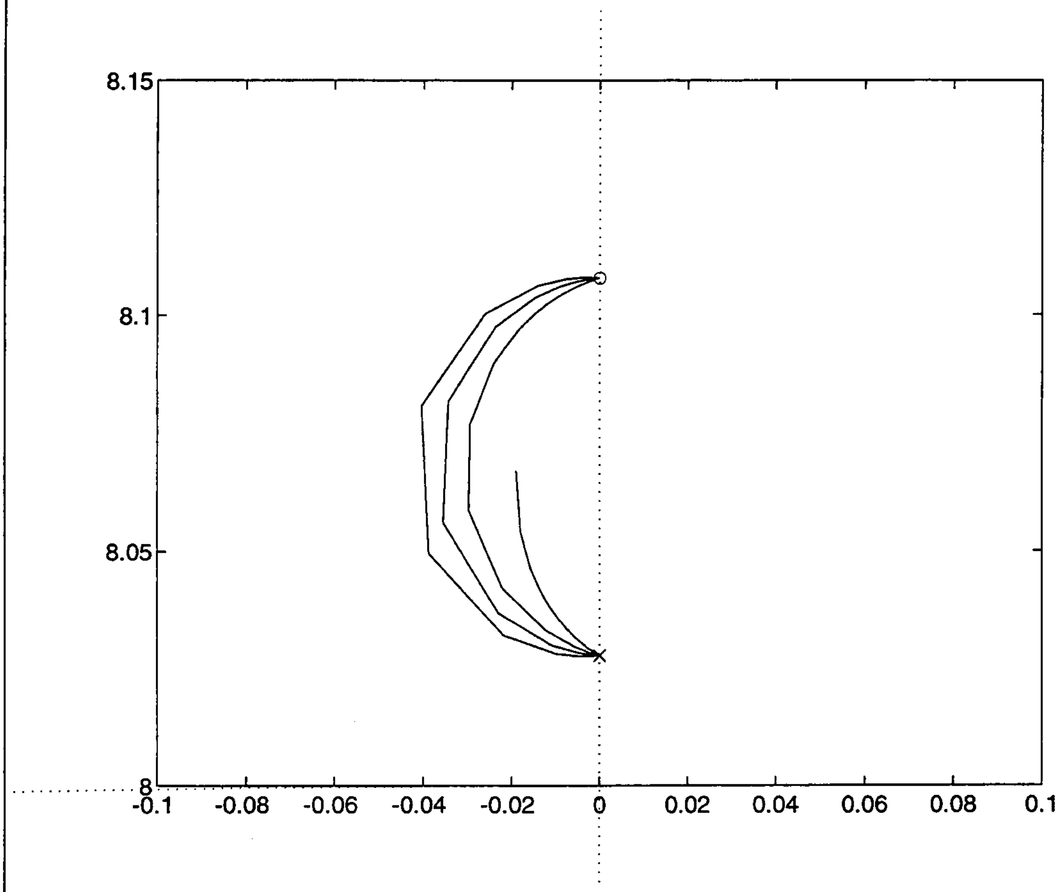

Figure 5.7: *Root locus contour for* ω_{c2} *varies from 1.3 to 2.4 Hz.: full view.*

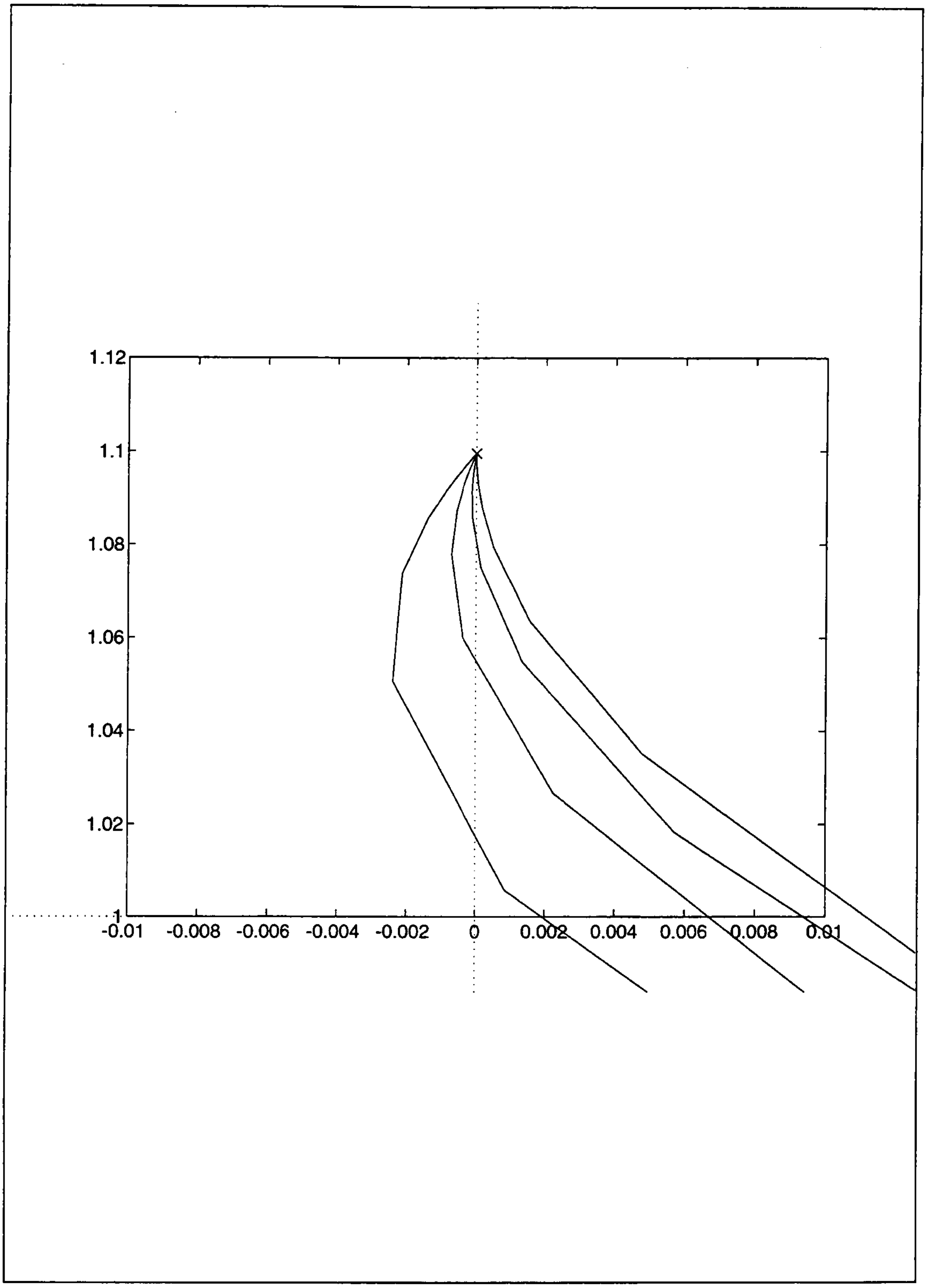

Figure 5.8: *Root locus contour for ω_{c2} ranging from 1.3 to 2.4 Hz.: crane pole detail.*

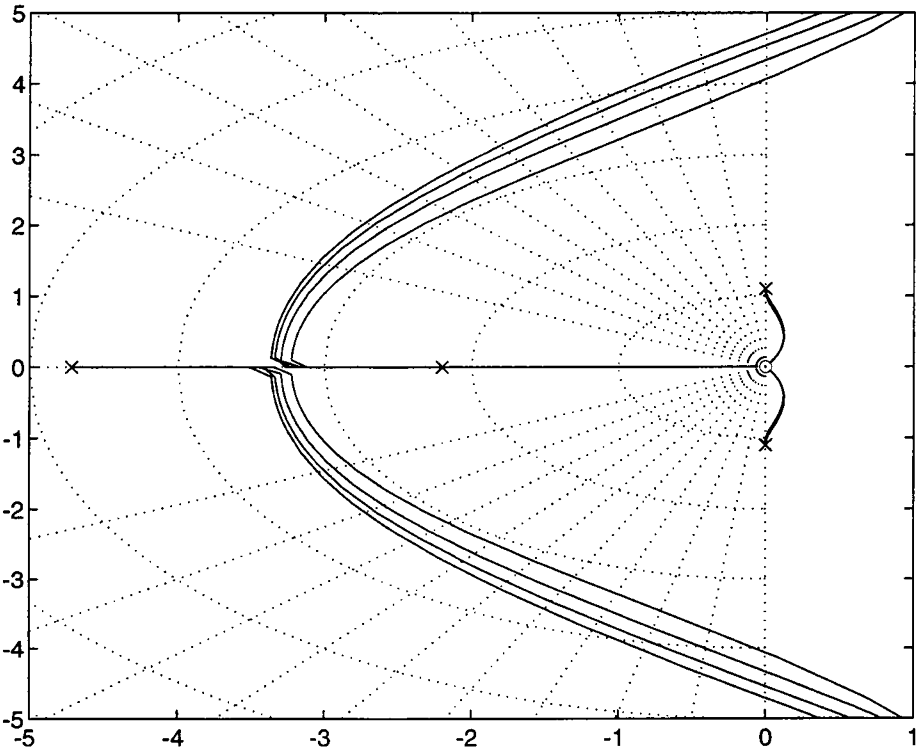

Figure 5.9: *Root locus contour for ω_{c2} ranging from 1.3 to 2.4 Hz.: overall close-up.*

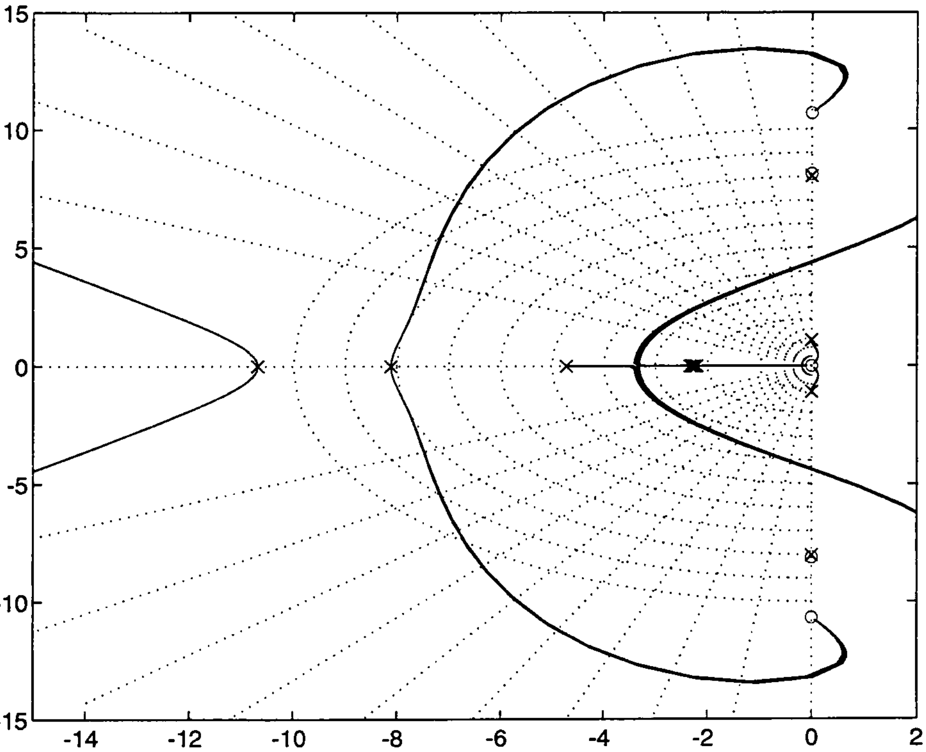

Figure 5.10: *Root locus contour for* ω_l *ranging from 0.35 to 0.37 Hz.: full view.*

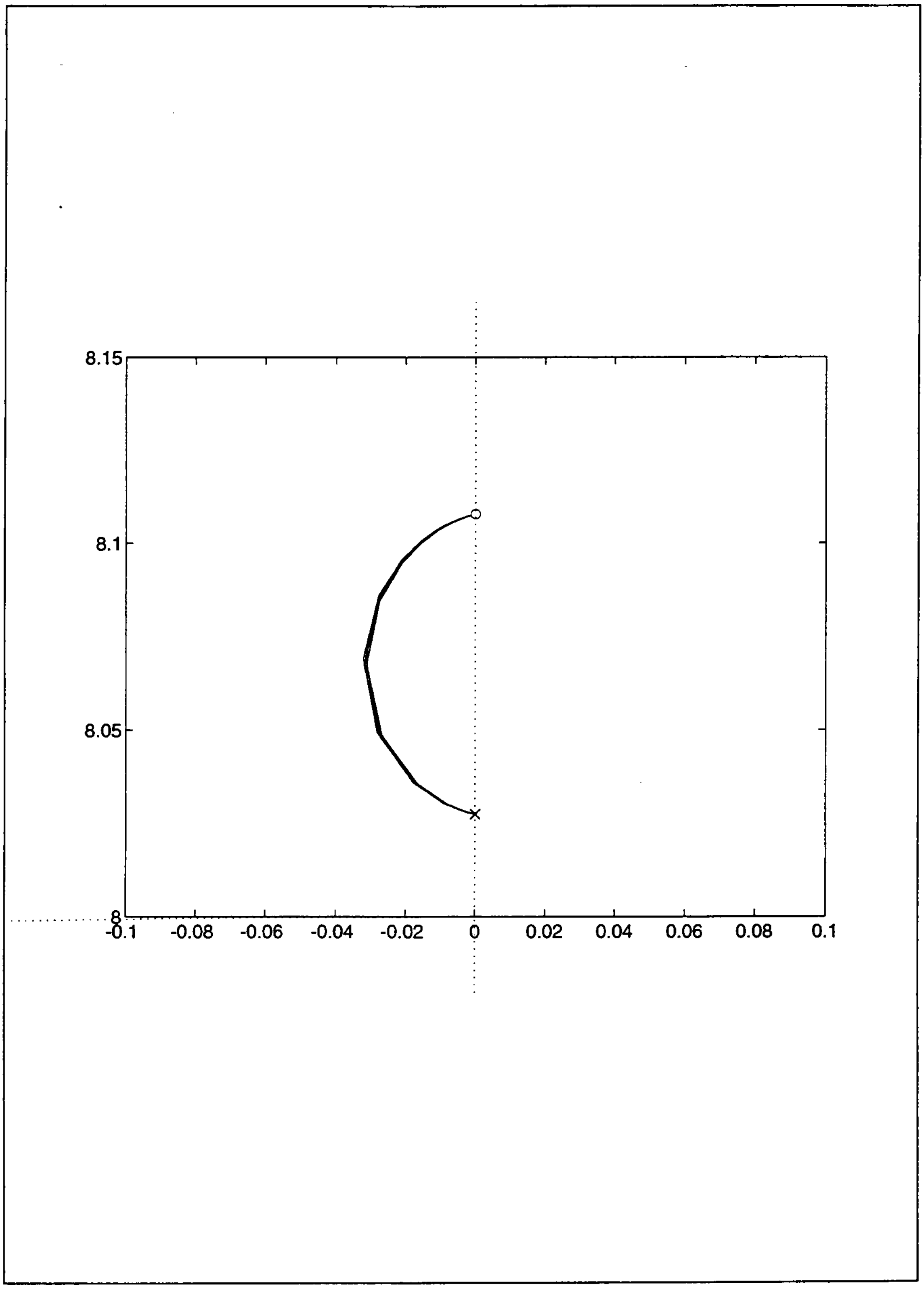

Figure 5.11: *Root locus contour for ω_l ranging from 0.35 to 0.37 Hz.: inclinometer pole detail.*

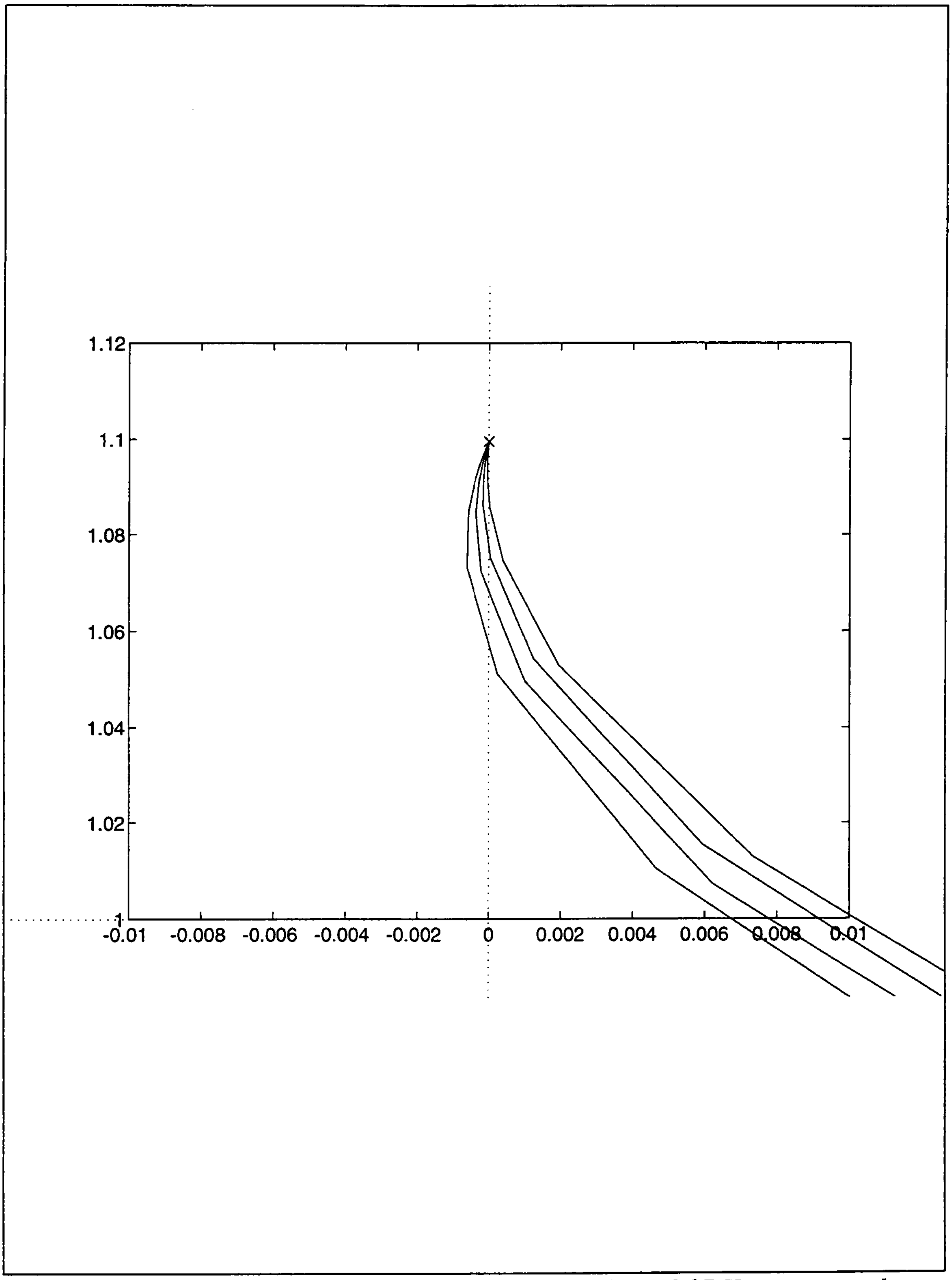

Figure 5.12: *Root locus contour for ω_l ranging from 0.35 to 0.37 Hz.: crane pole detail.*

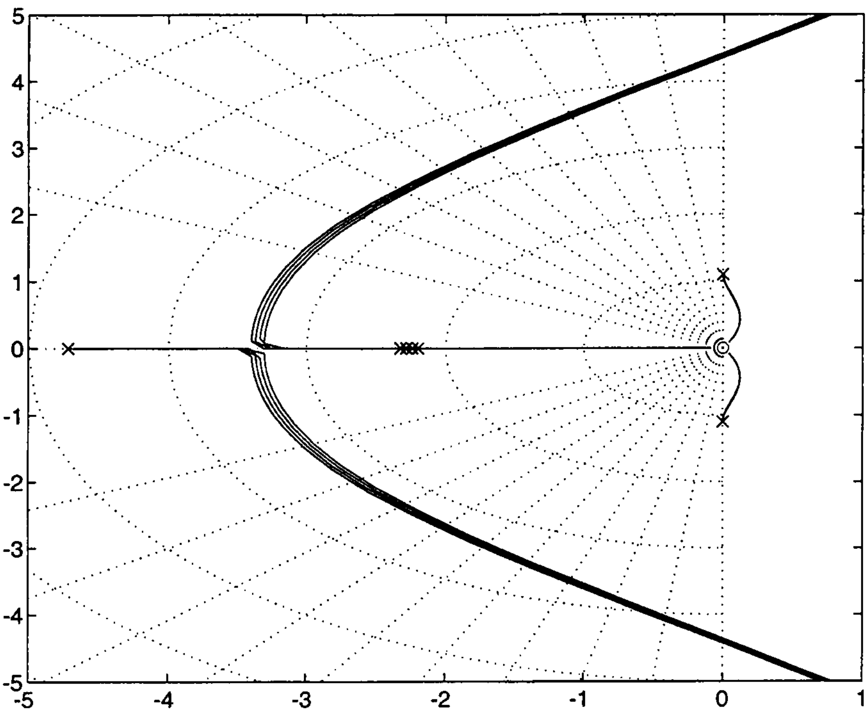

Figure 5.13: *Root locus contour for ω_l ranging from 0.35 to 0.37 Hz.: overall close-up.*

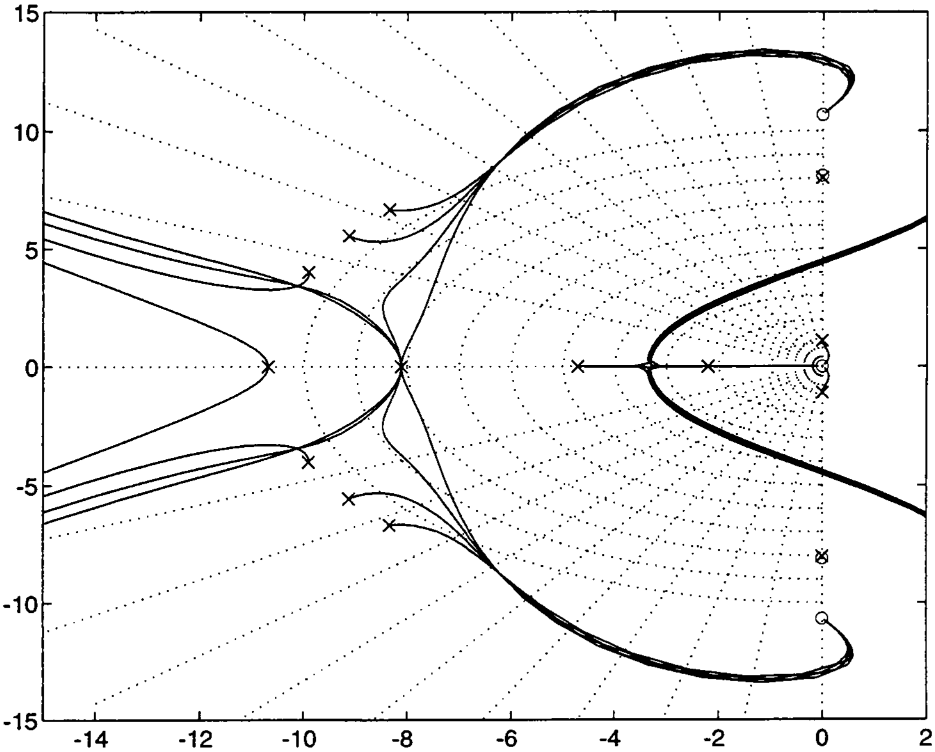

Figure 5.14: *Root locus contour for ζ_{c2} ranging from 0.78 to 1: overall view.*

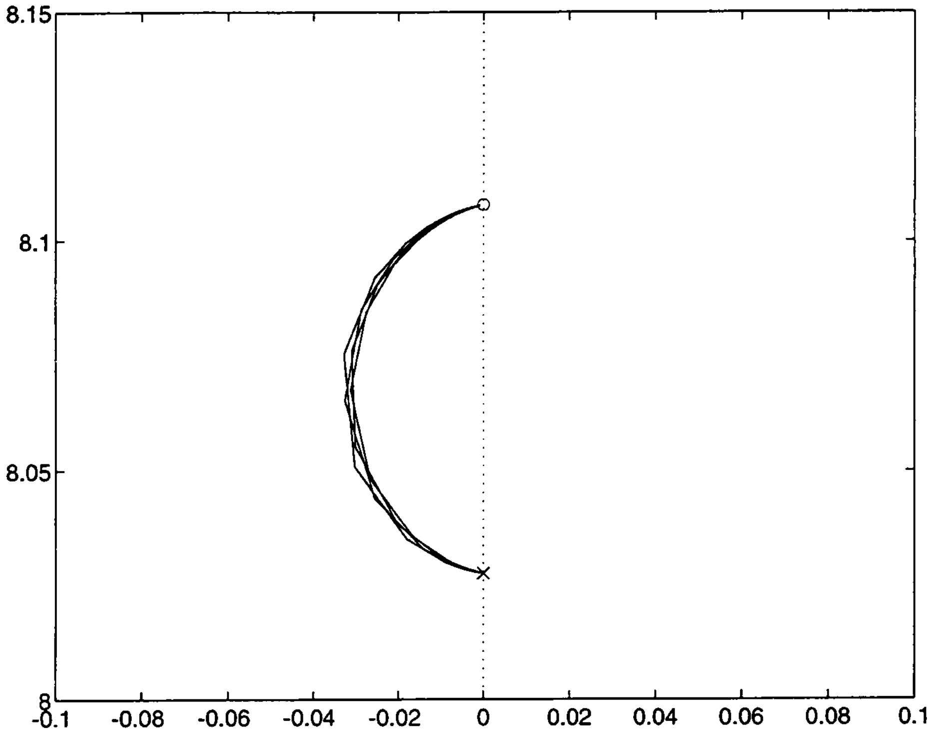

Figure 5.15: *Root locus contour for ζ_{c2} ranging from 0.78 to 1: inclinometer pole detail.*

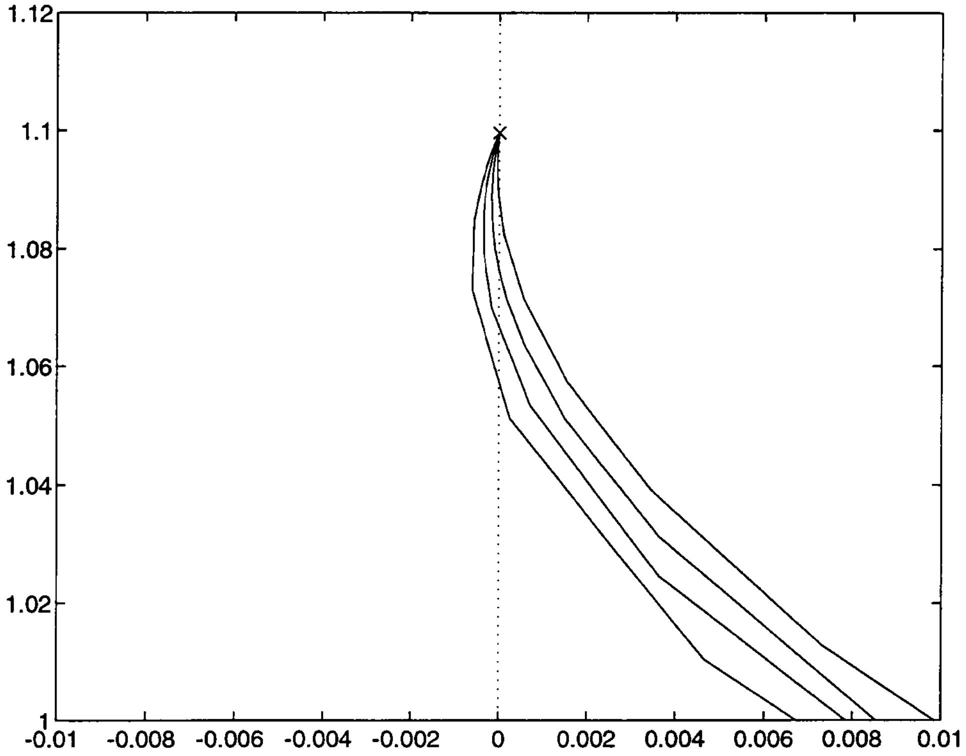

Figure 5.16: *Root locus contour for ζ_{c2} ranging from 0.78 to 1: crane pole detail.*

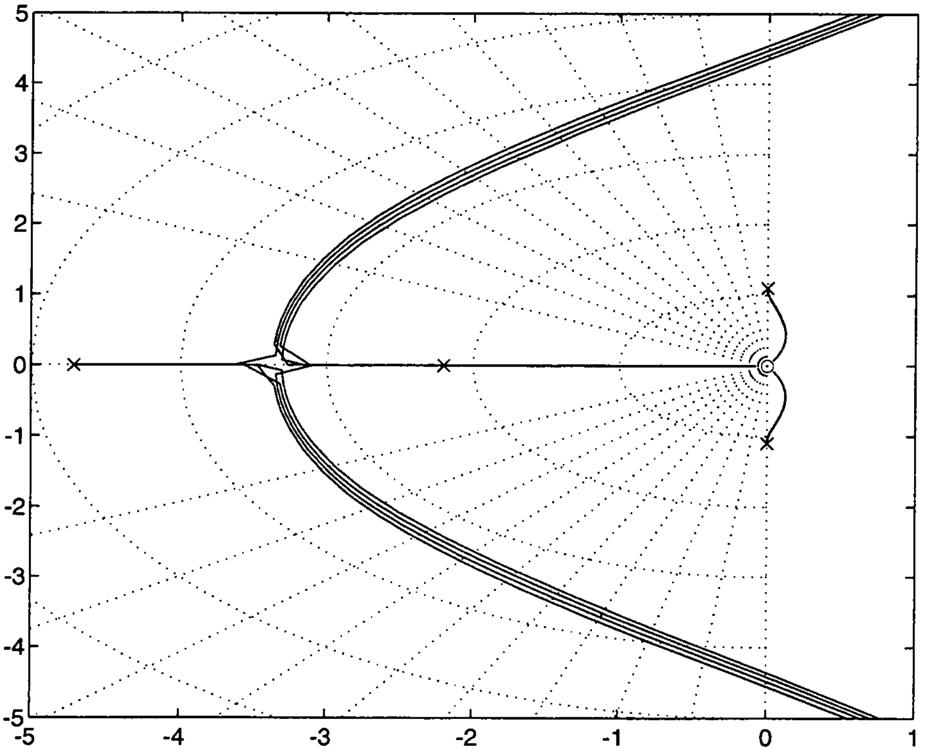

Figure 5.17: *Root locus contour for ζ_{c2} ranging from 0.78 to 1: overall close-up.*

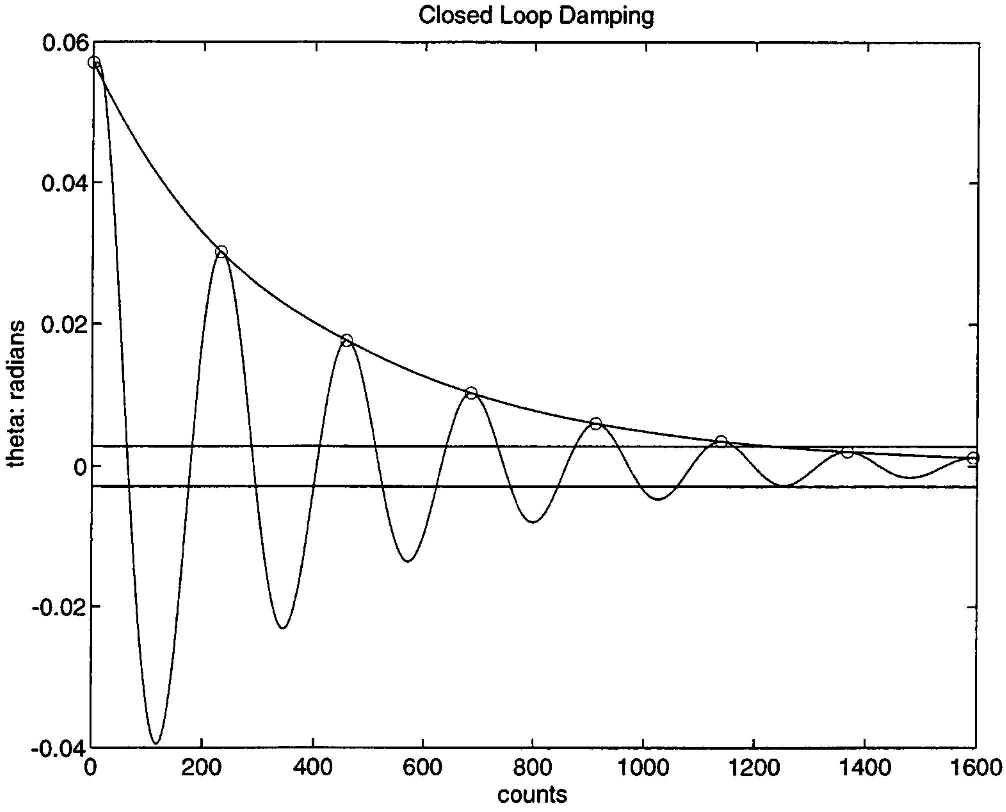

Figure 5.18: *Crane cable theta for ω_p = 85% of base; parallel lines depict 5% of starting amplitude, envelope of decay superimposed.*

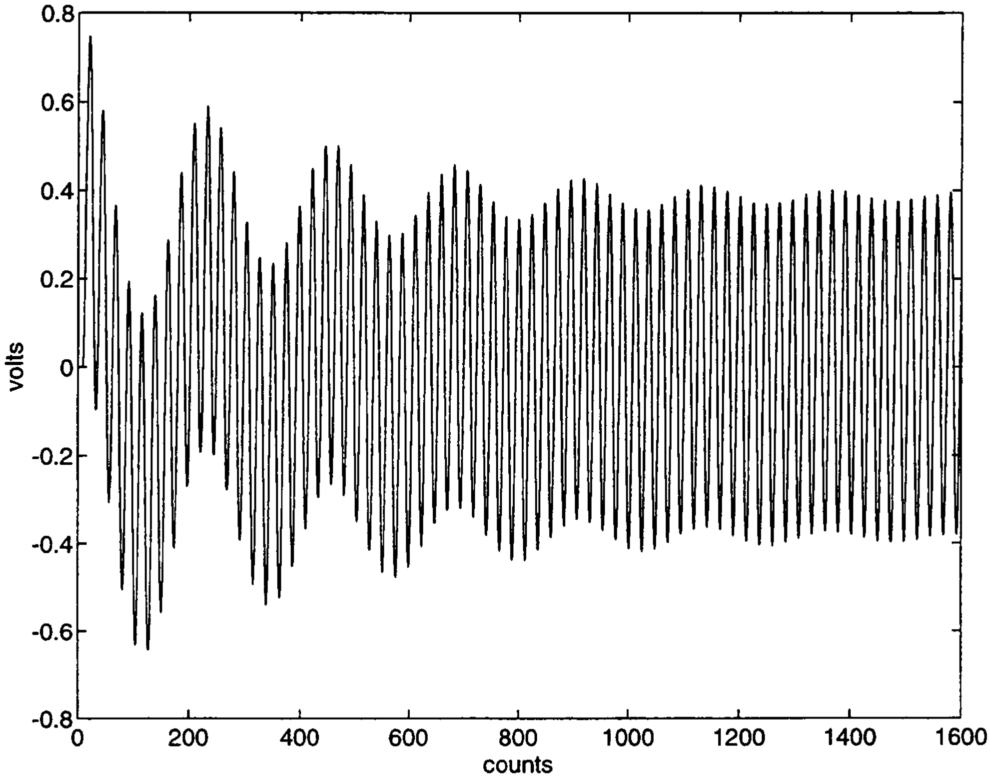

Figure 5.19: *Inclinometer output for ω_p = 85% of base.*

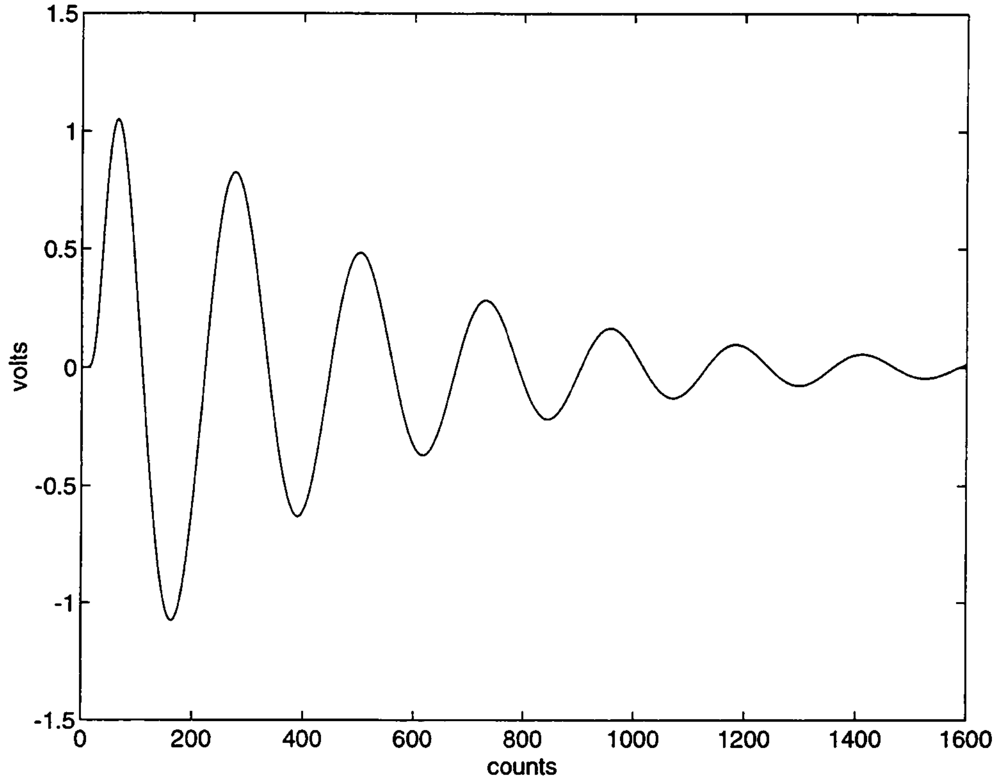

Figure 5.20: *Compensator output for ω_p = 85% of base.*

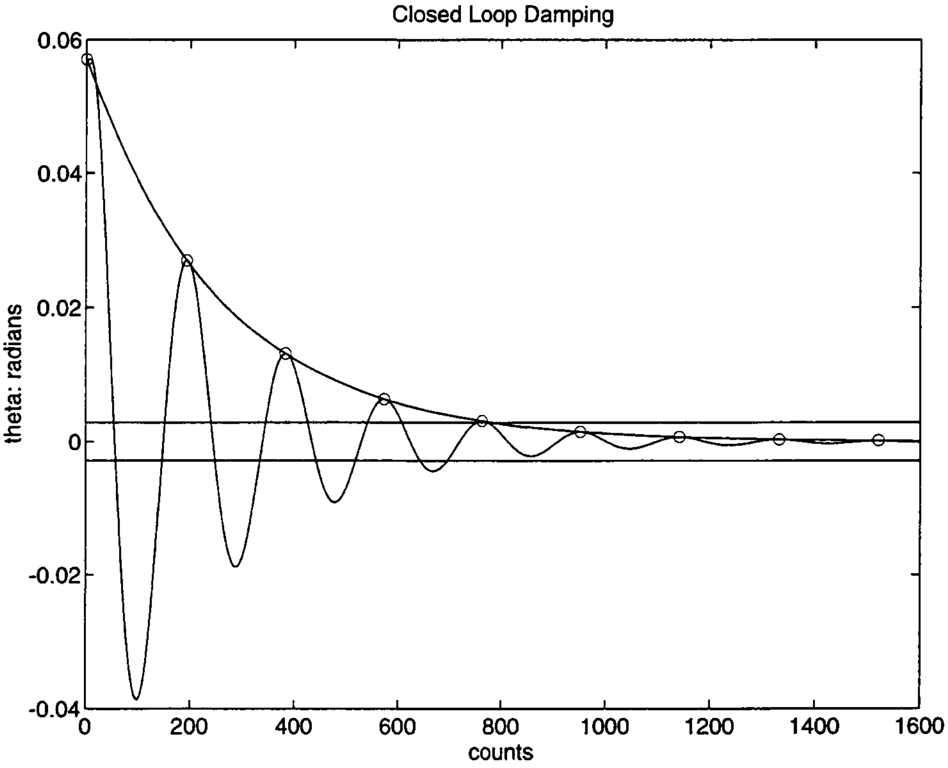

Figure 5.21:*Crane output for* ω_p *= base value; parallel lines indicate 5% of initial amplitude, decay envelope superimposed.*

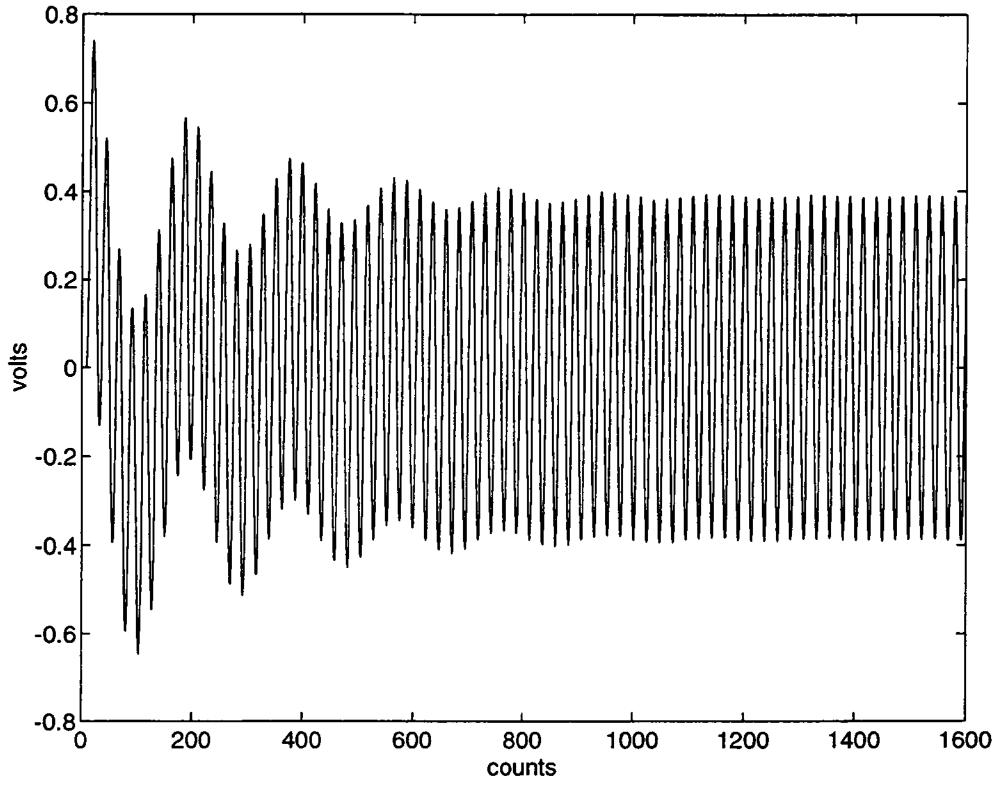

Figure 5.22: *Inclinometer signal for* ω_p = *base.*

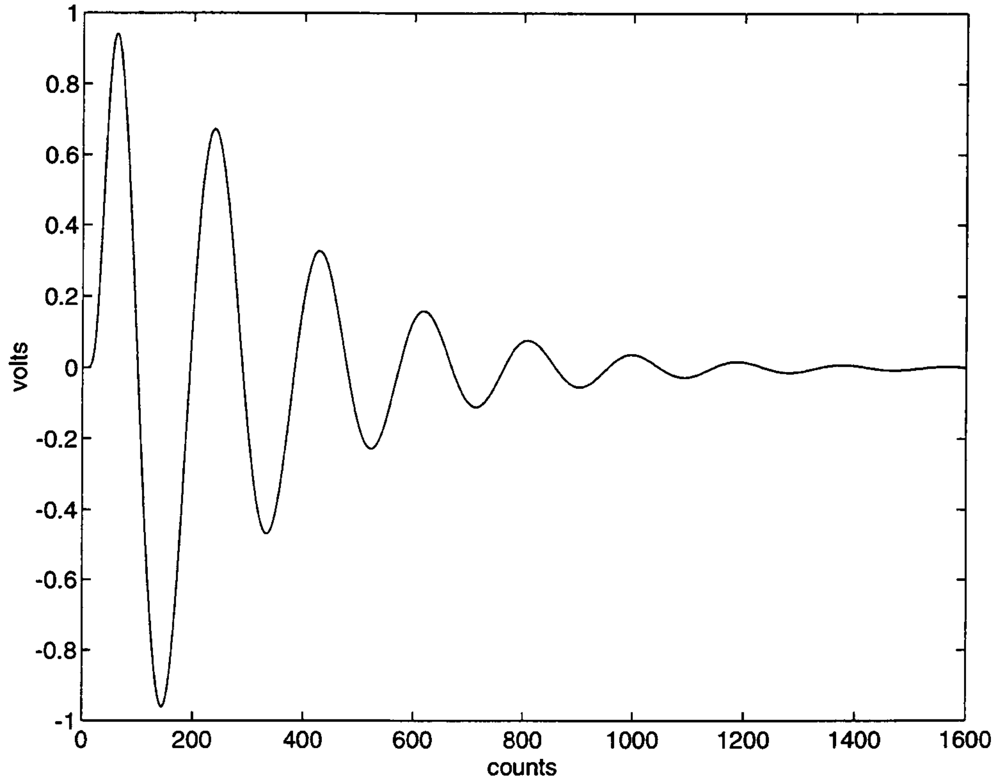

Figure 5.23: *Compensator output for* ω_p = *base.*

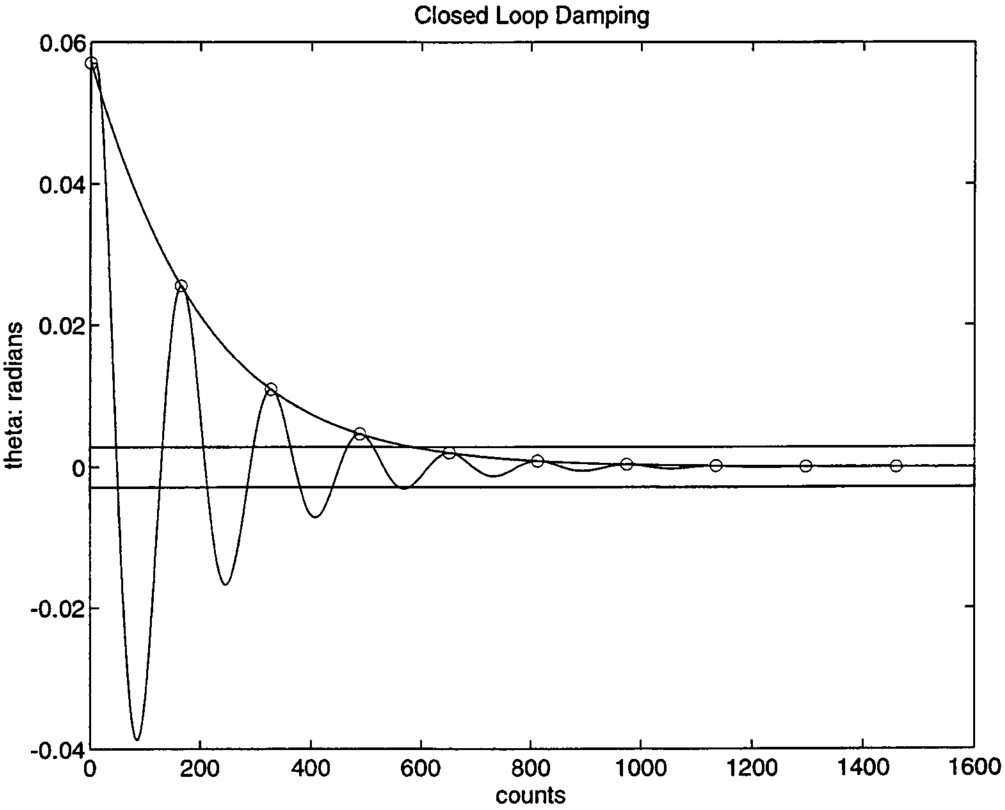

Figure 5.24: *Crane output for ω_p = 115% of base; parallel lines indicate 5% of initial amplitude, decay envelope superimposed.*

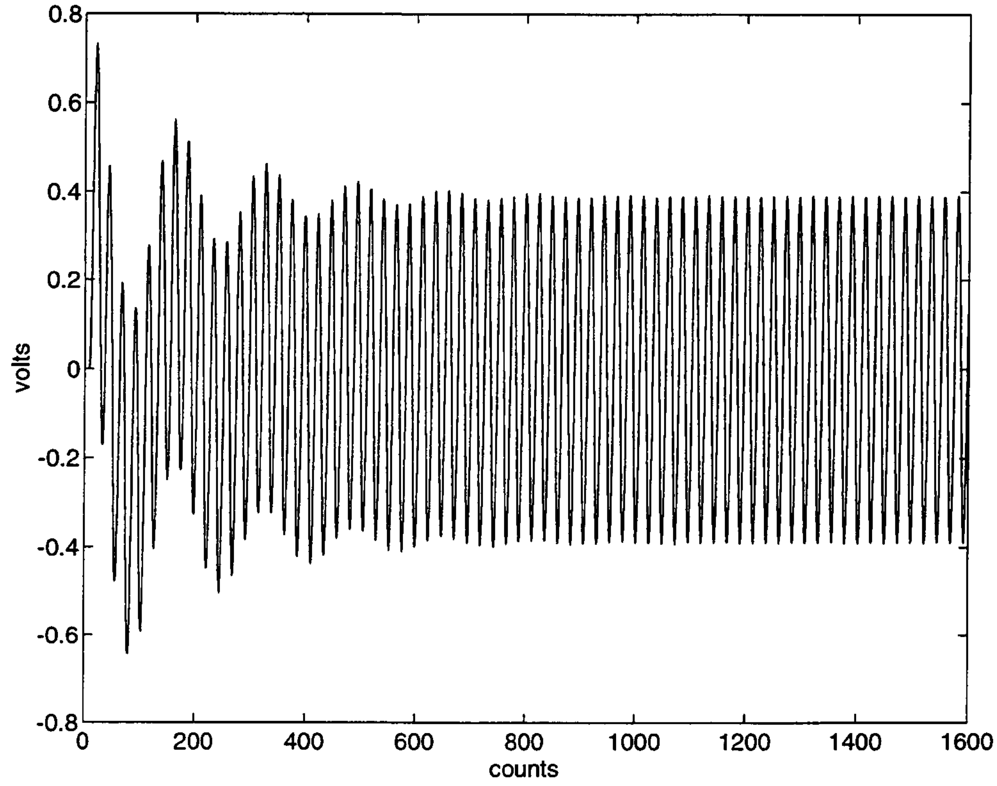

Figure 5.25: *Inclinometer signal for* ω_p = *115% of base.*

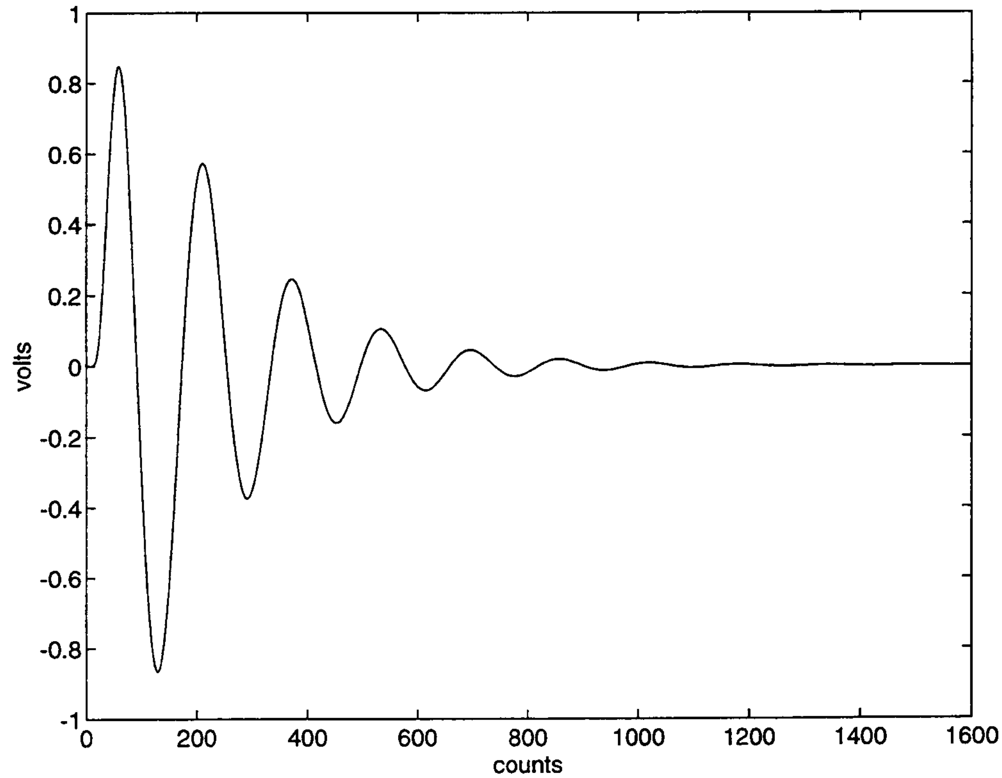

Figure 5.26: *Compensator output for* ω_p = *115% of base.*

Vita

Douglas A. Shamblin received his Bachelor of Science in Electrical Engineering from the University of Tennessee, Knoxville in December 1992 and a Master of Science from the University of Tennessee, Knoxville in August 1995. He worked as a graduate research assistant in the Computer Vision and Robotics Research Laboratory from September 1992 through August 1994.